UiT The Arctic University of Norway
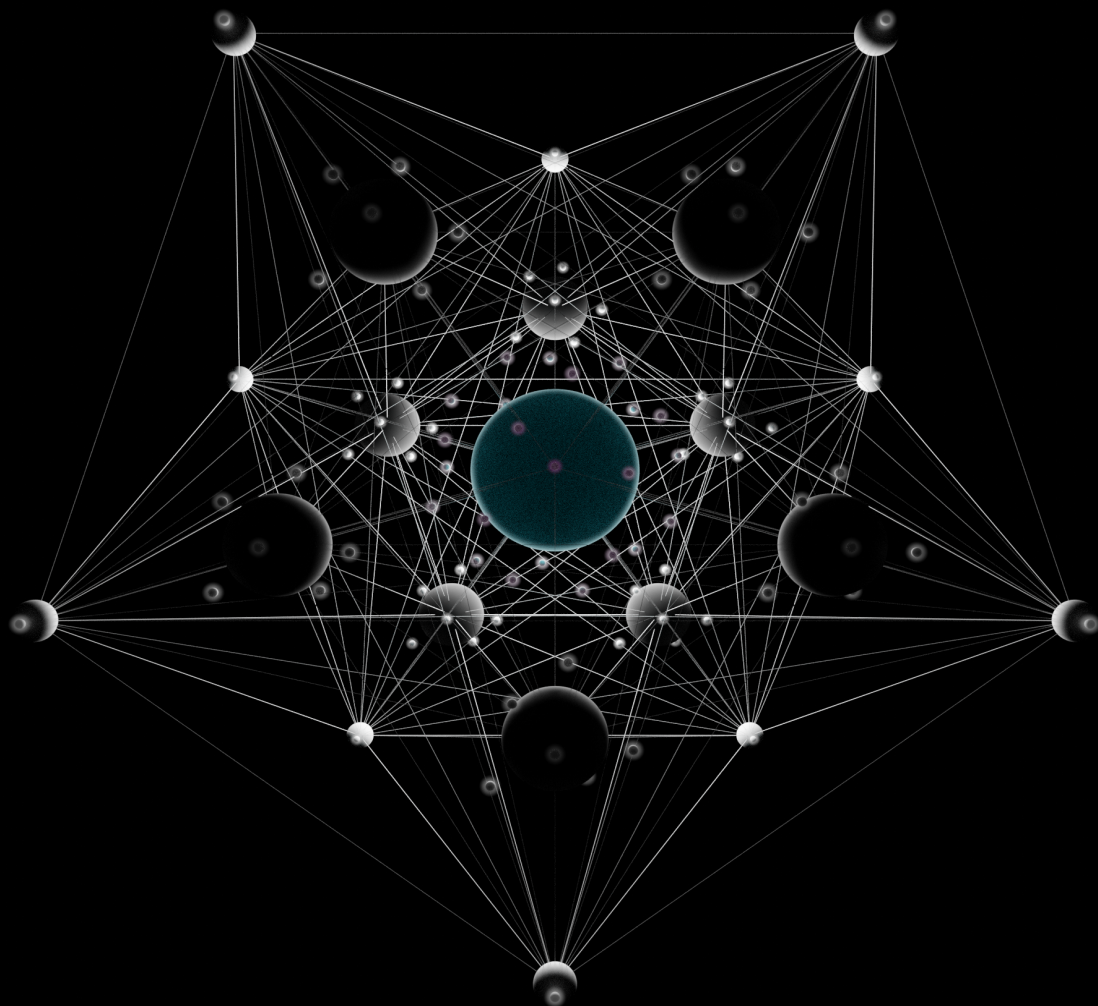
Faculty of Science and Technology

Department of Chemistry

Applications of Multiwavelets to Energies and Properties

Anders Brakestad

A dissertation for the degree of Philosophiae Doctor

December 2021

Applications of Multiwavelets to Energies and Properties

Anders Brakestad

A dissertation for the degree of Philosophiae Doctor

Department of Chemistry

Faculty of Science and Technology

UiT The Arctic University of Norway

Supervisor

Kathrin H. Hopmann

Professor

Co–Supervisor

Luca Frediani

Professor

December, 2021

Table of Contents

Abstract

The goal of quantum chemistry is to provide fast and accurate algorithms for the computation of molecular energies and properties. Over the years, a large number of methods have become available, and today computational chemists have a very rich toolbox of protocols that can be used to gain insight to chemistry. Gaussian type orbital (GTO) basis sets are at the core of most modern algorithms, and they have served the community well since they were first introduced. However, during the last 20 years, Multiwavelets (MWs) have emerged as a promising alternative to traditional GTO basis sets. Multiwavelets are built up from polynomial functions, and systematically approach completeness due to their robust mathematical foundation in multiresolution analysis. The in-house MW code MRChem has reached a level of maturity where it can be used to study chemical systems of 1000s of electrons. It provides functionality for the calculation of SCF energies, as well as electric and magnetic properties via density functional pertubation theory. This thesis presents the application of MWs in benchmark studies of static electric dipole polarizabilities (Paper I) and transition metal-ligand interaction energies (Paper II). Here we provide highly precise numerical results practically at the complete basis set limit, and with this reference we are able to quantify basis set incompleteness errors (BSIEs) in large GTO basis sets without ambiguity. The thesis also presents a prototype implementation of scalar relativistic effects via the zeroth order regular approximation into MRChem (Paper III, in preparation), and a preliminary quantification of BSIEs in several all-electron GTO basis sets for elements in the fifth row of the periodic table.

A popular science introduction to quantum chemistry

Our understanding of the universe has changed a lot during the evolution of our species. Within a particular scientific paradigm, our understanding usually advances systematically and in increments, but every once in a while we reach an insurmountable problem that simply cannot be solved within the existing paradigm. When such problems are overcome, it results in a paradigm shift that not just overcomes the problem, but completely alters the *premises* of the problem. One example of such a paradigm shift took place towards the end of the 1800s and early 1900s, when the scientific community discussed the atomic theory of matter and how matter interacts with radiation. The classical physical understanding of the time was largely based on three separate theories: i) Sir Isaac Newton's classical mechanics, ii) statistical thermodynamics founded by Ludwig Boltzmann, James Clerk Maxwell, and Josiah Willard Gibbs, and iii) Maxwell's equations for electromagnetism. However, these theories were pushed beyond their limits when attempting to describe how very small particles, such as electrons and protons, interact with each other and with electromagnetic radiation. A new theory of matter was needed, and I think few people at the time of its invention would predict its monumental effect on our societies.

The new theory was of course the quantum theory of matter, also called quantum mechanics. The term "quantum" refers to that only certain energy levels in atoms are allowed: the energy has become quantized or discretized. This is not the case in the classical mechanics

of Newton, where energy is continuous. The story of how quantum mechanics was invented is best read as an intricate crime novel, but to do it justice is beyond the scope of this short introduction. The road to a quantum understanding of matter culminated in the famous wave equation published by Erwin Schrödinger in 1926. In solving this equation, one obtains the wavefunction, which contains a lot of physically and chemically relevant properties and how these behave over time given some initial conditions. Not long after Schrödinger published his equation, Paul Dirac unified the quantum theory of matter with Albert Einstein's theory of special relativity, which resulted in perhaps the most important equation relevant for chemistry: the Dirac equation.

The development of modern chemistry in the 1700s and 1800s culminated in a systematic organization of known and unknown chemical elements in what we today call the periodic table of the elements. However, it was not until quantum theory had matured that we had a mathematical framework for understanding the underlying phenomena that govern chemical reactions. Paul Dirac himself wrote in a publication in 1929 titled "Quantum mechanics of many-electron systems":

"The underlying physical laws necessary for the mathematical theory of a large part of physics and the whole of chemistry are thus completely known, and the difficulty is only that the exact application of these laws leads to equations much too complicated to be soluble. It therefore becomes desirable that approximate practical methods of applying quantum mechanics should be developed, which can lead to an explanation of the main features of complex atomic systems without too much computation."

Dirac claimed that quantum theory fully explains the whole of chemistry. Although this is a very bold statement, it can be justified. The

most important particle in chemistry is the electron. In all chemical reactions at least one electron is transferred from one place to another, and all chemical bonds are due to electrons interacting with one another. Electrons exist in immediate contact with the surrounding environment at the atomic scale, and most chemically relevant interactions involve electrons. Therefore, if one has a mathematical framework that accurately describes how electrons behave, then one can make the argument that it is possible to mathematically explain chemistry.

The second part of his quote is also insightful. The Dirac and Schrödinger equations can only be solved with pen and paper (which in technical jargon is called being "solved analytically") for the smallest atom in the periodic table: the hydrogen atom. Dirac actually quite accurately defined the entire field of quantum chemistry, by realizing that we must develop approximations to the exact quantum theories in order to be able to gain quantum mechanical insight to chemistry. The overarching goal of quantum chemistry is to use the laws of quantum mechanics to solve chemistry problems, and perhaps most of the research in quantum chemistry has centered around the development of good approximations.

It was the computer that truly made quantum chemistry come alive. The computer allowed us to stop computing properties of systems with little relevance to society, and instead start to *explain* "known" chemistry or *predict* "unknown" chemistry. Quantum chemistry as a field has taken huge advantage of the developments in computer science, and if your game console can take advantage of a new type of hardware, chances are that quantum chemistry eventually also will benefit from it. The efficiency of central processing units (CPUs) are perhaps plateauing, but the use of graphics processing units (GPUs) in quantum chemistry is becoming more common. The largest super-computer in Norway, named Betzy after Mary Ann Elizabeth Stephansen, consists of approximately 170 000 CPUs, 336 000 GB, and a total disc storage of 2500 TB. With

access to such large computer architectures, one can distribute the computational workload over thousands of CPUs, which allows us to use more computationally demanding methods that otherwise would take too much time.

The field of quantum chemistry is highly diverse. Computer programming lies at the core of all the tools available to quantum chemists, since the theories need to be translated from mathematics to code in order to become useful. The development of new approximations to exact theories involves a combination of physical understanding and skills in mathematics, since it is important to capture as much of the physical essence in appropriate mathematical representations. The application of already-developed methods to problems of societal relevance requires chemical understanding and intuition. The day-to-day work of an applied quantum chemist requires skills in scripting automated workflows and data analysis, in order to work efficiently. The illustration in Figure 1 therefore summarizes the field of quantum chemistry (the central cog) and its influences (the outer cogs).

My PhD research represents the incremental and systematic advance of science, and touches upon several of the influences in Figure 1. I have been testing, and lately also developing, new software for quantum chemistry calculations that delivers higher precision than what can be achieved with conventional software. This involves submitting thousands of calculations national supercomputers to generate high-quality data, which is then analyzed in detail and archived. Our data serve the purpose as an objective reference against which the precision of other approximations can be compared, and we hope that our protocols and data can aid researchers in rational choice of computational protocols in the future, and help guide the development of future quantum chemistry approximations.

So what will quantum chemistry look like in the future? The increase in computational power is opening the possibility to use better
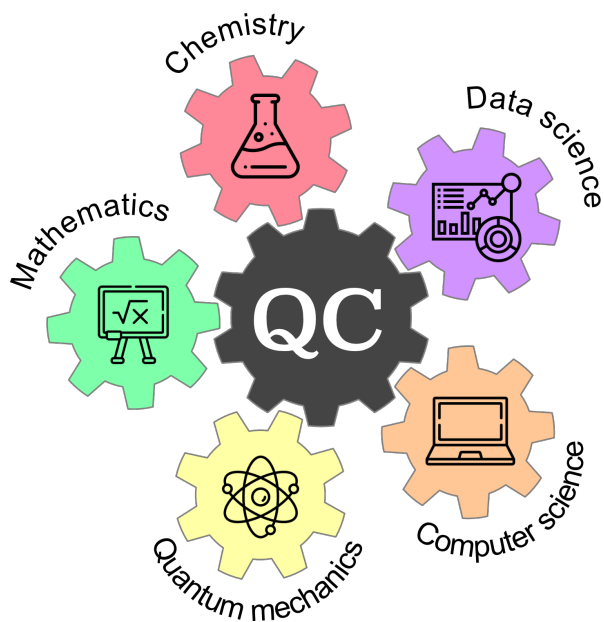
FIGURE 1: A summary of how the field of quantum chemistry is influenced by other research fields.

and improved algorithms that were too expensive to use for routine research calculations just a couple of decades ago, and allows us to some extent to move away from certain approximations and toward more exact physics in quantum chemistry. The full impact of machine learning in our field has not yet been reached, and the development of the quantum computer is still in its early stages. Both of these will undeniably affect the field of quantum chemistry. Fully quantum chemical descriptions have not yet stepped fully into the sphere of biochemistry, which could allow quantum chemistry to more directly aid in the development of new medicines, drugs, and enzymes. It is difficult to predict the future, but I think the constant feedback loop in Figure 1 will drive the development of smarter algorithms and better hardware, which will open the door to new and interesting applications.

Acknowledgements

For Heidi

List of Papers

The following scientific publications are included in this PhD thesis:

Paper I

Anders Brakestad, S. R. Jensen, P. Wind, M. D'Alessandro, L. Genovese, K. H. Hopmann, and L. Frediani. "Static Polarizabilities at the Basis Set Limit: A Benchmark of 124 Species". In: *Journal of Chemical Theory and Computation* 16.8 (2020), pp. 4874–4882. DOI: 10.1021/acs.jctc.0c00128

My Contributions Performed all calculations and data analysis, except for those used in a timing showcase. Wrote initial drafts of comp. details, results, discussion, and conclusions. Contributed to manuscript revisions. Submitted to journal.

Paper II

Anders Brakestad, P. Wind, S. R. Jensen, L. Frediani, and K. H. Hopmann. "Multiwavelets applied to metal–ligand interactions: Energies free from basis set errors". In: *Journal of Chemical Physics* 154.21 (2021), p. 214302. DOI: 10.1063/5.0046023

My Contributions Performed all calculations and data analysis, except for those used in a timing showcase. Wrote initial drafts of computational details and results sections. Contributed to manuscript revisions.

Paper III

Anders Brakestad, S. R. Jensen, K. H. Hopmann, and L. Frediani. "Scalar relativistic effects with Multiwavelets: Implementation and benchmark". *Manuscript in preparation*

My Contributions Performed prototype implementation of ZORA in the MRChem code, together with SRJ. Performed all GTO and MW calculations, performed data analysis and drafted computational details and results sections of the manuscript. Contributed to manuscript revisions. First authorship is shared between AB and SRJ.

List of Abbreviations

2c two-component. 52, 53

4c four-component. 51

5Z quintuple zeta. 29, 61

6Z sextuple zeta. 58

Ag silver. 94, 98

APW augmented plane wave. 35, 36

Ar argon. 29, 30

Au gold. 85, 87

BO Born-Oppenheimer. 11, 13, 14, 18, 51

BSIE basis set incompleteness error. 28–30, 61, 64, 78–81, 83, 94, 102

BSSE basis set superposition error. 29–32, 34, 35, 41, 79–81, 83, 102, 103

C carbon. 11, 28, 34, 81, 85

Ca calcium. 85

CBS complete basis set. 38, 57, 64, 78, 79, 83, 95, 103

CC coupled cluster. 3, 18, 58, 61

LAPW linearized augmented plane wave. 36

LCAO linear combination of atomic orbitals. 25

LDA local density approximation. 22

LR linear response. 46, 61, 62

MO molecular orbital. 15–17, 19, 20, 22–25, 27, 29, 37, 38, 40, 87, 92, 93

MRA multiresolution analysis. 3, 39, 101

MW multiwavelet. 3, 6, 38, 39, 41, 47, 61–64, 78, 81–83, 94, 97–99, 101–104

Na sodium. 85

NHC N-heterocyclic carbene. 11, 78

Ni nickel. 11, 34, 41, 81

O oxygen. 85

P Phosphorus. 85

PW plane wave. 34–37

QZ quadruple zeta. 29, 70, 72, 73, 75, 78, 79, 81, 102

Rb rubidium. 94, 97

RUD relative unsigned deviation. 58, 59, 69–75, 94, 95, 97–99

S sulfur. 75, 85

SCF self consistent field. 26, 27, 69, 92–94

CHAPTER

1

INTRODUCTION

1.1 Quantum chemistry and multiwavelets

Quantum chemistry is a rich field of research, that benefits from quantum mechanics, mathematics, chemistry, computer science, and data science. It developed naturally in the wake of the quantum revolution which took place at the end of the 1800s and the early 1900s, and became alive when the electronic computer was invented around the mid 1900s. The overarching goal of quantum chemistry is to provide the computational tools required to predict molecular and material properties, and to provide conceptual tools for rationalizing empirical observations [1]. Quantum chemistry therefore tries to provide a virtual laboratory where interesting chemistry can be explored, and where problems relevant to our society can be challenged.

One can make the claim that quantum chemistry to a certain extent has succeeded in its goal [2]. Today, we can use the tools of quantum chemistry to predict a large number of observables of interest to experimental chemists, and predict physical and chemical properties of molecules and materials that have never existed before. The reach of quantum chemistry is increasing as chemists come up with new areas

for research. New approximations, faster hardware and larger architectures further increase the number of types of problems that can be addressed by quantum chemistry.

However, the large number of tools available to the user comes with a cost. While all approximations available today together span a large space of interesting problems that can be addressed, individual approximations often span a much smaller space. Approximations, by their construction, introduce assumptions, which limits either the accuracy that can be achieved from the method or the transferability of the method, or both. A famous example of this challenge is the so-called "zoo" of density functional approximations (DFAs), in which it is not trivial for non-experts to navigate the hundreds of DFAs to choose from [3–5]. One runs into the danger that the choice of method to use is partly based on habit or popularity, and not solely on objective measures.

A similar "zoo" can be said to exist for basis sets, judging from the large number of basis sets available from the Basis Set Exchange [6, 7]. Gaussian type orbitals (GTO) basis sets are by far the most common type of basis sets in use today for molecular calculations, and a large number of them have been developed. This was acknowledged 35 years ago by Davidson and Feller [8], who noted that the choice of basis set often was made on the basis of habit. Although we have tremendously more computational resources today than what was available in the 80s, which reduces the basis set error variability since we can afford much larger basis sets, we still need to balance basis set precision and computational cost. The point made by Davidson and Feller is therefore still relevant today.

GTO basis sets are often arranged into "families" that are tailored to be used together with specific methodologies, and come in different sizes. The standard form of the basis sets is often not sufficient, and the user must decide whether to add additional polarization functions, whether to use diffuse functions, or whether to modify the default contraction

scheme for their application. Ideally one should also estimate the errors to expect from the selected basis set, and compare to the estimated errors from the other aspects of the computational protocol, but this is impossible to do *a priori*. While the expert is able to make informed decisions concerning these considerations [9], it is by no means trivial for non-experts.

Multiwavelets (MWs) have emerged as a powerful alternative to traditional GTOs [10]. Their foundation in the robust mathematics of multiresolution analysis (MRA) [11] leads to a basis set that is not empirically parametrized. Robust error control [12–14] means the user can set a finite but arbitrary target precision, and adaptive algorithms [15–17] ensure that the representations of molecular orbitals are automatically refined until the required precision is reached. The large number of available GTO basis sets reflect an underlying challenge in that no single basis set is good enough to describe all properties of interest to sufficient precision. Multiwavelets are in this sense a great step toward a black-box situation for basis sets, where just simple numerical considerations are required from the user, which makes them easy to use to non-experts. One can think of the MW basis set as being constructed to the necessary precision on-the-fly, and it should in principle be applicable for the computation of any property.

1.2 Why benchmark studies are important

Quantum chemistry is a field with a large number of methods available, that range from low accuracy (for example semi-empirical methods) to very high accuracy (large coupled cluster (CC) expansions). The main decisions a computational chemist needs to make when planning a project, is what electronic structure approximation to use and in which basis set the molecular orbitals should be expanded. Since approximations inherently come with errors, the user should ideally

make these decisions based on objective grounds that take the expected uncertainties into account.

The concept of "uncertainty" in computational chemistry is perhaps a bit different from how it is understood in experimental chemistry. When someone repeats an experimental protocol, they are essentially guaranteed to not obtain the same result twice. The protocol contains both random and systematic errors, both of which contribute to the overall uncertainty. The classical picture is that systematic errors limit the accuracy, while random errors limit the precision or repeatability. Accuracy is therefore related to the average value of multiple measurements, while precision is related to the variance of the measurements, and the various combinations of high/low accuracy/precision are often summarized as in Figure 1.1. Experimentalists therefore observe uncertainties in their data, and can visualize these using error bars.

The situation is slightly different in computational chemistry. When theoreticians perform a calculation multiple times, they are very likely to obtain identical numbers every time. A pocket calculator will always give 29.5 when asked to compute $\frac{354}{12}$, because computers do what they are instructed to do without randomness. Certain methods do rely on random number generators, such as Monte Carlo simulations, but even random numbers are not truly random since they are generated from a mathematical formula. If all random seeds were known, one should obtain identical results when repeating the calculation.

The most important error for theoreticians is therefore the systematic error. This represents deficiencies in the computational model, due to assumptions in the underlying theory. The strategy for quantifying systematic errors is essentially the same for experimental chemists and computational chemists: by comparison to an objective reference. One cannot know the error without having a reference (consider Figure 1.1 without the bull's eyes — the center of the target acts as an objective reference against which the score of each dart or arrow is measured).
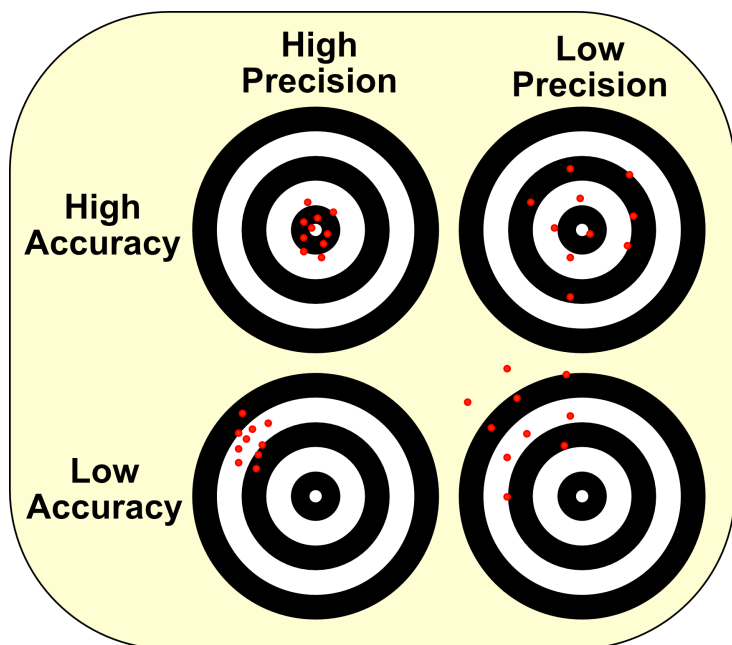
FIGURE 1.1: Visual representation of accuracy and precision. The center of the target acts as an objective reference against which the scores for each dart or arrow is measured.

Such reference values are typically obtained from different protocols that are based on different principles, and which are capable of estimating the same quantity with significantly smaller errors. For example, the accuracy of the B3LYP functional can be estimated by comparing to coupled cluster. However, the error in B3LYP is not uniform across all of chemistry. In order to get an idea of the inherent error in the B3LYP functional, we need to compare to objective references for a wide range of different chemical species. A closed-shell system built from main group atoms is likely to have a smaller error than an open-shell system that involves multiple transition metal centers.

The role of benchmark studies is to conduct these types of compar-

isons, in order to quantify the realistic uncertainty in different computational protocols. Benchmark studies are the compass which helps the user navigate in a cloudy landscape of different approximations. An important area where benchmarks are extremely helpful is in the evaluation of performance of DFAs. Two examples of such studies have been recently published [3, 18], where they ranked the performance of 100s of DFAs based on comparisons to more accurate methods. Although clear trends can be observed, a lot of commonly used functionals display similar uncertainties. A thorough computational protocol therefore repeats (some of) the calculations with multiple functionals, in order to obtain indirect validation of the results.

Benchmark studies help the community to make informed decisions based on objective metrics, and to guide new method development in fruitful directions. They help to close the gap between method developers, who often have a natural understanding of the inherent uncertainties of various electronic structure methods, and the general user community. It is vital to the integrity of science to be aware of the limitations of the obtained result, so that one does not draw conclusions that the data do not support. Data is very easy to generate in computational chemistry, and it is important to keep the pitfall above in mind, since a number does not necessarily mean insight.

1.3   Aims and organization of the thesis

The MW code MRChem can give results with finite but arbitrarily small basis set errors, and is guaranteed to converge to the complete basis set limit. The main goal of this thesis has been to use MRChem in benchmarks of basis set errors in calculations of energies and properties. In Paper I, we quantify basis set errors in static dipole polarizabilities obtained from the large GTO basis set aug-pc-4, and in Paper II, we investigate errors in a range of commonly used basis sets in calculations

of transition metal (TM)-ligand interaction energies. A secondary goal of this thesis has been to implement the zeroth order regular approximation (ZORA) into the MRChem code, and to investigate basis set errors in relativistic calculations. In Paper III (in preparation), we present a prototype implementation and show preliminary results.

The rest of this thesis is organized as follows. Chapter 2 provides an overview of the most relevant theoretical background on which our work is based. The next three chapters are dedicated to each of the three main topics of this thesis: basis set errors in static polarizabilities (Chapter 3), TM-ligand interaction energies (Chapter 4), and the implementation of scalar relativistic effects into the MRChem code (Chapter 5). Chapter 6 gives some concluding remarks and an comments on the future.

2

MOLECULAR ELECTRONIC STRUCTURE THEORY

This chapter will give a brief introduction to the key concepts in molecular electronic structure theory that underpin the work included in this thesis. I start with introducing the non-relativistic and time-independent Schrödinger equation, leading up to the basics of Hartree-Fock (HF) theory. Next, the principles of density functional theory (DFT) is outlined, which addresses the problem from a different angle. Then the concept of basis sets is introduced, and various aspects and challenges are highlighted for different types of basis sets. Finally, an overview of molecular properties and relativistic quantum chemistry is given.

2.1 Molecular quantum mechanics and Hartree-Fock theory

The fundamental equation in non-relativistic quantum chemistry is the time-independent Schrödinger equation

$$\mathcal{H}\Psi = E\Psi \qquad (2.1)$$

Here, the Hamiltonian operator $\mathcal{H}$ describes the total energy of the system, and can be decomposed into the following terms (in atomic units)

$$\mathcal{H} = \mathbf{T}^{\mathrm{N}} + \mathbf{T}^{\mathrm{e}} + \mathbf{V}^{\mathrm{NN}} + \mathbf{V}^{\mathrm{ee}} + \mathbf{V}^{\mathrm{Ne}} \tag{2.2}$$

$$= -\sum_{A=1}^{N} \frac{1}{2m_A} \nabla_A^2 \tag{2.3}$$

$$-\frac{1}{2}\sum_{i=1}^{n} \nabla_i^2$$

$$+\sum_{A=1}^{N}\sum_{B>A}^{N} \frac{Z_A Z_B}{|\vec{R}_A - \vec{R}_B|}$$

$$+\sum_{i=1}^{n}\sum_{j>i}^{n} \frac{1}{|\vec{r}_i - \vec{r}_j|}$$

$$-\sum_{A=1}^{N}\sum_{i=1}^{n} \frac{Z_A}{|\vec{R}_A - \vec{r}_i|}$$

where

$\mathbf{V}^{\mathrm{NN}}$ is the nucleus-nucleus repulsion operator
$\mathbf{V}^{\mathrm{ee}}$ is the electron-electron repulsion operator
$\mathbf{V}^{\mathrm{Ne}}$ is the nucleus-electron attraction operator
$\mathbf{T}^{\mathrm{N}}$ is the nuclei kinetic energy operator
$\mathbf{T}^{\mathrm{e}}$ is the electronic kinetic energy operator
$\{AB\}$ runs over nuclei
$\{ij\}$ runs over electrons
$\vec{R}, \vec{r}$ are the nuclear and electronic coordinates, respectively
Z is the nuclear charge
∇^2 is the Laplacian operator ($\frac{\partial^2}{\partial x} + \frac{\partial^2}{\partial y} + \frac{\partial^2}{\partial z}$)
n is the number of electrons
N is the number of nuclei

As the number of interacting particles grows, the complexity of the equations increases quickly. The potential energy of a medium sized nickel (Ni)–N-heterocyclic carbene (NHC) complex with 54 nuclei and 234 electrons is described by 1431 unique nucleus-nucleus interactions, 12 636 nucleus-electron interactions, and 27 261 unique electron-electron interactions. A visual representation of these interactions is given in Figure 2.1.

The Schrödinger equation can be solved analytically only for one- and two-particle systems, and several approximations need to be introduced in order to obtain solutions for larger systems in practice. Perhaps the most fundamental of these is the Born-Oppenheimer (BO) approximation, since it forms the basis of most routine quantum chemistry calculations today. The details can get quite involved, especially in rigorous treatments that involve the nuclear wavefunction, and the reader is referred to other works for these details [19]. However, an intuitive understanding can be gained from some simple qualitative considerations. In a hydrogen (H) atom the nucleus is about 1836 times heavier than one electron, and in a carbon (C) atom it is about 22 000 times heavier than one electron, which indicates that the timescale for the nuclear motion is much slower than the one for the electronic motion. A visual representation of this is given in Figure 2.2, as a way to gain some intuition. With this in mind, one can then consider the nuclei as stationary point charges (with zero kinetic energy), and instead solve the *electronic* Schrödinger equation for electrons moving in an electrostatic field generated by the nuclei

$$\mathcal{H}_{\mathrm{el}}(\mathbf{R})\Psi_{\mathrm{el}}(\mathbf{r};\mathbf{R}) = E_{\mathrm{el}}(\mathbf{R})\Psi_{\mathrm{el}}(\mathbf{r};\mathbf{R}) \tag{2.4}$$

where the electronic Hamiltonian operator is

$$\mathcal{H}_{\mathrm{el}} = \mathbf{V}^{\mathrm{NN}} + \mathbf{V}^{\mathrm{ee}} + \mathbf{V}^{\mathrm{Ne}} + \mathbf{T}^{\mathrm{e}} \tag{2.5}$$
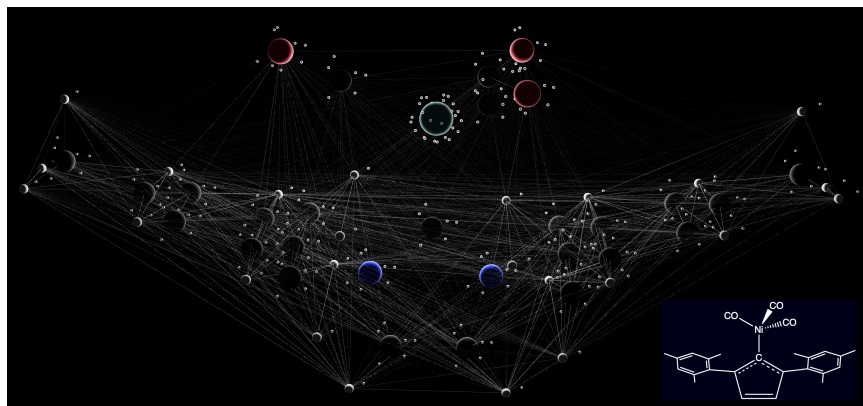
(a) Nucleus-Nucleus
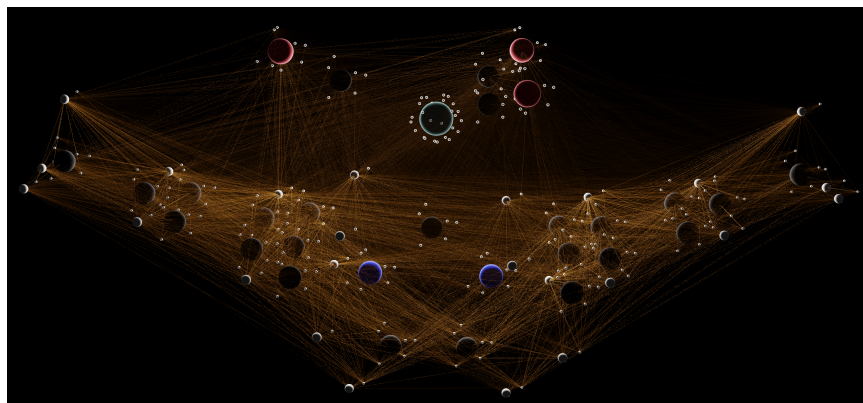
(b) Nucleus-electron
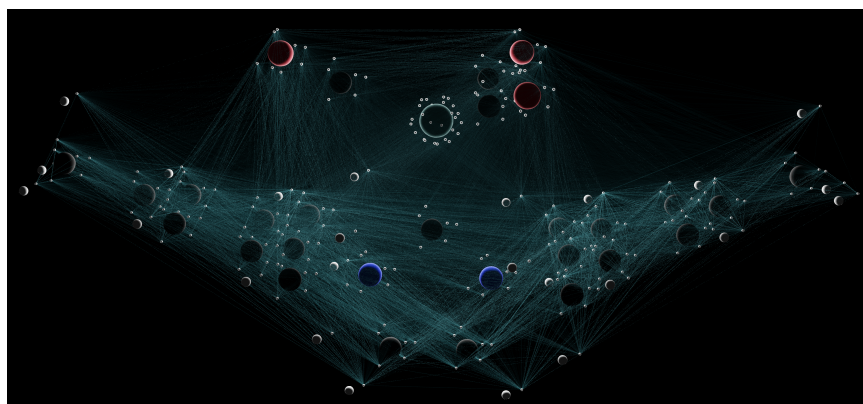
(c) electron-electron

12

FIGURE 2.1: Visual representation of the Coulomb interactions present in a TM complex (54 nuclei, 234 electrons). The inset in (a) the structure of the complex.
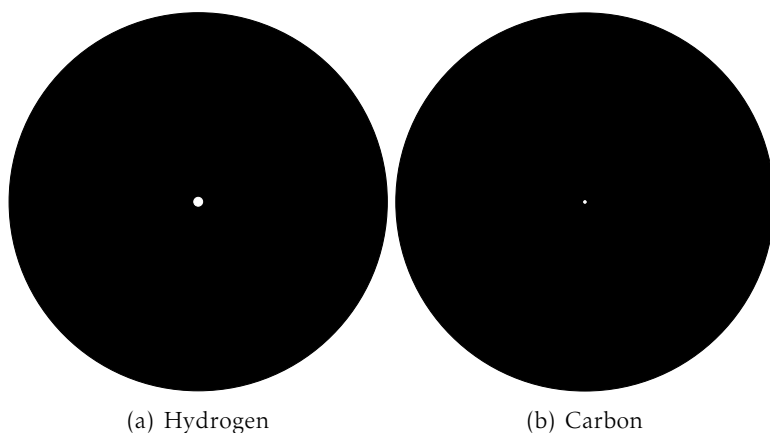
(a) Hydrogen   (b) Carbon

FIGURE 2.2: Visual representation to gain intuition of the much larger mass of a nuclei (black circle) compared to that of an electron (white circle), shown for hydrogenic (a) and carbonic (b) nuclei. Mass is here represented as area. The area of the nucleus is a factor of $\frac{r_N}{\sqrt{m_N/m_e}}$ larger than the area of the electron.

In addition to simplifying the equations, the BO approximation also simplifies the interpretation of the equations. The exact Hamiltonian operator does not depend on the nuclear coordinates, and the same Hamiltonian operator applies to all isoelectronic chemical systems with the same number and type of nuclei. In other words, the Hamiltonian operator does not depend on the atom connectivity. For example, a single Hamiltonian operator would describe all of the following systems

$$H_3C - CH_2 - OH \tag{2.6}$$

$$H_3C - O - CH_3 \tag{2.7}$$

$$H_3C - CH_3 + O \tag{2.8}$$

$$H_3C - CH + H_2O \tag{2.9}$$

$$3H_2 + C \equiv O + C \tag{2.10}$$

This means that the exact wavefunctions also would describe all of these chemical systems simultaneously, which complicates the interpretation of the particular system studied. By fixing the nuclear geometry at the beginning of the calculation via the BO approximation, we make the Hamiltonian operator unique to the molecular structure.

Up until this point we have not considered what form the (electronic) wavefunction should have. Electrons are fermions, and so one requirement is that the wavefunction must be antisymmetric with respect to the interchange of two electron coordinates. For an n-electron system, the antisymemetry requirement can be ensured by expressing the wavefunction as a linear combination of Slater determinants. In HF theory, one assumes that the electronic ground state can be described by a single Slater determinant, here written as $\boldsymbol{\Phi}$

$$\boldsymbol{\Phi}(\mathbf{x_1}, \mathbf{x_2}, \ldots, \mathbf{x_n}) = \frac{1}{\sqrt{n}} \begin{vmatrix} \phi_1(\mathbf{x}_1) & \phi_2(\mathbf{x}_1) & \ldots & \phi_n(\mathbf{x}_1) \\ \phi_1(\mathbf{x}_2) & \phi_2(\mathbf{x}_2) & \ldots & \phi_n(\mathbf{x}_2) \\ \vdots & \vdots & \ddots & \vdots \\ \phi_1(\mathbf{x}_n) & \phi_2(\mathbf{x}_n) & \ldots & \phi_n(\mathbf{x}_n) \end{vmatrix} \tag{2.11}$$

where each ϕ is a one-electron wavefunction, or spin-orbital.

For time-independent Hamiltonian operators, the energy for a trial wavefunction will always be higher than the energy for the exact wavefunction:

$$E^{\text{Trial}} \geq E^{\text{Exact}} \iff \frac{\langle \boldsymbol{\Psi}^{\text{Trial}} | \mathcal{H} | \boldsymbol{\Psi}^{\text{Trial}} \rangle}{\langle \boldsymbol{\Psi}^{\text{Trial}} | \boldsymbol{\Psi}^{\text{Trial}} \rangle} \geq \frac{\langle \boldsymbol{\Psi}^{\text{Exact}} | \mathcal{H} | \boldsymbol{\Psi}^{\text{Exact}} \rangle}{\langle \boldsymbol{\Psi}^{\text{Exact}} | \boldsymbol{\Psi}^{\text{Exact}} \rangle} \qquad (2.12)$$

with the equality holding if $E^{\text{Trial}} = E^{\text{Exact}}$. This is called the variational principle, and transforms the problem of computing the energy of a Slater determinant to a minimization problem: The set of molecular orbitals (MOs) that minimize the total energy represent the Hamiltonian eigenstates.

The starting point for obtaining an expression of the energy of a Slater determinant is the expectation value over the Hamiltonian operator (assuming a normalized wavefunction)

$$E = \langle \boldsymbol{\Phi} | \mathcal{H} | \boldsymbol{\Phi} \rangle \qquad (2.13)$$

A commonly used derivation involves introducing an antisymmetrization operator $\mathcal{A}$ that acts on a Hartree product (and produces a Slater determinant), which can be expanded into sums of permutations of increasing numbers of electron coordinates:

$$\mathcal{A} = \frac{1}{\sqrt{n!}} \left[\mathbf{1} - \sum_{ij} \mathbf{P}_{ij} - \sum_{ijk} \mathbf{P}_{ijk} - \ldots \right] \qquad (2.14)$$

According to the Slater-Condon rules, all permutations of more than two electron coordinates will vanish, since the Hamiltonian operator only contains up to a two-electron operator (electron-electron repulsion). By evaluating the permutation operator acting on the diagonal elements of the Slater determinant, one arrives at the following energy expression (expressed in terms of operator expectation values)

$$E = \sum_{i=1}^{n} \langle \phi_i | \mathbf{h}_i | \phi_i \rangle + \frac{1}{2} \sum_{ij}^{n} (\langle \phi_j | \mathbf{J}_i | \phi_j \rangle - \langle \phi_j | \mathbf{K}_i | \phi_j \rangle) + V_{\text{nuc}} \qquad (2.15)$$

where the one electron operator $\mathbf{h}_i$ (often called the core Hamiltonian) contains the electronic kinetic energy and the electron-nucleus attraction

$$\mathbf{h}_i = \frac{1}{2}\nabla_i^2 - \sum_{A=1}^{N}\frac{Z_A}{|\mathbf{R}_A - \mathbf{r}_i|} \tag{2.16}$$

and the Coulomb and exchange operators, $\mathbf{J}_i$ and $\mathbf{K}_i$, respectively, are defined as

$$\mathbf{J}_i|\phi_j(2)\rangle = \langle\phi_i(1)|\mathbf{g}_{ij}|\phi_i(1)\rangle|\phi_j(2)\rangle \tag{2.17}$$

$$\mathbf{K}_i|\phi_j(2)\rangle = \langle\phi_i(1)|\mathbf{g}_{ij}|\phi_j(1)\rangle|\phi_i(2)\rangle \tag{2.18}$$

$$\mathbf{g}_{ij} = \frac{1}{|\mathbf{r}_i - \mathbf{r}_j|} \tag{2.19}$$

$$\tag{2.20}$$

The nuclear repulsion is a constant shift of the energy, V_{nuc}, since the nuclear potential does not depend on the electronic coordinates. The $\mathbf{J}_j$ and $\mathbf{K}_j$ operators contain all the two-electron interactions, and are the so-called Coulomb and exchange operators, respectively. The former is the quantum analog to classical Coulomb interactions, and describes an increase in energy due to the repulsive forces felt by two interacting electrons. The latter, on the other hand, does not have a classical analog, and describes a *lowering* of the energy that originates from the antisymmetry requirement for the wavefunction.

Now that one has an expression for the energy associated with the Slater determinant wavefunction, one can attempt to find the set of MOs that makes the energy stationary with respect to variations in the MOs. The variational principle briefly introduced above transforms this into a minimization problem, where one is interested in finding the MOs that minimize the energy. The requirement that the MOs should remain orthonormal during the minimization naturally leads to the

use of Lagrangian multipliers in order to carry out such a constrained minimization. The details of this procedure will not be covered here; however, it will be noted that the idea of the Fock operator $\mathcal{F}$ emerges from the derivations (here in a restricted HF notation):

$$\mathcal{F}_i = \mathbf{h}_i + \sum_j^{n/2} (\mathbf{J}_j - \mathbf{K}_j) \tag{2.21}$$

The matrix representation of the Fock operator can be diagonalized to contain the optimized set of Lagrange multipliers on its diagonal, and these diagonal elements can be interpreted as the MO energies. The final result is the so-called HF equations, which can be expressed as

$$\mathcal{F}_i |\phi_i\rangle = \epsilon_i |\phi_i\rangle \, ; \epsilon_i = \langle \phi_i | \mathcal{F}_i | \phi_i \rangle \tag{2.22}$$

and the total energy in terms of MO energies becomes

$$E = \sum_i^n \epsilon_i - \frac{1}{2} \sum_{ij}^n (J_{ij} - K_{ij}) + V_{\text{nuc}} \tag{2.23}$$

The total energy does not equal the sum of the orbital energies, since these include a double counting of the repulsive two-electron interactions, and Equation (2.23) shows that the orbital energies are corrected by subtracting a portion of the Coulomb and exchange contributions. Further, the HF equations must be solved in an iterative manner, since both $\mathbf{J}$ and $\mathbf{K}$ depend on the optimized set of MOs.

HF theory is a so-called mean-field theory. This is because the two-electron integrals are computed such that each electron only interacts with the average electrostatic field generated by the other electrons. In other words, the instantaneous repulsion to all other electrons is only considered in an average fashion. The HF approximation provides a reasonable and qualitatively correct wavefunction, but its lack of explicit electron correlation makes it in general not good enough to

study molecular systems to sufficient accuracy to be used in predictions of chemical properties and reactivity. However, it is often used as the starting point of more accurate wavefunction methods (so-called post HF methods or correlated methods) that attempt to recover the explicit electron correlation, such as the CC and configuration interaction (CI) methods. These methods are outside the scope of this thesis, and will not be discussed.

2.2 Density functional theory

The wavefunction $\Psi(\mathbf{r})$ is a highly complex, $3n$ dimensional function. The electron density ρ, on the other hand, is a much simpler 3 dimensional function, is defined as

$$\rho(r_1) = N \int \Psi^*(r_1 \ldots r_N)\Psi(r_1 \ldots r_N)\mathrm{d}r_2 \ldots \mathrm{d}r_N \qquad (2.24)$$

Hohenberg and Kohn proved in 1964 [20] that the electron density uniquely defines the ground state energy, and therefore also the Hamiltonian operator: i) The electron density will have cusps at the nuclear positions, and hence the position of the nuclei can be determined; ii) The integral of the density over all space defines the number of electrons; and iii) The slope near nuclear cusps defines the nuclear charge.

The ground state energy is according to the Hohenberg-Kohn theorem a functional of the electron density:

$$E[\rho](\mathbf{r}) = T[\rho] + V_{\mathrm{Ne}}[\rho] + V_{\mathrm{ee}}[\rho] + V_{\mathrm{NN}} \qquad (2.25)$$

Within the BO approximation, the nuclear repulsion energy is just a constant shift in the total energy (as it does not depend on the electron density), and the nucleus-electron attraction term is expressed as

$$V_{Ne}[\rho] = -\sum_{A=1}^{N}\left[\int \rho(\mathbf{r})\frac{Z_A}{|\mathbf{r} - \mathbf{R}_A|}\right] \qquad (2.26)$$

The electron repulsion and kinetic energy contributions are not known exactly. Early attempts at finding approximate expressions go back to the 1920s and the so-called Thomas-Fermi model [21, 22]; however, this model turned out to predict all molecules to be unstable compared to their individual constituents, and therefore had no practical use in chemistry.[†] The philosophy in modern DFT is to decompose density functionals that are not known exactly into two parts: i) one part that one knows must contribute, and ii) the "remainder", which accounts for all that which is missing in the first part. In this spirit, the electron-electron repulsion term is split into Coulomb and exchange contributions (implicitly including all electron correlation):

$$V_{ee} = J[\rho] + K[\rho] \tag{2.27}$$

The Coulomb term is given exactly by the classical expression

$$J[\rho] = \frac{1}{2} \int \int \frac{\rho(\mathbf{r})\rho(\mathbf{r}')}{|\mathbf{r} - \mathbf{r}'|} \tag{2.28}$$

Efforts into developing accurate expressions for the kinetic and exchange energy contributions are ongoing, often referred to as "orbital-free density functional theory", but by far the most common formulation of density functional theory (DFT) today is the so-called KS formulation [23].

Kohn and Sham set out to find approximate ways to compute the kinetic and exchange contributions by reintroducing MOs into the theory, and in this way gave up on the benefit of the much lower dimensionality of the electron density compared to the wavefunction. Their motivation for doing this can be understood by recalling that a single Slater determinant is an exact ansatz for a wavefunction of non-interacting electrons, and the exact kinetic energy for such a system is expressed as expectation values over the kinetic energy operator:

[†]The later Thomas-Fermi-Dirac model did predict stable molecules, but was still not accurate enough for practical use.

$$\mathbf{T}_i^{\mathrm{HF}} = -\frac{1}{2} \langle \phi_i | \nabla^2 | \phi_i \rangle \tag{2.29}$$

Briefly, the clever idea in KS-DFT is to introduce a fictitious potential in the Hamiltonian for non-interacting electrons, but under the assumption that this potential reproduces the exact ground state density. The mantra is therefore, "if you can't solve it exactly, start from a simpler problem and extract from it as much as possible". The full electron-electron contribution in Equation (2.25) is not known, but at least we can factor out the Coulomb part and be left with a remainder. Similarly, the kinetic energy in Equation (2.29) is not exact, but it recovers most of the kinetic energy of the system, leaving out only a remainder. We are then left with the following sum of density functionals, with tilde indicating that they are exact for non-interacting electrons, and dagger indicating that they are unknown remainders

$$E[\rho](\mathbf{r}) = \tilde{T}[\rho] + V_{\mathrm{Ne}}[\rho] + J[\rho] + V_{\mathrm{NN}} + T^{\dagger}[\rho] + K^{\dagger}[\rho] \tag{2.30}$$

The kinetic energy and exchange remainders are usually collected into a single functional, called the exchange-correlation functional, and this represents the only missing term in obtaining an exact electron density. It contains all the deficiencies that the other terms introduce: it corrects for the incorrect expression of the kinetic energy, and it describes all explicit electron-electron correlation effects (the Coulomb correlation is, as in HF theory, a mean-field expression).

The set of optimum (KS) MOs is found in a similar manner as in HF theory by doing a constrained minimization with Lagrangian multipliers. The KS equations come out as

$$\mathcal{F}\phi_i = \epsilon_i \phi_i \tag{2.31}$$

$$\left(-\frac{1}{2}\nabla^2 + \left[\int \frac{\rho(\mathbf{r}')}{|\mathbf{r} - \mathbf{r}'|} + V_{xc} - \sum_{A=1}^{N} \frac{Z_A}{|\mathbf{r} - \mathbf{R}_A|}\right]\right)\phi_i \tag{2.32}$$

$$= \left(-\frac{1}{2}\nabla^2 + V_{\text{eff}}\right)\phi_i = \epsilon_i \phi_i$$

This must be solved in an iterative manner, due to the ρ-dependence in the Coulomb and exchange-correlation operators.

A lot of research has gone into various approximations to the exchange-correlation functional V_{xc}, and there are today hundreds of possible choices. Traditionally, two main strategies are used in the design and construction of new DFAs. One can study the mathematical properties of the exact density and deduce properties that the exact functional should have. Then one comes up with mathematical expressions that fulfill as many as these properties while at the same time are able to capture relevant physics. A common example of functionals developed in this manner is PBE [24]. Alternatively, one can come up with functional forms that contain undetermined parameters, which are fitted to experimental data or highly accurate *ab initio* calculations. Mathematically robust functionals are often said to be general, in the sense that they deliver predictable accuracy across a large range of different applications. Parametrized functionals, on the other hand, are biased toward the training data set. They can therefore deliver higher accuracy for systems and properties that resemble those included in the training set, but suffer when they are used outside of their comfort zone. Examples of highly parametrized functionals are found in the Minnesota class of functionals [25]. In practice, though, a combination of both strategies is often used, where reasonable mathematical robustness is combined with a small number of fitted parameters. The very popular functional B3LYP [26–28], for example, contains three parameters that have been fitted to empirical data.

It is not straightforward to come up with a procedure for systematically approaching the exact functional. However. there exists different levels of approximations that have been developed over the years. This classification is referred to as "Jacob's Ladder", a reference to the Old Testament and Abraham's son Jacob who dreamt about a ladder leading to Heaven. In the context of quantum chemistry, the ladder to heaven signifies the path toward the exact exchange correlation functional. The ladder is usually divided into five rungs: i) local density approximation (LDA), which evaluates the density at a single point in space, ii) generalized gradient approximation (GGA), which also takes the gradient of the density into account, iii) meta-GGA, which either uses the Laplacian of the gradient or the orbital kinetic energy density, iv) hybrid GGA and hybrid meta-GGA, which includes a fraction of exact HF exchange, and v) the random phase approximation and double-hybrids, in which not only occupied orbitals are considered, but also unoccupied orbitals. The validity of Jacob's Ladder is supported in large-scale benchmark studies where hundreds of density functionals are compared to coupled cluster calculations over a wide range of different chemical systems and different chemical properties [3, 18].

2.3   Basis sets

The HF and DFT theories outlined above are given in the so-called MO basis; the quantities that we solve for are the MOs. In principle, one can attempt to map these functions onto a uniform and 3-dimensional grid; however, this approach is associated with a few challenges, some of which are so severe that they strongly limit their practical uses. The main challenge is that in order to represent MOs well close to the nuclei, very fine grids are necessary. This comes with the cost of very expensive numerical routines routines and large memory footprints, which limits such approaches to small systems.

Another approach is to expand the MOs in a basis of simpler functions.

$$\phi(\mathbf{r}) = \sum_{i=1}^{\infty} c_i \chi_i(\mathbf{r}) \approx \sum_{i=1}^{N} c_i \chi_i(\mathbf{r}) \qquad (2.33)$$

This expansion is exact in the limit of an infinite number of basis functions, and any type of function can in principle be used, be it exponential functions, Gaussian functions, periodic functions, polynomial functions, or even combinations of these. However, in practice we must rely on basis set truncation in order to discretize the problem, and this introduces an error associated with the basis set used. Although any linear combination of functions can be used, there are some characteristics that make the basis computationally attractive, which are enumerated by the SAUCE principles [29]:

S The basis set construction should be parametrized in such a way that it can be **S**ystematically tuned to increase its completeness

A The basis functions should **A**ccurately reproduce the physics of the target function to facilitate rapid convergence

U The basis set should be **U**niversal in the sense that it should not be biased toward any chemical system

C The basis set should be **C**ompact, so that any given precision can be obtained with as few basis functions as possible

E The mathematical operations should be **E**fficiently evaluated in a computer code

Slater- and Gaussian type orbitals

The functional forms Slater type orbitalss (STOs) Equation (2.34) and GTOs Equation (2.35) are motivated by the analytical wavefunction for a

H atom, and consists of a normalization factor N, a spherical harmonics part Y and a radial part (in spherical coordinates):

$$\chi_{\zeta,n,l,m}(r,\theta,\phi) = N\,Y_{l,m}(\theta,\phi)r^{n-1}e^{-\zeta r} \tag{2.34}$$

$$\chi_{\zeta,n,l,m}(r,\theta,\phi) = N\,Y_{l,m}(\theta,\phi)r^{2n-2-l}e^{-\zeta r^2} \tag{2.35}$$

where n, l, m are quantum numbers, and r is the radial dependence. The radial part of an STO is exponential in r and cusps at the position of the nuclei, which agrees well with the nature of a molecular orbital. For this reason, relatively few Slater type functions are necessary to give a proper representation of an MO, both in terms of the nuclear cusp requirement and the exponential decay of the wavefunction. GTOs, on the other hand, contain an r^2 dependence, which eliminates the nuclear cusp and leads to a too rapid decay.

GTOs are still the most commonly used type of basis sets today, despite the inherently poorer description of a molecular orbital compared to STOs. The reason for their widespread use lies in their computational efficiency, due to the fact that the product of two Gaussian functions centered at two different nuclei is itself a Gaussian centered in the middle of the two original nuclei. A similar property does not hold for Slater type functions. This means that for GTOs a four-center integral is reduced to a two-center integral, which reduces the computational cost considerably. Due to much less frequent use of STOs in modern quantum chemistry software [‡], they will not be considered further here.

As mentioned above, a single GTO cannot correctly describe an orbital very close to or very far from a nucleus (due to the r^2 dependence). However, these shortcomings can to some extent be alleviated by forming linear combinations of "primitive" Gaussian functions, although the correct cusp behavior can never be fully recovered. Such linear combi-

---

[‡]The ADF quantum chemistry software [30] is perhaps the most well known and modern implementation of STOs

nations increase the computational cost associated with the basis set, but this is easily compensated for by the much more efficient evaluation of Gaussian integrals compared to Slater integrals.

The motivation for using atomic centered basis functions that are inspired from the analytical solution to the H atom, lies in the assumption that atoms in molecules retain much of their free-atom characteristics. Linear combinations of localized hydrogenic wavefunctions, or "atomic orbitals", should therefore be a reasonable approximation to the delocalized molecular orbitals. This is the origin of the so-called linear combination of atomic orbitals (LCAO) approach for constructing MOs. The basis set expansion transforms the HF and DFT equations from integrals over MOs to integrals over basis functions. The computed ground state orbitals are then defined by the optimized basis set coefficients.

GTO basis set temperament and contraction   The functional form of a GTO (Equation (2.35)) contains an exponent ζ in the radial part of the expression, and this must be determined for all primitive GTOs in the basis set. One could attempt an explicit optimization of all coefficients, but for large basis sets this becomes a highly multi-dimensional and non-linear optimization problem, with a large number of local minima in a flat parameter space. However, such optimized exponents have been studied extensively, and regular trends in the way these exponents behave for different types of orbitals (s, p, f, etc) have been found. These trends offer a way to greatly reduce the variational problem of optimizing basis set exponents, and today two main types of GTO basis sets are common: even-tempered basis sets and well-tempered basis sets. In even-tempered basis sets, one exploits that the ratio between two successive exponents is almost constant, so that all M exponents can be generated by a function that depends on just two parameters:

$$\zeta_i = \alpha\beta^i; i = 1, 2, \ldots, M \tag{2.36}$$

The parameters α and β are then optimized for a given nuclear charge and orbital type (s, p, d, etc).

Well-tempered basis sets also exploit the observation of constant-ratio exponents, but have four parameters to be optimized

$$\zeta_i = \alpha\beta^i\left(1 + \gamma\left(\frac{i}{M}^\delta\right)\right); i = 1, 2, \dots, M \qquad (2.37)$$

While the parameter space is larger, the parameters only need to be optimized once for each atom type, since all angular momenta share the same exponents and so different primitive GTO types (s, p, d, etc) will be described by the same radial part. Since the flexibility in well-tempered basis sets is larger than in even-tempered ones, the basis set precision is larger given the same number of basis functions. Both strategies allow for a much simplified procedure for generating basis function exponents, compared to the full variational optimization, regardless of basis set size.

Another important concept in the context of GTO basis sets is basis set contraction. A large number of Gaussian functions is necessary to obtain a precise description of a molecular orbital, and so the determination of the basis function coefficients (which is to be performed during the self consistent field (SCF)) quickly becomes expensive as the basis set grows. The computational cost grows with the number of basis functions M as M^4, and so it is desirable to keep the variational problem as small as possible. Further, energy-optimized basis set exponents are biased toward a precise description of the high-energy, but chemically uninteresting, core region. Molecular bonding takes place with valence electrons, and several properties require precise descriptions of diffuse valence electrons (for example polarizabilities and Rydberg states).

Basis set contraction is the procedure of constructing the full basis set as multiple linear combinations of sub sets of the primititve Gaussians. A qualitative argument for introducing contractions, is the

realization that the core electron distribution changes little upon molecular bonding, and by extension the basis function coefficients describing these electrons change little. One can therefore reduce the variational SCF problem by expanding the MOs in a set of fixed linear combinations of basis functions

$$\chi^{\mathrm{CGTO}} = \sum_i c_{i\alpha} \chi_i^{\mathrm{PGTO}} \qquad (2.38)$$

The primitive Gaussian coefficients are fixed for all basis functions included in a contracted basis function, and the contracted basis function coefficients are determined variationally. The number of contracted basis functions used to describe the valence region corresponds to the widely used "zeta classification" for organizing and comparing basis sets of similar size.

Two main contraction schemes exist: segmented and general contraction. Segmented contraction involves putting the restriction that a single primitive Gaussian function can only enter a single contracted function; the contracted orbital spaces therefore form disjoint sets, as no primitive Gaussians are shared among the contracted spaces. In general contraction, no such restriction is put on the construction of the contracted orbital spaces. All primitive Gaussian functions enter all contracted functions, but with different coefficients. It should be noted that most basis sets used today are not constructed purely by segmented or general contraction, but with a combination of the two.

Polarization and diffuse functions As noted above, energy-optimized basis sets are inherently biased toward the core region, since the magnitude of the energy is much larger for these orbitals compared to valence orbitals. However, most chemistry involves changes in the valence electron distribution, and the core region changes relatively little. In addition, the electron density in covalent bonds is only approxi-

mately described by atomic orbitals with the same angular momentum as the valence electrons. For example, a H s-orbital involved in bonding will not be spherically symmetric, but distorted: it becomes polarized. Therefore, the "bare" basis set will need some *ad hoc* augmentation to overcome these challenges.

Polarization functions are basis functions of higher angular momentum that are added to the basis set (higher compared to the atom's valence electrons). For example, the basis set for a C atom (valence electrons occupy p orbitals) is polarized by the addition of d-type functions. In mean field theories such as HF and DFT, where explicit electron correlation is neglected, it is usually sufficient to add a single set of polarization functions to each atom, but in correlated methods larger polarization sets are needed. Some basis sets also contain polarization functions for the core electrons, which can be necessary in calculations of properties where an accurate description of core orbitals is important.

Diffuse functions are basis functions with small exponents, normally of s or p type, and provide more flexibility in the basis set to better describe the tail region of molecular orbitals. Typically, this becomes important for energy calculations of negatively charged species (which has a more diffuse electron density), or for property calculations where the wavefunction tail is important (for example for polarizabilities). Although standard basis sets exists with polarization and diffuse functions added, it is still up to the user to correctly select a basis set that is able to describe the physics taking place in the system under investigation.

GTO basis set errors   In theory, basis set expansions are exact, but in practical calculations we must truncate the expansion and this introduces a basis set error. This is called the basis set truncation problem, and comes with several consequences that affect how computational chemists design and perform calculations. Two different, but not completely independent, errors will be discussed in this section: basis set

incompleteness errors (BSIEs) and basis set superposition errors (BSSEs). The first describes the mathematical error we introduce by truncating the basis set, and the second is a consequence of basis set truncation when using atom-centered basis functions.

BSIEs are always present, as one cannot use an infinite expansion in practice. However, by using large basis sets the error can in most cases be made sufficiently small so as not to have a significant effect on the computed property. This becomes challenging for large chemical systems, due to the high computational cost associated with quadruple zeta (QZ) or quintuple zeta (5Z) basis sets, and one must always balance the desired precision against the computational cost.

BSSEs are conceptually different, and arise in GTO basis sets for two reasons: i) the basis set is not complete, and ii) the basis functions are centered on the nuclei. The error is related to the fact that basis functions provide mathematical flexibility to all MOs regardless of which nuclei they are centered on. Consider a simple reaction of two argon (Ar) atoms forming a dimer. When the two atoms are infinitely far apart, there will be zero overlap between the basis functions centered on each Ar atom. As the atoms approach each other their basis functions start to overlap, and the total wavefunction is effectively being described by twice as many basis functions than what it was when atoms were infinitely far apart (although many basis functions may contribute very little to the overall description). As one computes the reaction, essentially two systems computed with different basis sets are compared. This basis set inconsistency when computing relative energies is referred to as BSSE, and it is something to always keep in mind when studying chemical reactivity and thermodynamics. BSSEs are the reason why finite GTO basis sets tend to be biased toward molecule formation compared to the individual fragments, and it is often stated in the literature that BSSEs lead to an overstabilization of the molecular complex. In the limit of a complete basis, the total wavefunction cannot improve by

using more basis functions, and so BSSEs vanish in this limit.

It is common to distinguish between so-called intermolecular BSSE and intramolecular BSSE. The term intermolecular BSSE is used when one is studying processes where one atomic or molecular fragment binds to or interacts with another. The Ar dimer case given above is an example of where intermolecular BSSEs appear. The term intramolecular BSSE, on the other hand, is used when studying processes where no chemical transformation takes place, for example conformational changes in a molecule or in relative stability comparisons. For example, consider a study where one wants to look at the basis set effect on the relative stability of ethanol compared to dimethyl ether [31]. Table 2.1 presents the individual ethanol and dimethyl ether energies, as well as the relative energy $E^{\text{Ethanol}} - E^{\text{Dimethylether}}$. The progression through the basis set series leads to different energies, although they seem to be converging. The "basis set effect" is what leads to these different energies, and it is a combination of both BSIEs and intramolecular BSSEs (and not BSIEs alone, which might be the most intuitive conclusion). This becomes clearer by realizing that the basis sets used in ethanol and dimethyl ether are actually slightly different (despite being called with identical names in the input file), since the positions of the nuclei are not the same, and therefore the micro-environment surrounding each nucleus is not the same. Intramolecular BSSEs will be more important in the molecular regions that differ the most, and will likely cancel in very similar regions. Ultimately, both intramolecular and intermolecular BSSEs share the same origin: the basis functions are centered on the nuclei and the basis set is incomplete.

Another interesting observation from Table 2.1 is that the number of converged digits in the total energies is lower than in the relative energies. This suggests that there is some cancellation of error going on in the subtraction. This is indeed the case for GTO basis sets, and is the reason why one can get fairly precise relative energies from rather

TABLE 2.1: Total energies for ethanol and dimethyl ether computed with the PBE functional and a series of Jensen's polarization consistent basis sets, ranging from single-zeta to pentuple zeta. The last column shows the relative stability of ethanol compared to dimethyl ether. The reference energies are computed with a multiwavelet basis using a precision of 1.0×10^{-6}. All energies are given in Hartrees.

Basis	Ethanol	Dimethyl Ether	ΔE
pc-0	-154.4009454549	-154.3905838028	-0.0103616521
pc-1	-154.8139631377	-154.7983217885	-0.0156413492
pc-2	-154.9135549488	-154.8952010119	-0.0183539369
pc-3	-154.9217016623	-154.9033219450	-0.0183797173
pc-4	-154.9223673965	-154.9039790822	-0.0183883143
MW6	-154.9224148223	-154.9040269783	-0.0183878440

imprecise total energies. However, it is impossible to know *a priori* precisely how such cancellations behave for a large set of chemical systems.

Intermolecular BSSEs come with additional, methodological consequences for the computational chemist. They directly affect computed relative energies, for example reaction energies or reaction barrier heights, and it is desirable to correct for this if possible. The most popular method for reducing or eliminating BSSEs is called the counterpoise (CP) correction, originally developed by Boys and Bernardi [32]. Assuming a purely rigid addition reaction, *i.e.*, the geometry of A and B does not change when forming the adduct, consider the following reaction

$$A + B \longrightarrow A-B \tag{2.39}$$

It has the following reaction energy

$$\Delta E = E_{AB}^{AB} - E_A^A - E_B^B \qquad (2.40)$$

where subscripts indicate the basis set used and the superscripts indicate the molecular fragment. The adduct A−B will be described by a larger basis set than its separated constituents A and B, and the reaction energy is therefore computed from single-point calculations effectively using slightly different basis sets. One can do a quasi-derivation of the CP correction [33] by assuming that the BSSEs originate due to the basis set inconsistencies just described. First, the correct reaction energy (without any BSSEs) will be one where the basis set descriptions are identical (using the same notation as in Equation (2.40))

$$\Delta E^{CP} = E_{AB}^{AB} - E_{AB}^A - E_{AB}^B \qquad (2.41)$$

The BSSE is then the difference between Equation (2.40) and Equation (2.41)

$$
\begin{aligned}
\text{BSSE} =& \Delta E - \Delta E^{CP} & (2.42)\\
=& E_{AB}^{AB} - E_A^A - E_B^B & (2.43)\\
& - E_{AB}^{AB} + E_{AB}^A + E_{AB}^B \\
=& (E_{AB}^A - E_A^A) + (E_{AB}^B - E_B^B) & (2.44)
\end{aligned}
$$

which is the usual way to present the CP correction. The CP-corrected reaction energy is then obtained by rearranging Equation (2.42)

$$\Delta E^{CP} = \Delta E - \text{BSSE} \qquad (2.45)$$

Equation (2.44) demands that the energy of fragments A and B should be computed in the basis set used for the adduct A−B. The way this is done in practice, is to introduce the "missing" basis functions from the adduct into the fragment calculations. These basis functions

are centered at so-called "ghost atoms" with zero charge, which serve as a means to smuggle the missing basis functions into the computational domain without modifying the Hamiltonian operator.

Recall that we here assumed a completely rigid addition reaction. In reality the geometry of the fragments will change as they start to interact, which means that the geometry of the isolated fragments will not be the same as their geometry when part of the adduct. The CP correction terms in Equation (2.44) are in practice computed for each fragment at the geometry that the fragment has in the adduct. Often one sees the correction in a slightly modified notation, where the origin of the particular geometry used is indicated in parenthesis

$$\Delta E^{CP} = E_{AB}^{AB}(AB) - E_A^A(A) - E_B^B(B) \tag{2.46}$$
$$- (E_{AB}^A(AB) - E_A^A(AB)) - (E_{AB}^B(AB) - E_B^B(AB))$$
$$= \left(E_{AB}^{AB}(AB) - E_{AB}^A(AB) - (E_{AB}^B(AB) \right) \tag{2.47}$$
$$- \left(E_A^A(A) - E_A^A(AB) \right)$$
$$- \left(E_B^B(B) - E_B^B(AB) \right)$$

where four four additional terms appear compared to Equation (2.41), since the E_X^X terms no longer cancel. This notation facilitates another interpretation by noting that the first three terms of Equation (2.47) are the rigid reaction energy in the CP basis, and the remaining terms represent non-rigidity corrections in the "original" basis for each fragment. To compute a CP-corrected reaction energy in accordance with Equation (2.47) increases the computational cost by roughly a factor of two or three, owing to the four extra single-point calculations (which uses a larger basis set than used in Equation (2.40)).

The CP correction can readily be applied for simple addition reactions such as Equation (2.39), where each fragment can be uniquely identified. It is trickier for reactions where some chemical transforma-

tion takes place, such that the individual fragments no longer can be identified in the adduct. For example, consider a reaction where CO_2 is inserted into a Ni-C bond.

$$
L-Ni-CH_3 + CO_2 \quad \longrightarrow \quad
\begin{array}{c}
O \\ \diagdown \\
C-CH_3 \\ \diagup \\
L-Ni-O
\end{array}
\tag{2.48}
$$
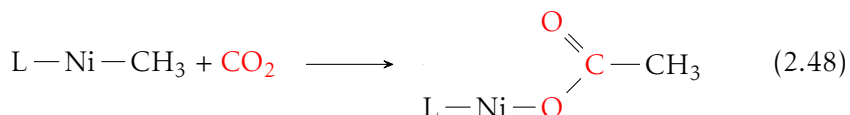
The original fragments are no longer present in the product, and so the partitioning into fragments for the CP procedure is not straightforward. For this reason many computational protocols omit the CP correction at the cost of extra BSSEs, in order to keep the protocol simple and not introduce arbitrary corrections the rigor of which is not clear.

Other types of basis sets

While GTOs are by far the most common type of basis sets used in computational chemistry, other types also are worth mentioning. Most notably among these are perhaps plane waves (PWs), real-space numerical methods, and effective core potentialss (ECPs). A short overview of the main principles will be given here.

PW basis functions $\phi(x)$ have the following functional form

$$
\phi(x) = e^{i\mathbf{k}\cdot\mathbf{r}}
\tag{2.49}
$$

As can be seen, they are complex periodic functions, and hence span an infinite space. Valence electrons in metallic materials behave much like free electrons, and so the use of PWs is a reasonable way to describe these electrons. PWs are also suited for extended, three-dimensional systems due to their non-locality, since the number of basis functions required depends on the size of the unit cell, and not on the number of electrons inside the unit cell, but can also be used to study molecular systems.

One challenge for PWs is that core electrons require very rapidly oscillating functions (high $\mathbf{k}$ values) in order to describe the electron density close to the nuclei, and the nuclear cusp is therefore almost impossible to describe sufficiently. Therefore a very large number of basis functions are needed to get decent precision in the computed energies, which limits the sizes of chemical systems within computational reach.

However, a PW description comes with some benefits. There is no parametrization required to construct a plane wave basis: The Bloch theorem defines $\mathbf{k}$ as a good quantum number, and the permissible values for $\mathbf{k}$ are given by the unit cell translational vector. In practice one then just needs to define the highest value of $\mathbf{k}$ that should be included in the basis set, since this uniquely defines the PW basis. The simplicity of construction leads to relatively effortless implementation in codes, and they are easy to use from a user-perspective. Since PWs are not centered on the nuclei, but rather extend over the entire computational domain, the source of BSSEs is eliminated. Reaction energies, or relative energies in general, can therefore be computed without the risk of contaminating the results with BSSEs.

There are efforts into alleviating the issues related to describing the nuclear cusps, such as various flavors of the augmented plane wave (APW) methods and pseudopotentials. The common theme here is to accept that PWs alone cannot describe core electrons satisfactorily, and instead use different types of functions to describe the challenging regions. As mentioned above, PW basis sets are most commonly used in the context of computational material science, where the systems of interest are infinitely extended, periodic crystals. The translational symmetry of periodic systems means that the crystal structure is uniquely defined by a unit cell.

In the original APW method [34, 35], the unit cell is partitioned into two different regions: non-overlapping, atom-centered spherical regions (S), and the remaining interstitial regions (I). Spherical regions

are described by solutions to the radial Schrödinger equation, and the interstitial regions are described by PWs:

$$\phi(\mathbf{r}) = \begin{cases} \Omega^{-1/2} \sum_{\mathbf{g}} c_{\mathbf{g}} e^{i(\mathbf{g}+\mathbf{k}) \cdot \mathbf{r}} & \mathbf{r} \in I \\ \sum_{lm} A_{lm} U_l(\mathbf{r}) Y_{lm}(\mathbf{r}) & \mathbf{r} \in S \end{cases} \tag{2.50}$$

Here, Ω is the cell volume, $c_{\mathbf{g}}$ and A_{lm} are expansion coefficients, Y are spherical harmonics, and U_l are solutions to the radial Schrödinger equation

$$\left[-\frac{d^2}{d\mathbf{r}^2} + \frac{l(l+1)}{r^2} + V(\mathbf{r}) - E_l \right] \mathbf{r} U_l(\mathbf{r}) = 0 \tag{2.51}$$

A later extension of the APW method is the linearized augmented plane wave (LAPW) method [36–40], which improves the overall description by expanding the spherical regions in functions that depend on both U and its derivative $\dot{U}$

$$\phi(\mathbf{r}) = \begin{cases} \Omega^{-1/2} \sum_{\mathbf{g}} c_{\mathbf{g}} e^{i(\mathbf{g}+\mathbf{k}) \cdot \mathbf{r}} & \mathbf{r} \in I \\ \sum_{lm} \left[A_{lm} U_l(\mathbf{r}) + B_{lm} \dot{U}(\mathbf{r}) \right] Y_{lm}(\mathbf{r}) & \mathbf{r} \in S \end{cases} \tag{2.52}$$

Close to an atomic nucleus the potential and wavefunction are strongly varying, but nearly spherically symmetric, and serves as the physical justification for this type of partitioning. The partitioning described above is sometimes referred to as the "muffin tin approximation": the muffin moulds and the connecting structure correspond to the atom-centered spheres and the interstitial regions, respectively. Care is taken to ensure that the wavefunction ϕ is continuous at the sphere boundary, since otherwise the kinetic energy is not well-defined. Many flavors of the (L)APW method are described in the literature, where the augmentation basis is constructed based on different criteria. It is beyond the scope of this thesis to give an account of these flavors, but an overview can be found in Singh and Nordström [41].

The ECP approach does not expand the core regions in basis functions, but replaces the explicit core electrons by parametrized, analytical functions that aim to reproduce the core potentials. They are therefore not strictly basis functions. These potentials are often referred to as pseudopotentials in the physics or computational material science community, but are more commonly called ECPs in the quantum chemistry community. Regardless of the terminology used, the purpose of the strategy is the same: avoid having to explicitly describe the challenging atomic core region of the wavefunction. In quantum chemistry, ECPs are usually combined with Gaussian basis functions used to describe the valence electrons. Additional benefits include a smaller computational cost, especially for the heavier atoms where the number of core electrons gets large. The parameters in an ECP are often fitted to calculations performed with relativistic quantum chemistry methods, and in this way allows for indirect relativistic corrections in an otherwise non-relativistic calculation.

Numerical methods attack the problem of how to compute MOs from a different angle. The Hamiltonian operator must be discretized in some manner; with GTOs and PWs the MOs are expanded in a finite linear combination of analytical functions. Numerical methods discretize the problem differently. For example, numerical atomic orbitals are similar to the GTO expansion, but the MOs are instead expanded in numerical basis functions obtained from solving Schrödinger-like radial equations [42]. Alternatively, the MOs themselves can be represented as functions on real-spaced grids, with all integrals and derivatives computed numerically via finite elements. Such an approach has the potential of yielding energies and properties to an arbitrary precision, provided a sufficiently dense grid over which the operators are evaluated. The main drawback for such numerical procedures is that they use uniform grids, and in order to obtain an accurate description of the nuclear cusp very fine grids are necessary. This increases both the

computational cost and the memory requirements for the calculation, which limits such methods to small systems.

2.4   Multiresolution and Multiwavelets

In the last few decades, a viable alternative to traditional GTO basis sets has been developed based on the MO basis introduced by Alpert [10, 43]. Their use in quantum chemistry was pioneered by Harrison in the early 2000s [12, 44–47]. They come with several desirable properties that make them very attractive for use in quantum chemistry. Although unfamiliar to most chemists, from a user-viewpoint they are much easier to use than GTOs, which suffer from being highly parametrized and whose precision for a particular application is difficult to evaluate by non-experts. With MWs, arbitrary precision with respect to the complete basis set (CBS) limit can be achieved by a single keyword in the input file that directly quantifies the basis set error requested from the calculation. The goal of this section is not to give a robust and thorough introduction of the theory underlying a MW description of quantum chemistry, but to give an overview of some of the main concepts and to highlight aspects of MWs that make them especially attractive in all-electron quantum chemical calculations. For more details, the reader is referred to the literature [11, 15].

Conceptually, the idea of MWs is relatively simple. Given a small set of $k+1$ orthogonal polynomials $\phi_j{}^k$ of order $\leq k$ on the unit interval, one can attempt to represent a function. Completeness can be approached by letting the polynomial order approach infinity. Another way to reach completeness is by splitting the interval in two, and then copying the basis functions by dilation and translation. The first split ($n = 1$) leads to the following set of basis functions (restricted to one dimension for clarity)

$$\phi_j^1(x) = 2^{1/2}\phi_j^0(2x - l), \qquad l = 0, 1 \tag{2.53}$$

and after n splits we have (omitting the "0" superscript for $n = 0$)

$$\phi_{j,l}^n(x) = 2^{n/2}\phi_j(2^n x - l), \qquad l = 0, 1, \dots, 2^n - 1 \tag{2.54}$$

The basis becomes complete in the limit $n \to \infty$. The idea is to start off with a crude representation of the target function, and systematically approach completeness by repeated dilation and translation of the basis, or by increasing the polynomial order (although in practice a combination of the strategies are used).

The use of MW basis functions is based on the general concept of MRA, which provides a recipe for the construction of an infinite series of subspaces of the Hilbert space L^2. The basis outlined above satisfies a set of mathematical properties required by MRA, and can be used to represent any square-integrable function to any finite but arbitrary precision. Two different but complimentary series of subspaces are actually constructed, one where so-called scaling functions live and one where so-called wavelet functions live. The scaling spaces V are constructed such that completeness in L^2 can be approached systematically

$$V_k^n = V_k^0 \subset V_k^1 \subset V_k^2 \subset \dots \subset L^2 \tag{2.55}$$

where the wavelet spaces are the orthogonal complement to the scaling spaces, and a wavelet space at scale n is a "difference" space that relates two sequential scaling spaces

$$V_l^{n+1} \ominus V_k^n = W_k^n; \qquad W_k^n \perp V_k^n \tag{2.56}$$

The scaling and wavelet basis together form what is called the MW basis. The most desirable features of the MWs are perhaps orthogonality, adaptivity and robust error control. An orthogonal multiresolution is trivially

achieved if the polynomial functions are chosen to be orthogonal, for example by using Legendre polynomials or interpolating polynomials. Using orthogonal basis functions avoid issues with linear dependencies, leading to better numerical stability in precise calculations. Adaptivity is made simple by disjoint support of the scaling and wavelet functions, as well as a separated representation of operators. Error control is made possible by the way the wavelet spaces are related to the scaling spaces, and by the vanishing moments of the wavelet functions.

Robust error control is a feature that allows an objective evaluation of the precision of the current representation of the target function. This is contrary to the other types of basis sets discussed in this chapter, where one has to systematically repeat calculations with increasingly large basis sets in order to estimate the basis set errors. One therefore gains information about regions of the grid used to represent an MO that are not delivering a representation to the precision specified by the user. Vanishing moments of wavelet functions are key to the robust error control. If the wavelet function has M vanishing moments, then any polynomial of order $M-1$ can be represented exactly in the scaling basis, and the error in the target MO representation will be of Mth order. This robust error control can be used to signal that the representation needs to improve in a particular region, so that the total error moves toward the threshold set by the user. This process can be made completely automatic and self-contained when combined with grid adaptivity.

Adaptivity refers to that each MO is represented by values on a grid specifically constructed to hold that orbital, and each grid represents the function in a multiresolution manner such that the grid is at its densest in rapidly varying regions of the function (usually very close to the nucleus), and less dense in slowly varying regions (valence and interatomic regions). This avoids the challenges that come with a uniform grid (very dense grids that lead to high memory requirements), since the grid is refined to higher density only in regions where the

wavelet basis indicates that refinement is necessary. A few technicalities needs to be sorted out for adaptivity to be feasible and practical. The standard way to represent operators in a basis is the straightforward matrix realization of the operators in the basis. For a multiwavelet basis, this has the drawback of coupling all length scales (n) in all dimensions, which leads to complicated algorithms for operator application. The scales can be decoupled so that the operator representation only directly includes interactions within one scale, and where interactions across scales are taken care of in a post-processing step of wavelet transforms. This operator representation is referred to as the non-standard form [48, 49], and achieves that adaptive refinement becomes much simpler, since applying the operator at a given scale does not affect or depend on nodes at different scales. Adaptivity also becomes simpler by the disjoint support of scaling and wavelet functions, since by construction the domains of two such functions at the same scale do not overlap. This means that adaptive refinement can be done at one interval without affecting function description in other intervals at other scales (due to the non-standard form of operators) or within one scale (due to the disjoint support).

MW basis functions are not centered at the nuclei, and therefore do not suffer from BSSEs. As mentioned earlier, this is a great benefit in studies of chemical reactivity, and since it gives more robust results and simplifies the computational protocol. The MW basis is great step toward a black-box situation for basis sets, due to the guaranteed precision and simple input parameters, making them user-friendly to non-experts. However, some thought needs to be invested when planning a set of calculations with multiwavelets. As an example, consider the reaction in Equation (2.48). The total energy of the Ni fragment will be at the order of 10^3 Ha, while the energy of CO_2 will be about one order of magnitude smaller. Since MWs do not benefit from cancellation of errors, it becomes necessary to make conscious decisions on the number of

significant digits required in each fragment in order to reach the desired precision in relative energies. A conservative strategy is identify the fragment with the largest energy, determine the appropriate precision for this and reuse for the other fragments. However, this is not the most computationally efficient route, and one could save computational resources by determining appropriate precisions for each fragment of the reaction. This workflow in terms of significant digits is different from how one thinks about GTO calculations, since for GTOs the number of correct decimals in relative energies is greater than in total energies.

2.5   Molecular properties

Most quantum chemistry software packages are centered around the calculation of ground states. The term "ground state" here refers to not just to the electronic ground state, but to a state that is not affected by any external forces (apart from the electric field generated by the nuclei). We can get a lot of information about the molecular system from these calculations, for example the ground state energy, the ground state electron density, electric multipoles, forces on the nuclei, and more. However, many properties also require information about states other than the unperturbed ground state. For example, magnetizabilities are related to how much a material will become magnetized in an external magnetic field, and polarizabilities are related to how the electron density is affected by an external electric field.

The calculation of molecular properties provides a link between theoretical chemistry and experimental chemistry. Depending on the property of interest, we introduce various pertubations to the Hamiltonian operator. For example, an external electric field allows us to compute electric properties such as the electric dipole or the dipole polarizability, while an external magnetic field allows us to compute magnetic properties. Several frameworks exist for computing how a

pertubation affects the system, and a fundamental assumption for all is that these pertubations are small. Two different methods will be outlined in this section: properties from numerical approximations to energy derivatives and properties from density functional pertubation theory (DFPT) via the modified Sternheimer equations. This will give some background for the methods used in Paper I.

Properties from energy derivatives

In the presence of a general vector pertubation λ, the total electronic energy can be expanded in a Taylor series in the pertubation (around $\lambda = \mathbf{0}$)

$$E(\lambda) = E(\mathbf{0}) + \mathbf{E}^{(1)} \cdot \lambda + \frac{1}{2}\mathbf{E}^{(2)} \cdot \lambda^2 + \frac{1}{6}\mathbf{E}^{(3)} \cdot \lambda^3 + \mathcal{O}(\lambda^4) \qquad (2.57)$$

Here, $E(\mathbf{0})$ is the unperturbed total energy, and the coefficients $\mathbf{E}$ are the responses of the system to the pertubation and represent molecular properties. When the pertubation is time-independent (static), the molecular properties can be computed as energy derivatives

$$\mathbf{E}^{(1)} = \left.\frac{\partial E(\lambda)}{\partial \lambda}\right|_{\lambda=\mathbf{0}} \qquad (2.58)$$

$$\mathbf{E}^{(2)} = \left.\frac{\partial^2 E(\lambda)}{\partial \lambda^2}\right|_{\lambda=\mathbf{0}} \qquad (2.59)$$

$$\mathbf{E}^{(3)} = \left.\frac{\partial^3 E(\lambda)}{\partial \lambda^3}\right|_{\lambda=\mathbf{0}} \qquad (2.60)$$

One example of a static pertubation could be nuclear displacements $\Delta\mathbf{r} = \mathbf{r} - \mathbf{r}_0$, from which the first order property would be the electronic gradient (a vector for each Cartesian component), and the second order property would be the electronic Hessian (a matrix of all second-derivatives). However, the pertubation relevant for Paper I is a static

43

external electric field **F**, for which we get the following Taylor expansion (around **F = 0**)

$$E(\mathbf{F}) = E(\mathbf{0}) + \mathbf{E}^{(1)} \cdot \mathbf{F} + \frac{1}{2} \mathbf{E}^{(2)} \cdot \mathbf{F}^2 + \frac{1}{6} \mathbf{E}^{(3)} \cdot \mathbf{F}^3 + \mathcal{O}(\mathbf{F}^4) \tag{2.61}$$

$$= E(\mathbf{0}) + \boldsymbol{\mu} \cdot \mathbf{F} + \frac{1}{2} \boldsymbol{\alpha} \cdot \mathbf{F}^2 + \frac{1}{6} \boldsymbol{\gamma} \cdot \mathbf{F}^3 + \mathcal{O}(\mathbf{F}^4) \tag{2.62}$$

$$= E(\mathbf{0}) + \sum_i \mu_i F_i + \frac{1}{2} \sum_{ij} \alpha_{ij} F_i F_j + \frac{1}{6} \sum_{ijk} \beta_{ijk} F_i F_j F_k + \mathcal{O}(\mathbf{F}^4) \tag{2.63}$$

where the summation indices ijk represent Cartesian directions, and we implicitly defined the electric dipole $\boldsymbol{\mu} = \mathbf{E}^{(1)}$, the static electric dipole polarizability tensor $\boldsymbol{\alpha} = \mathbf{E}^{(2)}$, and the first hyperpolarizability tensor $\boldsymbol{\beta} = \mathbf{E}^{(3)}$.

A quick route to evaluate these derivatives in an approximate manner is via numerical finite differences (FD). The starting point for deriving FD formulas is the definition of the first derivative (using the "central" form, and not in the more conventional "forward" form):

$$f'(x) = \lim_{h \to 0} \frac{f(x + \frac{h}{2}) - f(x - \frac{h}{2})}{h} \tag{2.64}$$

When h is non-zero, we get the following approximation to the derivative expressed as a difference functional with an error that is quadratic in h

$$f'(x) \approx \Delta_h[f](x) = \frac{f(x + \frac{h}{2}) - f(x - \frac{h}{2})}{h} + \mathcal{O}(h^2) \tag{2.65}$$

This is the central FD formula for approximating the first derivative. The same procedure can be repeated to obtain formulas for higher order derivatives, and the second derivative formula can be derived by inserting the appropriate difference functionals into the nominator of Equation (2.65)

$$f''(x) \approx \frac{\Delta_h[f](x + \frac{h}{2}) - \Delta_h[f](x - \frac{h}{2})}{h} + \mathcal{O}(h^2) \tag{2.66}$$

$$\approx \frac{\frac{f(x+\frac{h}{2}+\frac{h}{2}) - f(x+\frac{h}{2}-\frac{h}{2})}{h} - \frac{f(x-\frac{h}{2}+\frac{h}{2}) - f(x-\frac{h}{2}-\frac{h}{2})}{h}}{h} + \mathcal{O}(h^2) \tag{2.67}$$

$$\approx \frac{f(x+h) - 2f(x) + f(x-h)}{h^2} + \mathcal{O}(h^2) \tag{2.68}$$

When the derivative is evaluated at $x = 0$, the formulas for the first and second derivative simplify to (omitting the residual error term)

$$f'(0) \approx \frac{f(\frac{h}{2}) - f(-\frac{h}{2})}{h} \tag{2.69}$$

$$f''(0) \approx \frac{f(h) - 2f(0) + f(-h)}{h^2} \tag{2.70}$$

A visual representation of the FD procedure for a first-order derivative is shown in Figure 2.3, and the approximation in Equation (2.69) can be thought of as the average slope of the function $f(x)$ in the interval $[\frac{-h}{2}, \frac{h}{2}]$ FD formulas can be derived for derivatives of arbitrary order and to arbitrary accuracy [50]. The derivations above yield approximated derivatives with a quadratic error in h, and tables of FD coefficients can be consulted when smaller errors are required. In general, the number of function evaluations grows both with smaller derivative errors and higher derivative orders.

The above FD formulas can be applied to the calculation of static electric properties. For example, the ith component of the dipole vector μ is approximated by evaluating the total energy under the influence of an electric field with strength $\pm\frac{F_i}{2}$

$$\mu_i = \frac{\partial E}{\partial F_i} \approx \frac{E(\frac{F_i}{2}) - E(-\frac{F_i}{2})}{F_i} \tag{2.71}$$
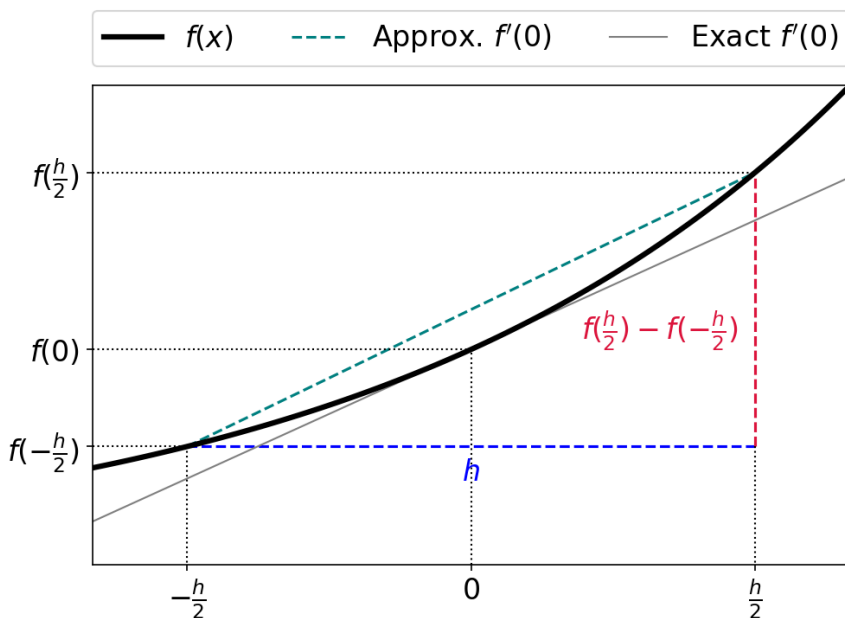
FIGURE 2.3: Visual representation of finite differences for a first-order derivative.

and the ith diagonal element of the static polarizability tensor α could be similarly approximated by either a second order FD formula by evaluating the total energy, or alternatively by a first order FD formula by evaluating the dipole

$$\alpha_{ii} = \frac{\partial^2 E}{\partial F_i^2} \approx \frac{E(F_i) - 2E(0) + E(-F_i)}{F_i^2} \tag{2.72}$$

$$= \frac{\partial \mu_i}{\partial F_i} \approx \frac{\mu_i(\frac{F_i}{2}) - \mu_i(-\frac{F_i}{2})}{F_i} \tag{2.73}$$

There is therefore some arbitrariness in whether the polarizability is called a linear response (LR) property or a quadratic response property, depending on the reference point used in the Taylor expansion.

It is important to recall that the total energy computed under the influence of an electric field is affected by all terms in the Taylor expansion in Equation (2.61). Therefore, the larger the magnitude of the pertubation the more important higher order terms will be. For example, when computing static polarizabilities by FD, one should keep in mind the potential for contamination from higher order terms that potentially can lead to incorrect results. It is therefore desirable to use a small field strength, in order to minimize higher order contributions to the total energy.

Another challenge to keep in mind relates to cancellation of digits. Consider the energy difference in the nominator of Equation (2.73). When one large number is subtracted from another large and similar number, many digits will be cancelled in the subtraction. It is therefore desirable to use a large field strength, in order to ensure that the energy difference is computed to sufficient numerical precision.

It then becomes clear that numerical precision and physical correctness in a calculation of a molecular property by FD are governed by two opposing guidelines for how to set the field strength. High correctness (or accuracy) requires a small field strength, but high numerical precision requires a large field strength. Proper calibration and testing is therefore necessary to strike a balance between the two, in order to arrive at a value that is sufficiently correct and sufficiently precise. This is easier to achieve with multiwavelets compared to GTOs, since the MW precision can be set strict enough to guarantee a particular numerical precision in a computed FD property. One can then get away with smaller field strengths, by an appropriate increase in MW precision. GTOs, on the other hand, rely on cancellation of errors, and the numerical precision will plateau at some point, limiting how small field strengths that can be used.

Properties from density functional pertubation theory

Another way to compute time-independent molecular properties is by time-independent pertubation theory. This theory is general and can be applied to any electronic structure theory, but is often referred to as DFPT when used within KS-DFT. The original Sternheimer equation published in 1954 [51] is based on linear pertubation theory, and serves as a starting point for our discussion. The modified Sternheimer equation [52] is a widely used method for computing polarizabilities, and will be discussed below. However, we start with the original formulation in order to motivate the modification.

Original Sternheimer The starting point is linear pertubation theory, where we introduce a pertubation to the system scaled by λ. The Fock operator $\mathcal{F}$, orbitals $|\phi_i\rangle$, and orbital energy ϵ_i then becomes

$$\mathcal{F} \rightarrow \mathcal{F}^{(0)} + \lambda \mathcal{F}^{(1)} \tag{2.74}$$

$$|\phi_i\rangle \rightarrow |\phi_i^{(0)} + \lambda \phi_i^{(1)}\rangle \tag{2.75}$$

$$\epsilon_i \rightarrow \epsilon_i^{(0)} + \lambda \epsilon_i^{(1)} \tag{2.76}$$

Inserting these into the KS equation (Equation (2.31)), one obtains

$$(\mathcal{F}^{(0)} + \lambda \mathcal{F}^{(1)})|\phi_i^{(0)} + \lambda \phi_i^{(1)}\rangle = (\epsilon_i^{(0)} + \lambda \epsilon_i^{(1)})|\phi_i^{(0)} + \lambda \phi_i^{(1)}\rangle \tag{2.77}$$

Expanding and neglecting quadratic terms in λ leads to

$$\lambda \mathcal{F}^{(0)}|\phi_i^{(1)}\rangle + \lambda \mathcal{F}^{(1)}|\phi_i^{(0)}\rangle = \lambda \epsilon_i^{(0)}|\phi_i^{(1)}\rangle + \lambda \epsilon_i^{(1)}|\phi_i^{(0)}\rangle \tag{2.78}$$

where the two fully unperturbed terms cancel due to the equality of the unperturbed KS equation. Rearranging the terms, we get the original Sternheimer equation

$$(\mathcal{F}^{(0)} - \epsilon_i^{(0)})|\phi_i^{(1)}\rangle = -(\mathcal{F}^{(1)} - \epsilon_i^{(1)})|\phi_i^{(0)}\rangle \qquad (2.79)$$

The perturbed Fock operator contains only the explicit external per-
tubation, and solving this equation will yield the perturbed electron
density. However, the original Sternheimer does not account for any
relaxation effects originating from the perturbed density, which leads
to polarizability predictions deviating from experimental values by
approximately 40 % [52].

Modified Sternheimer The modified Sternheimer extends the origi-
nal formulation by adding a self-consistency in the way the pertubation
is handled. The first-order perturbed operators become [53]

$$\mathbf{J}^{(1)}|\phi_i\rangle = \int \frac{\rho^{(1)}(r',r')\phi_i(r)}{|r-r'|} \qquad (2.80)$$

$$\mathbf{K}^{(1)}|\phi_i\rangle = \int \frac{\rho(1)(r,r')\phi_i(r')}{|r-r'|} \qquad (2.81)$$

$$\mathbf{V}_{xc}^{(1)}|\phi_i\rangle = \left[\frac{\partial^2 E_{xc}}{\partial\rho^2}[\rho^{(1)}(r,r)] \times \rho^{(1)}(r,r)\right]\phi_i(r) \qquad (2.82)$$

The modified Sternheimer equation is structurally identical to the origi-
nal one

$$(\mathcal{F}^{(0)} - \epsilon_i^{(0)})|\phi_i^{(1)}\rangle = -(\mathcal{F}_{\text{scf}}^{(1)} - \epsilon_i^{(1)})|\phi_i^{(0)}\rangle \qquad (2.83)$$

except an indication of the fact that the perturbed Fock operator now
contains both the explicit pertubation and the induced pertubations
in the potential operator. The equations therefore need to be solved
iteratively. Once the perturbed orbitals are computed, one can build the
density pertubation and subsequently compute the static polarizability
tensor.

2.6 Relativistic quantum chemistry

Non-relativistic quantum chemistry is an approximation that works very well for most elements encountered in organic and biologically relevant chemistry. However, the large nuclear charge of elements the heavier elements (approximately from row four or five and below), leads to an acceleration of core electrons to such high speeds that relativity no longer can be neglected in accurate calculations. This section will give a brief overview of relativistic quantum chemistry, with the main goal of introducing the ZORA method, in order to provide some theoretical context for Paper III.

The central equation in relativistic quantum chemistry is the Dirac equation, the relativistic equivalent to the Schröodinger equation, usually presented for a free electron as

$$[\beta c^2 + c(\alpha \cdot \mathbf{p})]\Psi = i\frac{\partial}{\partial t}\Psi \tag{2.84}$$

where c is the speed of light, $\mathbf{p}$ is a vector of momentum operators, α is a vector of 4×4 matrices, and β is a 4×4 matrix (the α and β matrices are collectively referred to as the Dirac matrices):

$$\mathbf{p} = \begin{bmatrix} p_x \\ p_y \\ p_z \end{bmatrix}; \quad \alpha = \begin{bmatrix} \alpha_x \\ \alpha_y \\ \alpha_z \end{bmatrix}; \quad \beta = \begin{bmatrix} \mathbf{I}_2 & \mathbf{0}_2 \\ \mathbf{0}_2 & -\mathbf{I}_2 \end{bmatrix} \tag{2.85}$$

in which the three Cartesian components of α are constructed from the Pauli spin matrices σ_i

$$\alpha = \begin{bmatrix} \mathbf{0}_2 & \sigma \\ \sigma & \mathbf{0}_2 \end{bmatrix} \tag{2.86}$$

$$\sigma_x = \begin{bmatrix} 0 & 1 \\ 1 & 0 \end{bmatrix}; \quad \sigma_y = \begin{bmatrix} 0 & -i \\ i & 0 \end{bmatrix}; \quad \sigma_z = \begin{bmatrix} 1 & 0 \\ 0 & -1 \end{bmatrix} \tag{2.87}$$

In quantum chemistry, however, we are not interested in free electrons, but rather electrons bound by the electric potential generated by the fixed nuclei under the BO approximation. The time-independent Dirac equation under these assumptions expressed in two-component form (with each component representing two equations) is given as

$$\begin{bmatrix} V & c\sigma \cdot \mathbf{p} \\ c\sigma \cdot \mathbf{p} & V - 2c^2 \end{bmatrix} \begin{bmatrix} \Psi^L(\mathbf{r}) \\ \Psi^S(\mathbf{r}) \end{bmatrix} = E \begin{bmatrix} \Psi^L(\mathbf{r}) \\ \Psi^S(\mathbf{r}) \end{bmatrix} \tag{2.88}$$

where the energy scale has been aligned with the non-relativistic energy, E signifies the positive energy solutions, V is the attractive electron-nucleus Coulomb potential, and σ is the vector of its Cartesian components from Equation (2.87).

Thus, Equation (2.88) is a set of four coupled differential equations, the solution to which is a wavefunction with four-component (4c). Such an equation can only be solved analytically for a H atom, or other H-like, one-electron systems. The solutions to the 4c Dirac equation lead to both positive and negative energies, where the positive energies are associated with electronic states and the negative ones with positronic states. Negative energies can safely be discarded except when dealing with high-energy processes [54]. Note that the wavefunction Ψ in Equation (2.88) is expressed in terms of a large component (Ψ^L) and a small component (Ψ^S). This terminology refers to that two of the four components are numerically larger than the other two when considering the electronic solutions (the situation is opposite when considering the positronic solutions).

While codes exist today that solve the 4c problem [55–58], most routine calculations within computational chemistry account for relativistic effects only in an approximate manner. A popular method for approximating relativistic effects is the ZORA method [59, 60], which is implemented in several mainstream quantum chemistry software packages.

The starting point for ZORA is the so-called unnormalized elimination of the small component (UESC) procedure, where the small component of the wavefunction has been eliminated by substitution.[§] The resulting two-component (2c) UESC expression, which is still exact, is given by

$$\left(\frac{1}{2}(\sigma \cdot \mathbf{p})\kappa(E,\mathbf{r})(\sigma \cdot \mathbf{p}) + V \right)\Psi^L(\mathbf{r}) = E\Psi^L(\mathbf{r}) \qquad (2.89)$$

where κ is a multiplicative operator that depends on the energy

$$\kappa(E,\mathbf{r}) = \left(1 + \frac{E - V}{2c^2} \right)^{-1} \qquad (2.90)$$

Equation (2.89) is not used in practice, since it is not an eigenvalue problem (the energy appears on both sides of the equation), but serves as a starting point for approximations. The first step toward ZORA is to rewrite the expression for κ

$$\kappa(E,\mathbf{r}) = \left(1 - \frac{V}{2c^2} \right)^{-1} \left(1 + \frac{E}{2c^2 - V} \right)^{-1} \qquad (2.91)$$

and to expand the second factor in a Taylor series (recognizing that it has the same functional form as $f(x) = \frac{1}{1+x}$) around $x = 0$

$$\left(1 + \frac{E}{2c^2 - V} \right) = \sum_{k=0}^{\infty} (-1)^k \left(1 + \frac{E}{2c^2 - V} \right)^{-k} \qquad (2.92)$$

Truncating the expansion to zeroth order, we get the 2c ZORA equations

$$\left(\frac{1}{2}(\sigma \cdot \mathbf{p})\left(1 - \frac{V}{2c^2} \right)^{-1}(\sigma \cdot \mathbf{p}) + V \right)\Psi^{2cZORA}(\mathbf{r}) = E\Psi^{2cZORA}(\mathbf{r}) \qquad (2.93)$$

[§]A more general derivation of the ZORA equations involves the elimination of the small components via a Foldy–Wouthuysen transformation. This approach allows for the derivation of multiple levels of approximations, as well as different ZORA flavors, in a unified procedure.

This is a 2c problem; however, in practice one usually uses the scalar relativistic version of this. We can use Dirac's relation to separate the spin-dependent part from the spin-free part

$$(\sigma \cdot \mathbf{p})\kappa(\sigma \cdot \mathbf{p}) = \mathbf{p} \cdot \kappa \mathbf{p} + i\sigma \cdot \mathbf{p} \times \kappa \mathbf{p} \tag{2.94}$$

The scalar relativistic ZORA eigenvalue problem is the obtained by completely neglecting the spin-dependent term

$$\left(\frac{1}{2}\mathbf{p} \cdot \left(1 - \frac{V}{2c^2}\right)^{-1} \mathbf{p} + V \right) \Psi^{\text{ZORA}}(\mathbf{r}) = E\Psi^{\text{ZORA}}(\mathbf{r}) \tag{2.95}$$

Scalar relativistic ZORA is relatively simple to incorporate into existing non-relativistic quantum chemistry codes, since the approximation essentially involves replacing the standard kinetic energy operator with a ZORA kinetic energy operator

$$T^{\text{ZORA}} = \frac{1}{2}\mathbf{p} \cdot \kappa \mathbf{p} \tag{2.96}$$

$$= \frac{1}{2}\mathbf{p} \cdot \left(1 - \frac{V}{2c^2}\right)^{-1} \mathbf{p} \tag{2.97}$$

The non-relativistic limit can be recovered by letting the speed of light approach infinity

$$\lim_{c \to \infty} T^{\text{ZORA}} = \frac{1}{2}\mathbf{p} \cdot (1 + 0)^{-1}\mathbf{p} = \frac{1}{2}\mathbf{p}^2 = T \tag{2.98}$$

One significant drawback of the ZORA method is that it is not gauge invariant. This means that a constant shift in the potential does not lead to a constant shift in the energy. The effect is more pronounced for core orbitals, and will for example lead to challenges in the calculation of ionization potentials for heavy atoms [61].

3

Static polarizabilities with Multiwavelets

3.1 What are static polarizabilities and why do we compute them?

The "static electric dipole moment polarizability" is an electric property of atoms and molecules. The name is quite a mouthful, and one can best gain an intuitive understanding of this property by deconstructing its name. An electric dipole moment is a property that chemists are familiar with: It is the property that describes the strength of charge-separation in polar molecules, such as water or ethanol, and goes back to the old rule-of-thumb that polar solvents dissolve polar molecules, and vice versa. A water molecule has a permanent dipole, but this dipole is susceptible to be affected, or perturbed, by nearby electric charges. The extent to which the dipole moment of a water molecule is perturbed is described by the electric dipole polarizability, which quantifies the dipolar change caused by an external electric field. Finally, an electric dipole moment polarizability is said to be static if the external electric field has a constant frequency (if the frequency varies, then the property

is referred to as dynamic). It is common to refer to the property as "static polarizability", or simply "polarizability", and this convention will be used from now on in this chapter.

Polarizabilities are interesting to compute for many reasons, but I will focus on three here: Accurate enzyme-ligand interactions, DFA transferability, and quantum chemistry method development. Polarizabilities are very relevant when considering dispersion forces between non-covalently bonded molecular fragments [62, 63]. Induced dipole interactions result directly from the electron density being perturbed by some external electric charge, and the nature of this pertubation is what we refer to as the polarizability. One example of this could be the presence of transition metal cations in the active site of an enzyme, which can interact with the electrons of incoming ligands and modify their bonding to the enzyme. Enzyme-ligand interactions is a large field within computational chemistry, and due to the large size of the enzyme such calculations are often performed with molecular force-fields. Force-fields are simple functions with parameters fitted to experimental data or quantum chemistry calculations. Polarizabilities are usually part of the reference data used in the fitting process, and it is important that they are computed accurately in order for the force-field to work as intended.

Polarizabilities are also a good metric for assessing the transferability of a given DFA [64]. Most DFAs contain empirical parameters that have been fitted to a set of experimental or high-quality *ab initio* data. There is therefore an inherent bias in the DFA construction that on average makes chemical species similar to those used in the fitting process more likely to yield lower errors. The connection between polarizabilities and transferability can be understood by realizing that electrons in molecules are in the presence of the electric field generated by the nuclear charges. When the molecule changes so does the electric field felt by the electrons. In polarizability calculations one applies an

external electric field to the chemical system, and calculates how the electronic wavefunction is affected by the pertubation. Therefore, a DFA that accurately captures the effects from an external electric field can, to some extent, also be expected to produce accurate electron densities over a range of chemical systems.

Finally, a more philosophical reason for why polarizabilities are interesting to compute accurately, is related to quantum chemical method development. Our calculations are based on mathematical models that are intended to describe the laws of physics, which we then apply to chemical problems. We must know the limitations of our models, both for the sake of not obtaining spurious data without our knowledge, and for the sake of directing future developments within the field of quantum chemistry toward areas where our currently available methods are lacking. It is therefore important to investigate how well common computational protocols perform in the calculation of various properties, regardless of their relevance, since what is irrelevant today may become relevant tomorrow.

3.2 Previous benchmarks on polarizabilities

Polarizabilities have been the subject of several benchmark studies in the past, but for most of them the main focus is on the accuracy of predicted polarizabilities by comparison to high-level quantum chemistry calculations or experimental data. Still, some studies include a section on how the polarizabilities converge with respect to the basis set used, and a brief overview will be given here. It should be noted that the purpose of the following basis set comparisons was more related to gaining a fair understanding of the basis set effects on polarizability calculations, and not to attempt a rigorous basis set benchmark in search for CBS polarizabilities. Any criticism presented in the following paragraphs should therefore not be interpreted as scientific criticism, but rather be

viewed in the light of highlighting a lack of basis set benchmarks on polarizabilities in general. The following cited studies are an exhaustive compilation of studies where basis set effects have been investigated, but represent those most relevant to this thesis that I could find.

Hickey and Rowley [65] performed an investigation into the accuracy of polarizability predictions from common quantum mechanical methods. The chemical species studied made up a set of 46 main group species from the first three rows of the periodic table, all uncharged and in closed-shell electron configurations. They included a study of the basis set effects in combination with common DFAs, based on the following basis sets: cc-pV[D,T]Z, aug-cc-pV[D,T]Z, and Sadlej-cc-pVTZ. However, they did not summarize the basis set effects in a single figure. Therefore, I have compiled their raw data from the published SI and computed relative unsigned deviations (RUDs), using the aug-cc-pVTZ basis set as reference, which are presented in Figure 3.1. The basis sets aug-cc-pVDZ and Sadlej-vpTZ (which is cc-pVTZ with additional basis functions specifically intended for calculations of polarizabilities) seem to perform equally well, with the largest deviation around 10 %. The non-augmented basis sets, on the other hand, perform much worse, particularly for aug-cc-pVDZ which displays multiple deviations larger than 40 %.

A rather thorough investigation of basis set convergence on polarizabilities was published by Hammond et al. [66]. Their main goal was to benchmark polarizabilities for water clusters with highly accurate CC protocols, and use this data to assess the accuracy of common DFAs. However, they also computed polarizabilities at the HF level of theory for a single water molecule with three different flavors of Dunning basis sets, with sequences ranging from double zeta (DZ) to sextuple zeta (6Z). The main drawback here is mainly that only HF was used and that only a single water molecule was tested. This naturally limits how universal the basis set convergence is for polarizabilities. Later in the
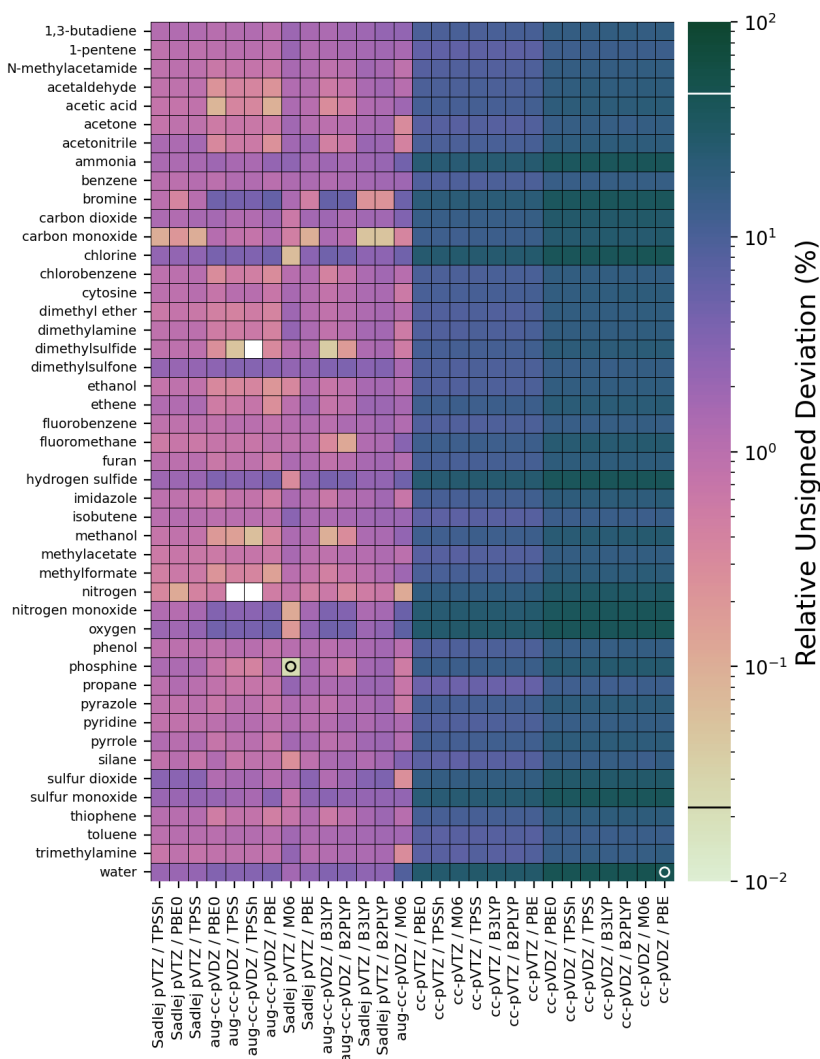
FIGURE 3.1: Estimated basis set errors based on RUDs with aug-cc-pVTZ polarizabilities as the reference [65]. The data has been compiled from their published SI.

paper they did present tests for different basis set families combined with various DFAs, but only water clusters of varying sizes were tested, which limits the scope of the conclusions that can be drawn.

Maekawa and Moorthi [67] computed static (and dynamic) polarizabilities with a selection of hybrid DFAs, for a set of 105 organic species spanning most common functional groups. Basis set effects were tested on a small subset of these (benzene, naphthalene, anthracene, and naphthacene) with the basis sets aug-cc-pVDZ and aug-cc-pVTZ. For benzene, they tested the two basis sets on the same geometry (optimized at the B3LYP/cc-pVDZ level of theory), and found that the polarizability at the DZ level converged to the first decimal (in units of $Å^3$), which is similar to what Hickey and Rowley [65] found. For the remaining three molecules they presented polarizabilities which had been geometry-optimized with two different basis sets, and it is therefore difficult to gain much knowledge purely about the basis set convergence (their motivation for this was that they were interested in seeing how well different protocols would predict experimental results).

A common theme throughout published computational studies on polarizabilities is that basis sets with diffuse functions outperform analogous basis sets without diffuse functions. It seems this piece of knowledge can be traced back to a seminal paper by Werner and Meyer [68] from 1976, in which they did a thorough investigation into the appropriate basis set construction for obtaining polarizability estimates to within experimental errors. This trend is also intuitive, since the polarizability is a property that relies on a good description of the tail of the wavefunction, which is precisely the region diffuse were designed to describe.

3.3   Summary of Paper I

The aim of this study was three-fold: i) We wanted to summarize recent efforts in the group aimed toward implementing algorithms in MRChem for computing static polarizabilities in a DFPT framework, ii) we wanted to provide a high-quality reference data set of polarizabilities obtained from MW calculations, and iii) using this data set, we wanted to quantify BSIEs in polarizabilities computed with large GTO basis sets. The starting point for our investigation was a benchmark study by Hait and Head-Gordon [64]. They had performed numerical polarizability calculations for 132 small main group species with a large number of DFAs, and compared them to more accurate CC polarizabilities. The basis set used for DFT calculations was aug-pc-4, a large 5Z GTO basis set with added diffuse and polarization functions. This particular basis set has been used and assumed complete for electric properties [64, 69], and we aimed to test this assumption by comparing to polarizabilities from MWs.

Our set of chemical systems consisted of 32 spin-polarized and 92 spin-unpolarized species (124 in total, see Table 3.1). The remaining 8 species (when compared to the 132 species in ref [64]) we were not able to converge to a convincing solution, and so they were discarded from our analysis. We limited our computational investigation to the PBE DFA [24], since MRChem did not support analytical polarizability calcualations with hybrid functionals at the time. In addition to using the numerical polarizabilities provided by ref [64], we also computed analytical GTO polarizabilities using the ORCA quantum chemistry code [70]. With MRChem we computed numerical polarizabilities with the FD approach and analytical polarizabilities within the LR framework.

On the basis of these two computational approaches (FD and LR) and basis set types (GTO and MW), we ended up with four distinct sets of polarizability data: i) MW–FD, ii) MW–LR, iii) GTO–FD, and iv)

TABLE 3.1: The 124 species and their spin multiplicities used in Paper I, sorted alphabetically. The number of closed-shell and open-shell species are 92 and 32, respectively. Closed-shell species are indicated in blue, while open-shell species are indicated in red.

^{1}AlF	^{1}Ar	^{1}Be	^{2}BeH	^{1}BeH$_2$	^{1}BF	^{1}BH$_2$Cl
^{1}BH$_2$F	^{1}BH$_3$	^{1}BHF$_2$	^{3}BN	^{2}BO	^{2}BS	^{2}C$_2$H
^{1}C$_2$H$_2$	^{2}C$_2$H$_3$	^{1}C$_2$H$_4$	^{1}CH$_2$BH	^{2}CH$_2$F	^{1}CH$_2$NH	^{1}CH$_2$PH
^{1}CH$_3$BH$_2$	^{1}CH$_3$Cl	^{1}CH$_3$F	^{1}CH$_3$NH$_2$	^{1}CH$_3$OH	^{1}CH$_3$SH	^{1}CH$_4$
^{1}Cl$_2$	^{1}ClCN	^{1}ClF	^{2}CN	^{1}CO	^{1}CO$_2$	^{1}CS
^{1}CSO	^{1}F$_2$	^{1}FCN	^{2}FCO	^{2}FH$-$OH	^{1}FNO	^{2}H
^{1}H$_2$	^{2}H$_2$CN	^{1}H$_2$O	^{2}H$_2$O$-$Li	^{1}HBO	^{1}HBS	^{1}HCCCl
^{1}HCCF	^{1}HCHO	^{1}HCHS	^{1}HCl	^{1}HCN	^{2}HCO	^{1}HCONH$_2$
^{1}HCOOH	^{1}HCP	^{1}He	^{1}HF	^{1}HNC	^{1}HNO	^{1}HNS
^{2}HO$_2$	^{1}HOCl	^{1}HOF	^{1}HOOH	^{2}Li	^{1}Li$_2$	^{1}LiBH$_4$
^{1}LiCl	^{1}LiCN	^{1}LiH	^{1}Mg	^{1}Mg$_2$	^{4}N	^{1}N$_2$
^{1}N$_2$H$_2$	^{1}N$_2$H$_4$	^{2}Na	^{1}Na$_2$	^{1}NaCl	^{1}NaCN	^{1}NaH
^{1}NaLi	^{2}NCO	^{1}Ne	^{3}NH	^{2}NH$_2$	^{1}NH$_2$Cl	^{1}NH$_2$F
^{1}NH$_2$OH	^{1}NH$_3$	^{1}NH$_3$O	^{1}NOCl	^{1}NP	^{3}O$_2$	^{1}O$_3$
^{2}OCl	^{1}OCl$_2$	^{2}OF	^{1}OF$_2$	^{2}OH	^{4}P	^{1}P$_2$
^{1}P$_2$H$_4$	^{3}PH	^{2}PH$_2$	^{1}PH$_2$OH	^{1}PH$_3$	^{1}PH$_3$O	^{1}S$_2$H$_2$
^{2}SCl	^{1}SCl$_2$	^{2}SF	^{1}SF$_2$	^{1}SH$_2$	^{2}SiH$_3$	^{1}SiH$_3$Cl
^{1}SiH$_3$F	^{1}SiH$_4$	^{1}SiO	^{3}SO	^{1}SO$_2$		

GTO–LR. The key comparison in our work was MW–FD vs GTO–FD, *i.e.*, an assessment of the basis set convergence in the polarizabilities published in ref [64]. However, since the FD approach was used to estimate the diagonal elements of the polarizability tensor, we also needed to double check that no significant errors from the FD treatment had contaminated either the MW or the GTO data sets. For this purpose we made the comparisons MW–FD vs MW–LR and GTO–FD vs GTO–LR. Finally, we also compared MW–FD to GTO–LR as a double check that our error analysis was correct. Note that for our internal MW validation (MW–FD vs MW–LR) we also used the LDA DFA, since we had some troubles converging the LR calculations with PBE.

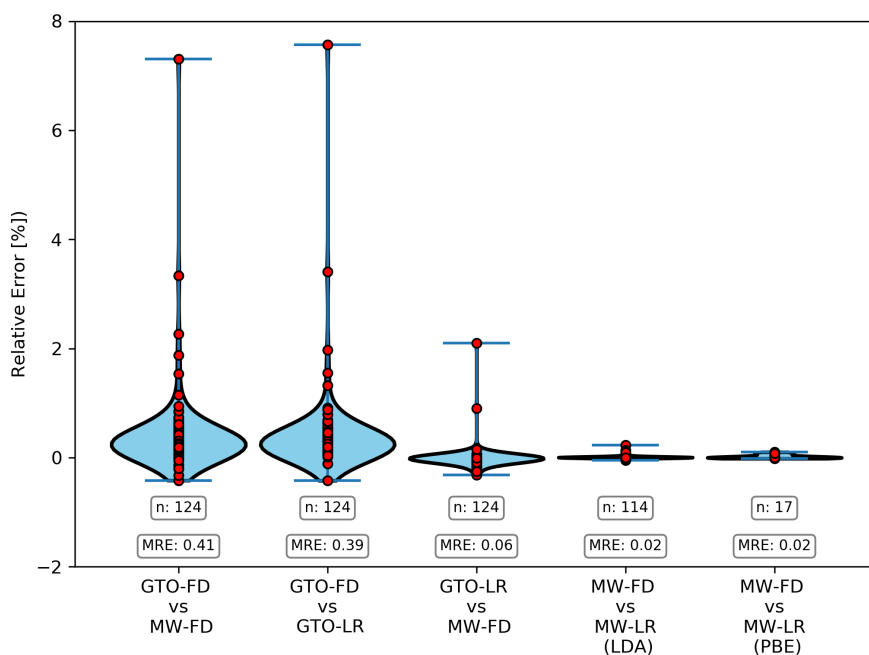Figure 3.2 summarizes the polarizability comparisons described

FIGURE 3.2: Summary of polarizability error distributions (in %) for four types of protocol comparisons. Red dots indicate data points. The internal validation of our MW results demonstrates that the MW-FD polarizabilities are virtually free from field strength-related effects. GTO–FD polarizabilities display quite large errors, considering the size of the aug-pc4 basis set that was used, while GTO–LR display much smaller errors.

above. The first thing to notice is that when comparing GTO–FD with MW–FD, we observe a few quite large relative errors of up to about 8 %. This is more than what we expected to see if the error was solely due to basis set effects, due to the very large size of the aug-pc-4 basis set. Comparing GTO–FD to GTO–LR we see more or less identical error distributions. This indicates that the FD approach has introduced some artefacts into the polarizability estimates. To get a fair estimate of the BSIEs for polarizabilities, we then compared GTO–LR to MW–FD. The error distribution is much more compressed, with smaller maximum errors and a smaller range of errors. A large majority of the species investigated display errors less than 0.5 %, which demonstrates that aug-pc-4 is capable of delivering polarizabilities very close to the CBS limit. More detailed discussions about the various comparisons can be found in Paper I.

Another interesting outcome from the study is related to the FDs approach. The careful use of finite differences with GTO basis sets requires a balancing of two different types of errors. A too strong applied field will lead to higher order responses (*e.g.*, hyperpolarizabilities) contaminating the property. On the other hand, if one attempts to control higher order responses by applying a too weak field, then the desired response is so small that one is likely to cancel out the significant digits when using the FD formula. A general rule is therefore to apply the weakest field that yields a sufficient number of significant digits in the estimated property; however, this cannot be known *a priori*, and will vary based on the molecular system studied (and possibly also the DFA used).

A robust use of FD is much easier with MWs. The reason is simply that the user can explicitly set the precision of the calculations with respect to the CBS limit, and in that way combat higher order effects by tighter thresholds. The number of significant digits in the polarizability can therefore be systematically increased by varying the MW precision.

A similar strategy is not possible for GTOs, and one must eventually rely on unpredictable error cancellations.

4

TM-LIGAND INTERACTION ENERGIES WITH MULTIWAVELETS

4.1 Why the interest in transition metals?

TMs belong to a group of elements with a broad spectrum of academic and industrial interest. Most notably, they are extensively used as catalysts for a diverse set of chemical reactions, for example in the upgrading of oil [71], in the synthesis of pharmaceuticals [72], in the production of ammonia from the Haber-Bosch process [73], and in the reduction of combustion waste products in car engines [74]. Although the quantum mechanical details of their electronic structure is a bit complex, one can perhaps understand their suitability as catalysts from a few general properties: partially filled d-orbitals, low redox potentials, larger size, and rich coordination chemistry.

Partially filled orbitals in general tend to imply greater potential for chemical reactivity. For example, the noble gases (or other molecules with noble gas electron configurations) with their full electron shells are known for being (to a large extent) chemically inert. As defined by International Union of Pure and Applied Chemistry (IUPAC) [75],

TMs are those elements which in their elemental or cationic form have partially filled d-orbitals. What makes TMs different from main group elements (with partially filled p-orbitals) is the more closely spaced energy levels. One consequence of this is that many TMs can exist in multiple oxidation states, and the potential barriers separating these states are often low. This makes it energetically easy to convert from one oxidation state to another, which is likely one of the properties that has lead to iron (Fe) being used in biological redox reactions. Another manifestation of the lower inter-oxidation state barriers is the relatively low redox potentials. If one looks at a standard table of redox potentials, one will find that TMs are neither at the top or the bottom, but somewhere in the middle. It should be noted, however, that it is not just the metal that determines inter-state barriers; the nature of the ligands also play an important role in determining the electronic properties of a TM complex.

Lastly, the larger sizes of TMs compared to main group elements also increase their usability in chemical synthesis. Larger atoms can simply accommodate a higher number of ligands bonded to it, which leads to greater flexibility in the design of both catalysts and scaffolds. For example, this opens up the possibility of designing complex catalysts with large and bulky side groups that are stereo- or regioselective, or the designing of catalysts that can bind multiple ligands and promote a reaction between them.

4.2 Previous benchmarks on basis set effects on metal-ligand properties

Due to their favourable properties, as described above, TMs and their interactions with other compounds have been the subject of a large number of computational benchmark studies. However, they are often more difficult to study computationally than main group systems, because

i) chemically relevant complexes often have open-shell configurations leading to poorer SCF convergence behavior, ii) low-lying electronic states might demand a multireference wave function method to get a qualitatively correct description, iii) high-quality, all-electron basis sets are not always defined for all TMs, iv) relativistic effects may become non-negligible and important if high accuracy is needed, and v) the high number of electrons can lead to expensive reference calculations for large sets of transition metals complexes. These difficulties have limited the number of comprehensive benchmark investigations of large TM complexes. However, they can to some extent be alleviated by limiting the included systems to only involve first-row TMs with well-defined ground electronic states in closed-shell configurations.

While most TM benchmarks focus on the functional performance (*i.e.*, the deviation from experiment or highly correlated methods), some do include tests on the basis set convergence. Basis set investigations in (a small sample of) such studies will be summarized below, where studies have been selected that have included either multiple TM systems or multiple basis sets. The presented data have been compiled from the published SIs. In order to facilitate a logarithmic axis in the data visualization, data points have been dropped where estimated errors was zero, or the corresponding reference value was zero, to avoid RUDs that were zero or infinite in magnitude. As stated in the previous chapter, the analysis given below should not be interpreted as scientific criticism against the cited works, but rather be seen as an attempt to reuse published data to gain insight into questions that were not part of the main research objectives.

Tekarli et al. [76] computed enthalpies of formation for a set of 19 first row TM complexes (closed and open-shell), with 44 DFAs and two different basis sets (cc-pVTZ and cc-pVQZ). The authors focused on the magnitude of the basis set effects when the computed enthalpies were compared to experimental ones. However, this makes it hard to

judge the quality of the basis set alone, since experimental errors are likely not uniform across all the complexes. Figure 4.1 presents a more detailed view of their basis set effects, by computing RUDs for triple zeta (TZ) compared to QZ enthalpies and plotting these in a heatmap. This way of presenting the data gives a semi-quantitative distribution of RUDs where trends and outliers can quickly be identified visually. Using the color gradient scale, one can see that for most complexes and functionals, the enthalpies changed by less than approximately 5 % upon going from TZ to QZ, and that the vast majority of complexes changed less than 10 %. The maximum RUD in the data set is close to 200 % (but this may to some extent be due to rounding errors from SI numbers with few decimals). Certain complexes seem to produce larger errors than others; most notably CuF consistently produces larger errors than other complexes for most of the included functionals. Further, basis set convergence is clearly not uniform across functionals, and BH&HLYP seems to produce larger RUDs for several complexes than other functionals.

In another study, Jiang et al. [77] computed enthalpies of formation for a set of 192, small TM complexes, with the B3LYP and M06 functionals, and checked the effects on the enthalpies from increasing the basis set from cc-pVTZ to cc-pVQZ, by comparing the computed enthalpies to experimental ones. They explain that the particular functional/basis set combination was used for all steps in obtaining enthalpies, *i.e.*, geometry optimizations, single points evaluations, and thermal corrections, which means that the geometries used are not identical for the two basis sets. While this may mask some of the effects of the basis sets, the effect on the geometry can likely be assumed to be minor [31] (also supported by Figure 4.4 below). Comparison to experiment further camouflage effects purely due to the basis sets, since other sources of errors are introduced into the data analysis. Therefore, I compiled their raw enthalpies of formation data from the published SI, and computed
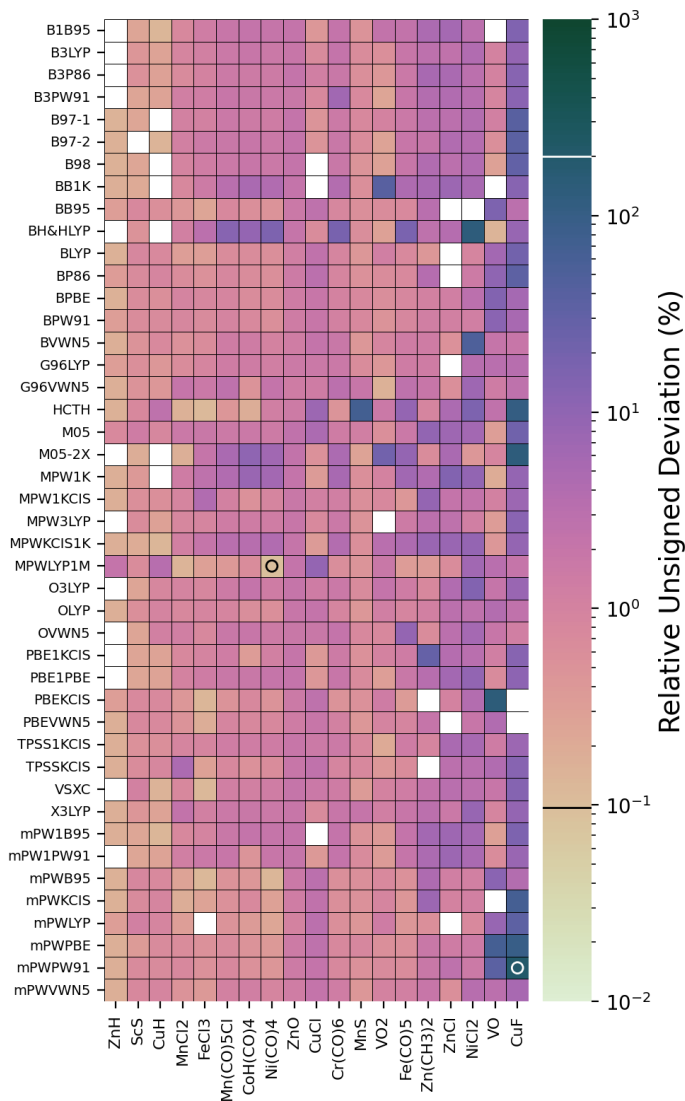
FIGURE 4.1: Estimated basis set errors in enthalpies of formation (in %) for a set of 19 TM complexes, based on RUDs computed with cc-pVTZ and cc-pVQZ, for 43 different functionals [76]. The data is compiled from their published supporting information.
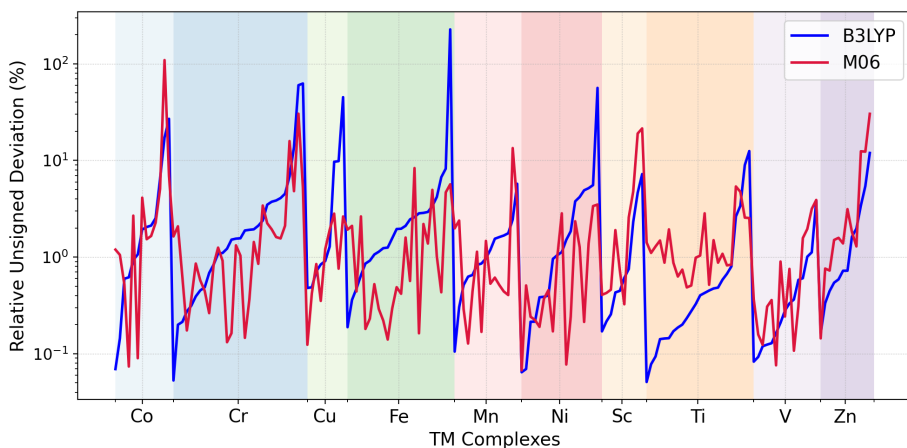
FIGURE 4.2: Estimated basis set errors in enthalpies of formation for a set of 192 TM complexes, based on RUDs in enthalpies computed with cc-pVTZ and cc-pVQZ for two different functionals [77]. Shaded regions in the plotting area indicate data involving the same TM. The data is compiled from their published supporting information.

RUDs based on enthalpies from TZ and QZ basis sets. The resulting estimates of the basis set errors at the TZ level for the two functionals are presented in Figure 4.2. The data range is rather large, spanning about four orders of magnitude. A large majority of the studied TM complexes show absolute deviations smaller than 5 %, regardless of the functional, but a few pathological cases display errors close to 100 % or above.

Aoto et al. [78] published an article where they set out to determine whether experimental data or high-level calculations best serve as reference values in benchmark studies for TM compounds. While their main question is a bit unrelated to the basis set issues that we are interested in here, they did assess basis set convergences by computing dissociation energies for 60 TM diatomics, as well as equilibrium bond lengths and

harmonic vibrational frequencies, with several basis sets increasing in size from DZ to QZ for 10 different DFAs. For the 3d systems they used all-electron basis sets, but for 4d and 5d systems they used a combination of valence orbital basis sets and effective core potentials. Their basis set evaluation was based on comparison to experimentally estimated properties, and they found that the choice of basis set had only a minor effect on the functionals' deviations from experiment. Using their raw data published in the SI, I have estimated basis set errors for the dissociation energies, bond lengths and harmonic frequencies, by computing RUDs. For my analysis I just considered the 3d systems, since the all-electron basis sets used makes the analysis more robust. Further, I judged the aug-cc-pVQZ basis set to be the most complete of the ones they tested, and so RUDs were computed relative to this basis set. The estimated basis set errors for dissociation energies, bond lengths, and harmonic frequencies are summarized in Figures 4.3 to 4.5 for all combinations of molecule/functional/basis set.

For dissociation energies, most RUDs appear to be below approximately 4 %, although errors up toward 20 % can be observed. The QZVP basis set performs the best, with most errors below 2 %, with augmented TZVP closely following. Augmented VDZ ranges from displaying very low errors to very large errors, highlighting the unpredictability in performance of small basis sets. Non-augmented TZVP displays errors up toward 10 % for most included functionals. Complexes containing titanium (Ti) and vanadium (V) seem to produce lower errors on average consistently for all combinations of functional and basis set than most other complexes. Further, the BLYP and M06 functionals seem to produce quite large errors for complexes containing Fe, and zinc (Zn)-containing complexes lead to relatively large errors especially for non-augmented TZ basis sets. A general trend seems to be that basis sets augmented with diffuse functions perform markedly better than non-augmented ones, with performance not far from one zeta-level
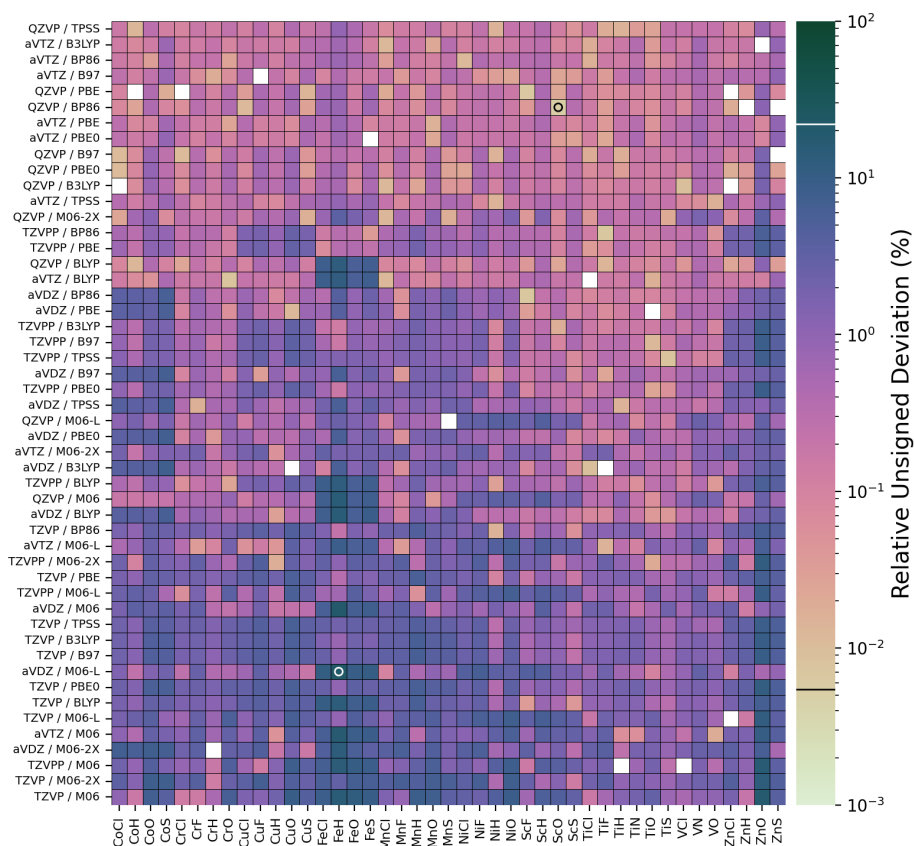
FIGURE 4.3: Estimated basis set errors in dissociation energies for TM diatomics for a variety of common combinations of DFA and basis set [78]. The largest and smallest errors have been highlighted with circles in the corresponding cells, and they have been indicated as horizontal lines in the color bar. Completely white cells correspond to missing data points that have been omitted due to either being zero or infinite.

higher.

The situation looks much better for the equilibrium bond lengths, as the largest RUD is smaller than 2 %, and the majority of cases showing

errors smaller than 1 %. A trend here is that the aug-cc-pVDZ basis set produces markedly larger errors than the other basis sets, and that the basis set expansion seems "practically converged" at the TZ level. Another interesting observation is that complexes containing chlorine (Cl) and sulfur (S) produce larger errors compared to other complexes. This trend seems to be consistent throughout most basis sets and functionals, but is most easily seen in the aVDZ basis set. This is perhaps due to the more diffuse electron density present for S and Cl compared to their second-row analogs, although an augmented DZ basis set perhaps should be expected to perform similar to non-augmented TZ.

The largest RUD for harmonic frequencies was approximately 10 %, which was observed for CrO at the M06-L/TZVPP level. Augmented TZ and QZ basis sets perform the best, with errors smaller than 1 % (although about half of the data points have been discarded due to zero of infinite errors). Augmented DZ and non-augmented TZ basis sets appear to give errors approximately of the same order of magnitude.

In summary, by making use of published data from benchmark studies, one can gain some understanding of the basis set effects on TM properties. For energetics and diatomic harmonic frequencies, it seems one can come a long way with a TZ basis set augmented with diffuse functions. Equilibrium bond distances in diatomics, on the other hand, seemed sufficiently converged at the DZ level. However, one should keep in mind that several studies did not include basis sets beyond TZ quality, and so a proper investigation of the basis set limit could not be done based on their data. Basis set effects are also not uniform across different DFAs, and it seems safe to conclude that the choice of GTO basis sets in calculations of TM complexes is still not completely black-box.

FIGURE 4.4: Estimated basis set errors in equilibrium bond lengths for TM diatomics for a variety of common combinations of DFA and basis set [78]. The largest and smallest errors have been highlighted with circles in the corresponding cells, and they have been indicated as horizontal lines in the color bar. Completely white cells correspond to missing data points that have been omitted due to either being zero or infinite.
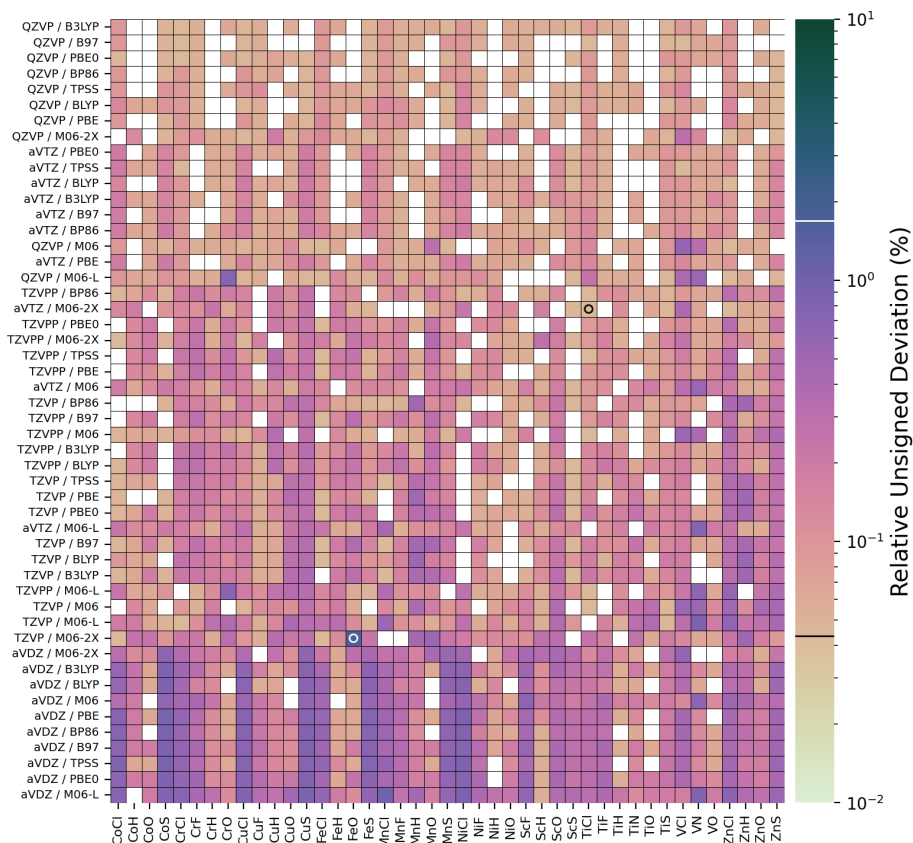
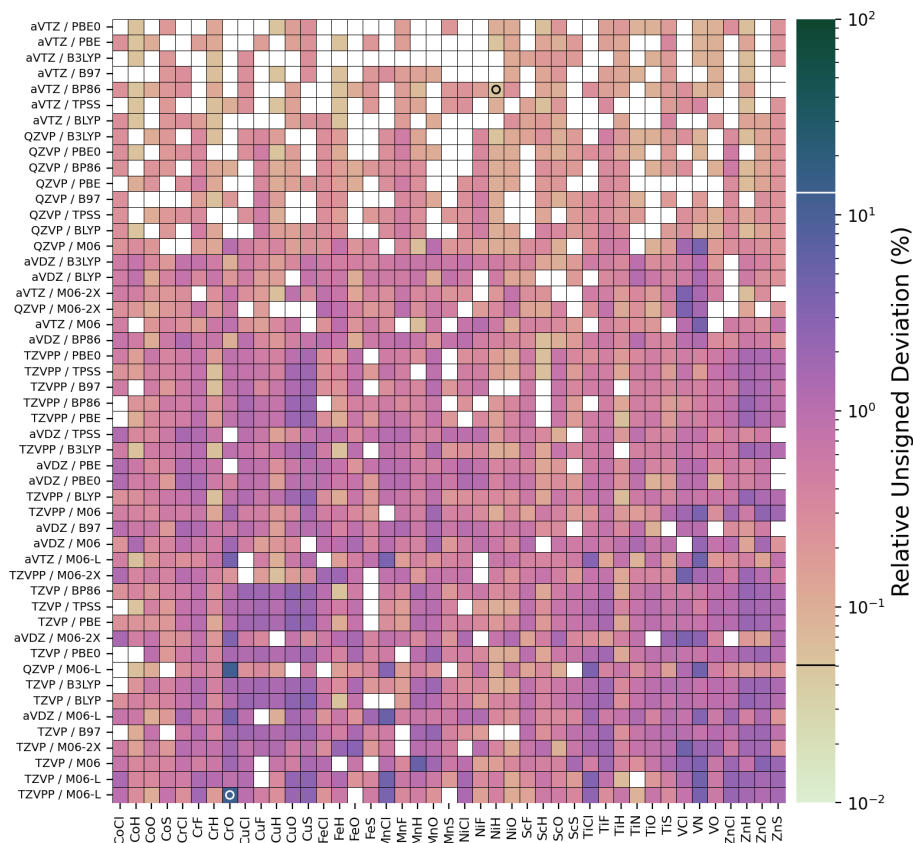**FIGURE 4.5:** Estimated basis set errors in harmonic frequencies for TM diatomics for a variety of common combinations of DFA and basis set [78]. The largest and smallest errors have been highlighted with circles in the corresponding cells, and they have been indicated as horizontal lines in the color bar. Completely white cells correspond to missing data points that have been omitted due to either being zero or infinite.

4.3 Summary of Paper II

Benchmarks with the main intention to compute TM properties at the CBS limit and to study the convergence to it, are relatively few in number. The aim of this paper was to partially close the gap by providing a set of CBS association energies computed with MWs, and compare to a diverse set of commonly used GTO basis sets. We also intended to compare CP-corrected association energies to uncorrected ones. This will aid the applied computational chemistry community in making rational choices on which basis sets to use in studies of energetics for metal-ligand interactions. In addition, the MW basis allowed us to quantify BSIEs in the largest, all-electron GTO basis sets available for TM complexes. Further, such a reference data set can be of use in the development of new methods and algorithms in quantum chemistry. The fact that a MW basis is guaranteed to converge to the actual CBS limit, and that the user can define a precision with respect to this limit, makes it the ideal protocol when collecting reference data in basis set convergence studies.

We selected 26 association reactions that spanned three different 3d TM frameworks and multiple ligands that exhibit different interactions with the metal (π donation from alkenes, σ donation from H_2, σ-donation from common solvents, and σ donation from NHCs). All chemical species were in closed-shell electron configurations, and an overview of these systems are shown in Figure 4.6. We computed association energies with the PBE functional together with 25 commonly used basis sets (Ahlrichs, Dunning, Pople, and Jensen families) ranging from DZ to augmented QZ quality, with and without CP corrections. In addition, we performed a thorough validation of the basis set convergence in association energies for all reactions at increasing levels of MW precision, to secure benchmark quality energies and to demonstrate the systematic convergence behavior of MWs.
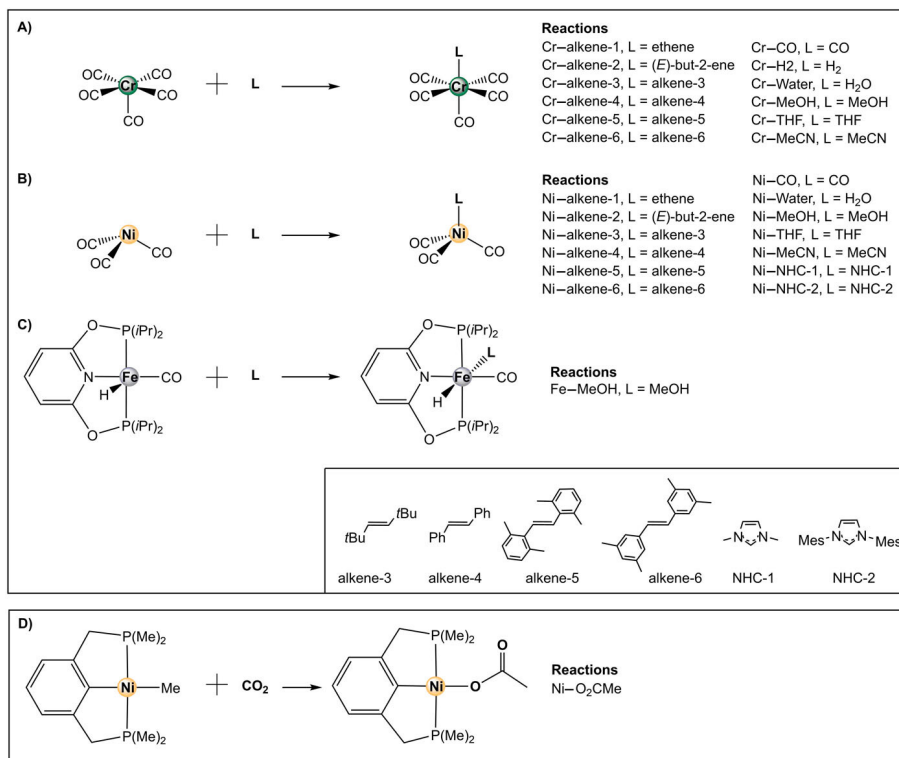
FIGURE 4.6: Overview of the 26 different reactions studied in our CBS analysis of TM-ligand association energies. Figure reproduced from Paper II with permission from AIP Publishing.

We investigated two types of errors associated with GTO basis sets: BSSEs and BSIEs. For BSSEs we found, unsurprisingly, that both the magnitude of the error (Figure 2 in Paper II) and its ratio to the association energy (Figure 4 in Paper II) decreased as the basis sets increased. Jensen basis sets consistently performed the best for TZ and QZ basis sets, but aug-cc-pVDZ led to the smallest BSSE among the DZ basis sets. The Pople basis set 6-311G(d,p) performed uncharacteristically poorly compared to other TZ basis sets, and more akin to DZ basis sets, but this has previously been attributed to a poor construction of the basis set
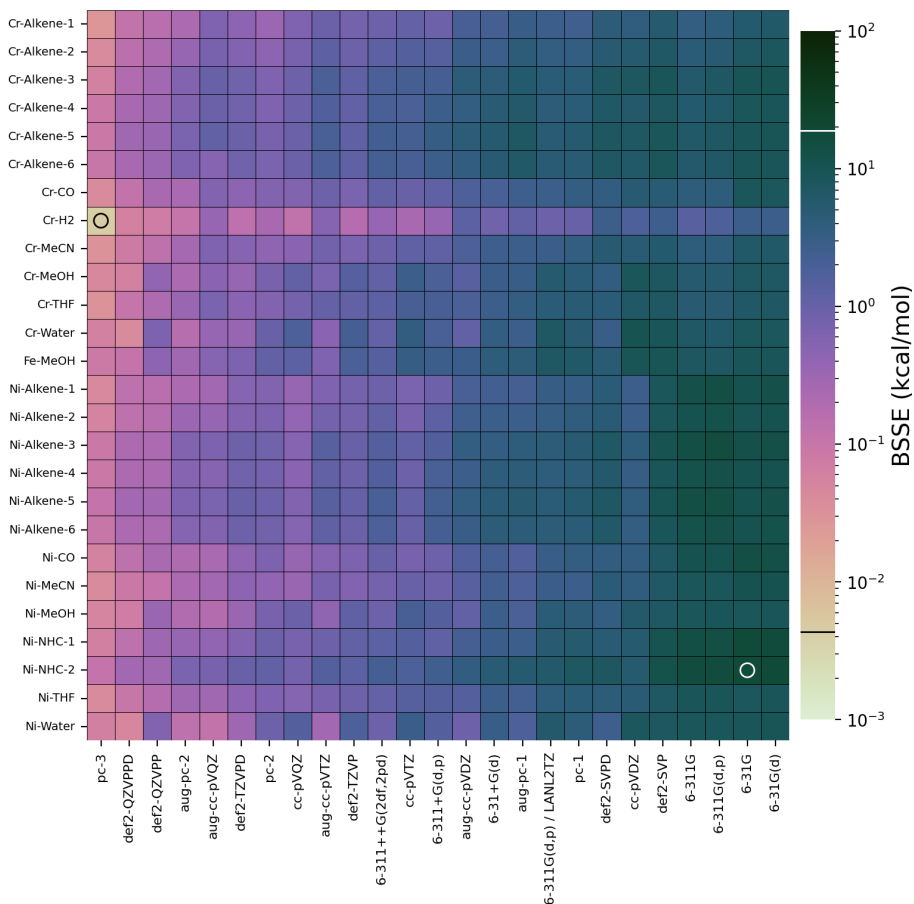
FIGURE 4.7: Overview of basis set superposition errors (kcal/mol) for a range of GTO basis sets, computed for 26 TM-ligand association reactions.

[79]. The BSSEs in kcal/mol are presented as a heatmap in Figure 4.7. The largest BSSE is seen for the Ni–NHC-2 reaction computed with the 6-31G basis set, and the smallest one for the $Cr-H_2$ reaction computed with the pc-3 basis set.

For BSIEs, the same trend of smaller errors for larger basis sets

was observed, and the Jensen basis sets delivered the smallest errors at the TZ and QZ level, with CP-uncorrected pc-3 delivering BSIEs consistently below approximately 0.2 kcal/mol. Most DZ and TZ basis sets greatly benefited from the CP correction, but for QZ basis sets this was not so clear. We also found that CP-uncorrected association energies tended to be too low while CP-corrected energies tended to be too high, in support of previous investigations [80]. Figure 4.8 summarizes BSIEs in CP-uncorrected reaction energies, presented as a heatmap, with MW5 errors also included as level of comparison (the reference used in the evaluations of BSIEs was MW7).

Another highlight of our study concerns the simplification of computational protocols. While we specifically studied association reaction where a CP correction easily can be carried out, more complex association schemes are common throughout organometallic chemistry, and the CP correction is often ambiguous and not easy to use. Any CP correction will always either involve performing multiple single-point energy calculations or, in the case of automated CP algorithms, the generation of more complex input files where each fragment is uniquely defined. We highlighted this point by computing CP-corrected and uncorrected association energies for a CO_2 insertion reaction, where CO_2 is inserted into a Ni–C bond. Here, a CP correction is not straightforward to do; if one tries to split up the reaction into several sub-steps, compute CP corrections for these individually and then add them up, then a highly complex computational protocol is necessary. Each CP correction requires four additional single-point calculations in addition to the uncorrected one, which quickly adds up both in manual labor and CPU time. The MW basis solves this difficulty by attacking the problem at its roots: MW basis functions do not follow the nuclei, but are instead represented as values on a fixed grid. The computed association energy is therefore completely free of BSSEs, and the only error present due to the basis set is the one originating from the finite basis set. A practically

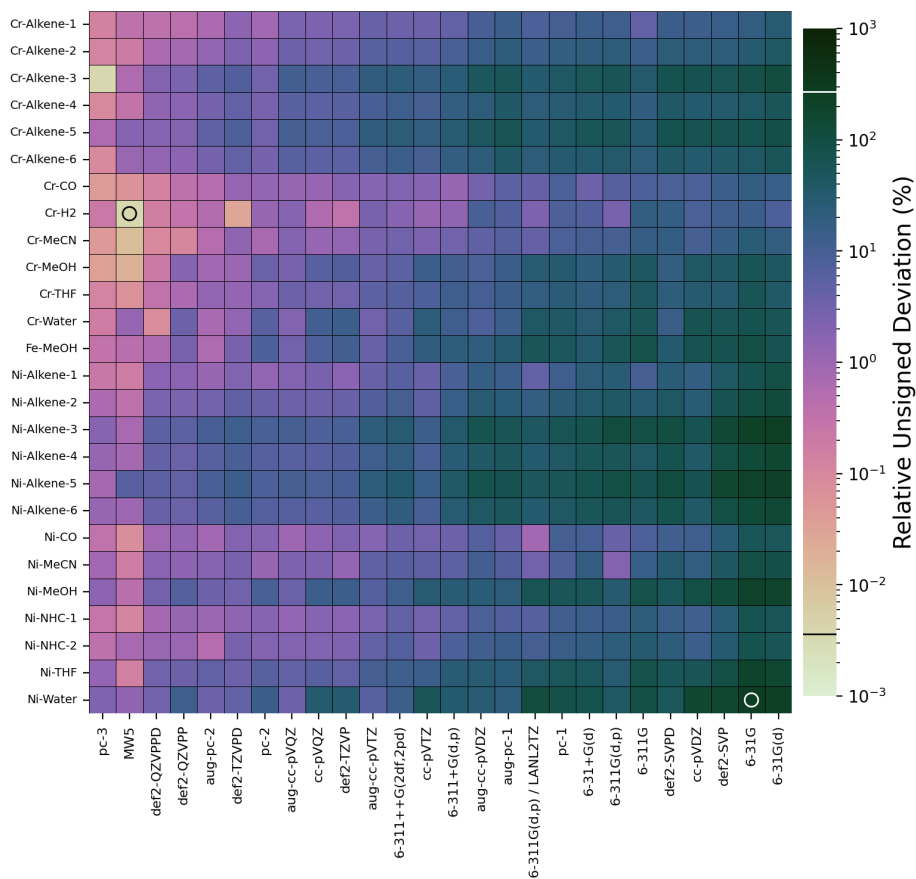**FIGURE 4.8:** Basis set incompleteness errors for CP-uncorrected association energies. For comparison, MW results with a precision of 1×10^{-5} are also included. Reference energies were computed with MWs with a precision of 1×10^{-7}.

complicated computational protocol involving a multi-step mechanism with several incoming and outgoing species (*e.g.*, a catalytic cycle) can be simplified greatly by the use of a MW basis set, and the resulting energies will have a quantifiable basis set error.

To summarize, we provided highly precise TM-ligand association energies for 26 reactions to within at least 1 cal/mol of the CBS limit. Using this reference data set, we quantified BSIEs in commonly used GTO basis sets when applied to the same set of reactions. We also demonstrated how a MW basis simplifies the computational protocol for studies of complex reaction pathways, since the computed association energies are guaranteed to be free from BSSEs. All of our raw data has been deposited as a DataVerse at the UiT Open Research portal, and is freely available [81]. Hopefully our reference data set can be used in future validation studies of TM-metal interactions or method developments.

5

Scalar relativistic effects with Multiwavelets

5.1 Why the need for relativistic effects?

Non-relativistic quantum chemistry is sufficient to describe a lot of interesting chemistry. The elements most important for life and our biological processes (C, H, oxygen (O), Phosphorus (P), S, Cl, sodium (Na), calcium (Ca), Fe, and a few more trace elements), do not require a relativistic treatment in order to obtain reasonably accurate energies and geometries. However, as one moves down the periodic table, the increasing nuclear charge leads to very high velocities of the core electrons. A rule of thumb is that elements of the first three rows of the periodic table do not exhibit significant relativistic effects, elements in the fourth row start to be affected slightly (but they can still be neglected to decent accuracy), but from row five and below relativity needs to be accounted for. Relativistic effects appear to be particularly strong for gold (Au), an observation referred to as "the gold maximum of relativistic effects" [82].

The theory of special relativity leads to several new effects. All of

these could be termed "relativistic effects", since they would not occur in a non-relativistic framework. Elementary expositions of the theory often mention phenomena such as time dilation, Lorentz-Fitzgerald contraction, and simultaneity [83, 84]. However, effects related to time are not relevant for the relativistic treatment of time independent quantum chemistry. The effects relevant to quantum chemistry are classified as scalar relativistic effects and spin-orbit coupling effects. Scalar relativistic effects manifest due an increase of the electron mass when electrons approach the speed of light. This is essentially a consequence of the famous Einstein equation

$$E = \frac{mc^2}{\sqrt{1 - \frac{v^2}{c^2}}} \tag{5.1}$$

since if the energy decreases then the mass must increase (the ratio $\frac{E}{m}$ is equal to a constant). Spin-orbit coupling take into account the electron spin, and becomes necessary when highly accurate energies are needed, or when computing properties that rely on the explicit treatment of electron spin.

It is, however, worth to consider what is meant when stating that a particular effect or phenomenon is due to a relativistic treatment of quantum chemistry. We can perhaps classify relativistic effects into three categories. The first category contains phenomena that are simply not possible to describe mathematically outside of a relativistic framework. One example could be spin-orbit coupling, which leads to magnetic interactions in the Hamiltonian. For example, spin-orbit coupling allows for the study of spin-mixed conical intersections, which play an important role in non-adiabatic processes taking place in photochemical reactions and chemiexcitation [85, 86]. While spin-orbit effects can be included in an *ad hoc* way, for example with pertubation theory, they regardless need to be accounted for in order to compute properties that rely on them. The second category contains phenomena that

are described in a qualitatively incorrect manner in a non-relativistic calculation. Two famous examples are that non-relativistic quantum chemistry incorrectly predicts the color of Au to be silver and the state of mercury (Hg) to be a solid at room temperature. Another interesting example is an investigation of the transfer of a methyl group from a cobalt corrinoid to a $Hg^{II}(SCH_3)$ substrate [87], where the authors found that a spin-orbit relativistic treatment predicted a concerted mechanism, while a non-relativistic calculation predicted a step-wise mechanism. The third category is perhaps the most common one, and contains phenomena that are described with decent accuracy in a non-relativistic framework, but which needs relativity to be included when high accuracy is needed. Scalar relativistic effects, for example, have been found to be important for certain properties computed for 3d-transition metals [88, 89].

A popular method for including scalar relativistic effects is the scalar version of the ZORA. More details about this approximation are given in Section 2.6. This method can be implemented in many quantum chemistry software packages, since the general design of the non-relativistic SCF implementation does not need to change much. Effectively one just need to replace the non-relativistic kinetic energy operator with the ZORA version

$$T^{NR} = \frac{1}{2}\mathbf{p}^2 \tag{5.2}$$

$$T^{ZORA} = \frac{1}{2}\mathbf{p} \cdot \left(1 - \frac{V}{2c^2}\right)^{-1} \mathbf{p} \tag{5.3}$$

$$= -\frac{1}{2}\nabla \cdot \kappa \nabla; \quad \kappa = \left(1 - \frac{V}{2c^2}\right)^{-1} \tag{5.4}$$

This high similarity to the non-relativistic problem should in principle mean that ZORA MOs exhibit similar basis set errors to corresponding non-relativistic MOs. The relativistic contraction of core s and p orbitals should require slightly more tight Gaussian functions, while the

relativistic expansion of d and f orbitals should require slightly more diffuse Gaussian functions. However, these requirements come naturally out of the parameter optimization procedure used in the construction of a basis set optimized for ZORA, and therefore poses no challenges to the user. Therefore, the challenge lies not in the physical description of ZORA orbitals, but rather in the development of all-electron GTO basis sets for heavy elements in general. The small number of all-electron basis sets for heavy elements is an indication of the difficult and time-intensive process of parametrizing large GTO basis sets for heavy elements.

5.2   Deriving the ZORA equations

During the prototyping of a ZORA implementation into the MRChem software, several different algorithms were attempted. Normally, the error in the energy should be quadratic in the orbital errors, but we were not able to achieve this until recently. Attempt 1 as defined below ended up being the successful implementation, but the derivations for the other attempts are also shown for completeness. We believe the source of the poorer energy convergence was related to numerical errors in the Laplacian operator ∇^2.

The starting point for all ZORA implementations is the definition of the Fock operator $\mathcal{F}$

$$\mathcal{F}\phi_i = (T^{\text{zora}} + V)\phi_i = \sum_j F_{ij}\phi_j \tag{5.5}$$

$$= (-\frac{1}{2}\kappa\nabla^2 - \frac{1}{2}\nabla\kappa \cdot \nabla + V)\phi_i = \sum_j F_{ij}\phi_j \tag{5.6}$$

The boxed equations below represent the implemented attempts. The general strategy is to isolate $(\nabla^2 - 2F_{ii})\phi_i$ on the left hand side, so

that the Helmholtz operator $\mathcal{G}$ can be applied to yield a self-consistent expression for orbital ϕ_i in the integral formulation.

Attempt 1

We divide Equation (5.6) by κ

$$-\frac{1}{2}\nabla^2\phi_i - \frac{1}{2}\frac{\nabla\kappa}{\kappa}\cdot\nabla\phi_i + \frac{V}{\kappa}\phi_i = \frac{1}{\kappa}\sum_j F_{ij}\phi_j \tag{5.7}$$

and then take out the diagonal terms $j = i$

$$-\frac{1}{2}\nabla^2\phi_i - \frac{1}{2}\frac{\nabla\kappa}{\kappa}\cdot\nabla\phi_i + \frac{V}{\kappa}\phi_i = \frac{F_{ii}}{\kappa}\phi_i + \frac{1}{\kappa}\sum_{j\neq i} F_{ij}\phi_j \tag{5.8}$$

Using that

$$\frac{1}{\kappa} = 1 - \frac{V^{\text{zora}}}{2c^2} \tag{5.9}$$

and rearranging, we get

$$-\frac{1}{2}(\nabla^2 - 2F_{ii})\phi_i = \frac{1}{2}\frac{\nabla\kappa}{\kappa}\cdot\nabla\phi_i - \frac{V}{\kappa}\phi_i - \frac{F_{ii}}{2c^2}V^{\text{zora}}\phi_i + \frac{1}{\kappa}\sum_{j\neq i} F_{ij}\phi_j \tag{5.10}$$

Converting to integral form, we finally get

$$\boxed{\phi_i = -2\mathcal{G}\left[\left(-\frac{1}{2}\frac{\nabla\kappa}{\kappa}\cdot\nabla + \frac{V}{\kappa} + \frac{F_{ii}}{2c^2}V^{\text{zora}}\right)\phi_i - \frac{1}{\kappa}\sum_{j\neq i} F_{ij}\phi_j\right]} \tag{5.11}$$

Attempt 2

We start by adding $\pm\frac{1}{2}\nabla^2\phi_i$ to Equation (5.6)

$$-\frac{1}{2}\nabla^2\phi_i + \frac{1}{2}\nabla^2\phi_i - \frac{1}{2}\kappa\nabla^2\phi_i - \frac{1}{2}\nabla\kappa\cdot\nabla\phi_i + V\phi_i = \sum_j F_{ij}\phi_j \tag{5.12}$$

Rearrange

$$\frac{1}{2}(1-\kappa)\nabla^2\phi_i - \frac{1}{2}\nabla^2\phi_i - \frac{1}{2}\nabla\kappa\cdot\nabla\phi_i + V\phi_i = \sum_j F_{ij}\phi_j \qquad (5.13)$$

Take out the diagonal elements $j = i$

$$\frac{1}{2}(1-\kappa)\nabla^2\phi_i - \frac{1}{2}\nabla^2\phi_i - \frac{1}{2}\nabla\kappa\cdot\nabla\phi_i + V\phi_i = F_{ii}\phi_i + \sum_{j\neq i} F_{ij}\phi_j \qquad (5.14)$$

and rearrange

$$-\frac{1}{2}(\nabla^2 - 2F_{ii})\phi_i = -\frac{1}{2}(1-\kappa)\nabla^2\phi_i + \frac{1}{2}\nabla\kappa\cdot\nabla\phi_i - V\phi_i + \sum_{j\neq i} F_{ij}\phi_j \quad (5.15)$$

Convert to integral form

$$\boxed{\phi_i = -2\mathcal{G}\left[\left(\frac{1}{2}(1-\kappa)\nabla^2 - \frac{1}{2}\nabla\kappa\cdot\nabla + V\right)\phi_i - \sum_{j\neq i} F_{ij}\phi_j\right]} \qquad (5.16)$$

Attempt 3

We start from the unexpanded form of the kinetic energy operator

$$T^{\text{zora}} = -\frac{1}{2}\nabla\cdot\kappa\nabla \qquad (5.17)$$

Substitution of $\phi_i \rightarrow \phi_i = \frac{1}{\sqrt{\kappa}}\tilde{\phi}_i$ (and storing the factor of -1/2 on the left hand side for convenience) yields

$$-2T^{\text{zora}}\frac{\tilde{\phi}_i}{\sqrt{\kappa}} = \nabla\cdot\kappa\nabla\frac{\tilde{\phi}_i}{\sqrt{\kappa}} \qquad (5.18)$$

Using the quotient rule, the right hand side can be developed

$$\nabla \cdot \kappa \nabla \frac{\tilde{\phi}_i}{\sqrt{\kappa}} = \nabla \cdot \kappa \left[\frac{\sqrt{\kappa} \nabla \tilde{\phi}_i - \tilde{\phi}_i \nabla \sqrt{\kappa}}{\kappa} \right] \tag{5.19}$$

$$= \nabla \sqrt{\kappa} \cdot \nabla \tilde{\phi}_i + \sqrt{\kappa} \nabla^2 \tilde{\phi}_i - \nabla \tilde{\phi}_i \cdot \nabla \sqrt{\kappa} - \tilde{\phi}_i \nabla^2 \sqrt{\kappa} \tag{5.20}$$

$$= \sqrt{\kappa} \nabla^2 \tilde{\phi}_i - \tilde{\phi}_i \nabla^2 \sqrt{\kappa} \tag{5.21}$$

The final expression for the kinetic energy operator then becomes (reinstating the factor -1/2 on the right hand side)

$$T^{\text{zora}} = -\frac{1}{2} \sqrt{\kappa} \nabla^2 \tilde{\phi}_i - \frac{1}{2} \tilde{\phi}_i \nabla^2 \sqrt{\kappa} \tag{5.22}$$

The starting point for deriving the self-consistent equations then becomes

$$(T^{\text{zora}} + V) \frac{\tilde{\phi}_i}{\sqrt{\kappa}} = \sum_j F_{ij} \frac{\tilde{\phi}_j}{\sqrt{\kappa}} \tag{5.23}$$

$$-\frac{1}{2} \sqrt{\kappa} \nabla^2 \tilde{\phi}_i + \frac{1}{2} \nabla^2 \sqrt{\kappa} \tilde{\phi}_i + \frac{V}{\sqrt{\kappa}} \tilde{\phi}_i = \frac{1}{\sqrt{\kappa}} \sum_j F_{ij} \tilde{\phi}_j \tag{5.24}$$

Divide by $\sqrt{\kappa}$

$$-\frac{1}{2} \nabla^2 \tilde{\phi}_i + \frac{1}{2} \frac{\nabla^2 \sqrt{\kappa}}{\sqrt{\kappa}} \tilde{\phi}_i + \frac{V}{\kappa} \tilde{\phi}_i = \frac{1}{\kappa} \sum_j F_{ij} \tilde{\phi}_j \tag{5.25}$$

Take out diagonal elements $j = i$, and use that $\frac{1}{\kappa} = 1 - \frac{V^{\text{zora}}}{2c^2}$

$$-\frac{1}{2} \nabla^2 \tilde{\phi}_i + \frac{1}{2} \frac{\nabla^2 \sqrt{\kappa}}{\sqrt{\kappa}} \tilde{\phi}_i + \frac{V}{\kappa} \tilde{\phi}_i = F_{ii} \tilde{\phi}_i - \frac{F_{ii}}{2c^2} V^{\text{zora}} \tilde{\phi}_i + \frac{1}{\kappa} \sum_{j \neq i} F_{ij} \tilde{\phi}_j \tag{5.26}$$

Rearrange

$$-\frac{1}{2} (\nabla^2 - 2F_{ii}) \tilde{\phi}_i = -\frac{1}{2} \frac{\nabla^2 \sqrt{\kappa}}{\sqrt{\kappa}} \tilde{\phi}_i - \frac{V}{\kappa} \tilde{\phi}_i - \frac{F_{ii}}{2c^2} V^{\text{zora}} \tilde{\phi}_i + \frac{1}{\kappa} \sum_{j \neq i} F_{ij} \tilde{\phi}_j \tag{5.27}$$

Convert to integral form

$$\tilde{\phi}_i = -2\mathcal{G}\left[\left(\frac{1}{2}\frac{\nabla^2\sqrt{\kappa}}{\sqrt{\kappa}} + \frac{V}{\kappa} + \frac{F_{ii}}{2c^2}V^{\text{zora}}\right)\tilde{\phi}_i - \frac{1}{\kappa}\sum_{j\neq i}F_{ij}\tilde{\phi}_j\right] \qquad (5.28)$$

Attempt 4

Here we reformulate Equation (5.16) fully in terms of $1 - \kappa$, using that $\nabla\kappa = -\nabla(1 - \kappa)$

$$\phi_i = -2\mathcal{G}\left[\left(\frac{1}{2}(1-\kappa)\nabla^2 + \frac{1}{2}\nabla(1-\kappa)\cdot\nabla + V\right)\phi_i - \sum_{j\neq i}F_{ij}\phi_j\right] \qquad (5.29)$$

5.3 Tests and validations

We have performed several tests to validate the implementations. Table 5.1 shows SCF convergence parameters for Attempts 1 and 2, such as energy changes and MO residuals, for the elements of row 5 in the periodic table. The key thing to note here is the much better energy convergence obtained in Attempt 1, most likely because there is no ∇^2 term in Equation (5.11). We can also see that the two attempts result in the same energies (at least to within the precision and convergence), a further indication that the implementations are correct.

Table 5.2 shows a comparison of energies obtained for a small set of main group atoms and molecules, where the ZORA non-relativistic limit is compared to regular non-relativistic calculations. Note that the noble gas atoms are in their helium-like ionic configurations (Ne^{8+}, Ar^{16+}, and so on). The data shows that the correct non-relativistic limit is obtained when using very large light speeds. While not a rigorous proof that the implementation is bug-free, it serves at least as one form

TABLE 5.1: Comparison of SCF convergence data at the MW8 precision level for ZORA attempts 1 and 2, where ΔE is the energy update, E is the total energy, and δ is the MO residual. All numbers are given in atomic units.

Atom	ΔE^{A1}	ΔE^{A2}	E^{A1}	E^{A2}	δ^{A1}	δ^{A2}
Rb	1.8e-08	1.4e-04	-3013.6351932639	-3013.6346413261	1.6e-06	1.9e-06
Sr	4.8e-08	1.4e-04	-3215.7852970112	-3215.7845703612	1.5e-06	1.7e-06
Y	3.9e-06	1.7e-06	-3425.7021986142	-3425.7021668255	1.8e-06	8.9e-07
Zr	1.6e-09	nan	-3643.6343461367	nan	9.0e-07	nan
Nb	1.2e-08	1.4e-04	-3869.7494369446	-3869.7489442815	1.1e-06	1.7e-06
Mo	1.5e-08	8.6e-05	-4104.1814757869	-4104.1809948135	1.0e-06	9.8e-07
Tc	8.3e-08	1.2e-04	-4346.9529323659	-4346.9523017123	1.2e-06	1.3e-06
Ru	7.0e-08	2.3e-05	-4598.3180774254	-4598.3173794074	1.8e-06	1.6e-06
Rh	4.8e-09	1.2e-04	-4858.4093472367	-4858.4088005040	5.3e-07	1.0e-06
Pd	5.9e-09	6.7e-05	-5127.4060602754	-5127.4052534048	6.4e-07	1.0e-06
Ag	6.9e-08	2.5e-05	-5405.3863408027	-5405.3854221617	1.0e-06	1.6e-06
Cd	8.0e-08	4.1e-06	-5692.4062620562	-5692.4048906514	2.4e-06	1.5e-06
In	8.0e-08	2.3e-04	-5988.4129111014	-5988.4114647375	8.1e-07	1.4e-06
Sn	4.5e-07	1.2e-04	-6293.6521885078	-6293.6515265108	1.9e-06	1.8e-06
Sb	9.4e-08	nan	-6608.2620334194	nan	9.1e-07	nan
Te	3.3e-08	5.3e-05	-6932.3098799744	-6932.3090488738	1.0e-06	6.9e-07
I	3.6e-09	9.0e-05	-7265.9967158775	-7265.9960042123	3.8e-07	1.4e-06
Xe	2.8e-07	2.5e-04	-7609.4698878767	-7609.4676868306	1.1e-06	1.5e-06

TABLE 5.2: Comparison of energies obtained with Attempt 1 at the ZORA non-relativistic limit (evaluated at $1000c$) and regular non-relativistic calculations at the MW6 precision level. The last column, ΔE, shows the absolute energy difference between the non-relativistic energy and the ZORA non-relativistic limit energy. All numbers are given in atomic units.

Atom	E^{zora}_{1000c}	E^{NR}	ΔE
He	-2.892935491418813	-2.892935491135128	2.8368463134e-10
Ne^{8+}	-93.79226382987301	-93.79226358279418	2.4707883028e-07
Ar^{16+}	-312.6875153796463	-312.6875127465987	2.6330475861e-06
Kr^{34+}	-1273.201397756162	-1273.201353956275	4.379988695e-05
H_2O	-76.38852580283374	-76.38852568901055	1.1382319087e-07
LiH	-8.047347899171163	-8.04734789762583	1.5453327506e-09

for sanity check. Attempts 3 and 4 gave similar results to Attempt 2, in the sense that they resulted in the same energy and the same energy convergence.

5.4 Comparison with GTOs

Having found an implementation that yields the expected quadratic convergence of the energy, we proceeded to compute energies with all-electron GTO basis sets for a preliminary comparison of GTO basis set errors. The GTO basis sets included in this comparison were the ANO-RCC-VQZP [90–92], ANO-R3 [93, 94], SARC-ZORA-TZVPP [95], UGBS [96], and Sapporo-QZP-2012-Diffuse basis sets [97]. All basis sets were obtained with the Python Application Programming Interface to the Basis Set Exchange [6, 7, 98], and the GTO calculations were performed with ORCA [70] version 5.0.1.[†] The resolution of the identity approximation was turned off (`!nori`), extra tight SCF convergence was requested (`!verytightscf`), and the largest default integration grid "defgrid3" was used (`!defgrid3`), in order to try and isolate the basis set errors.

An overview of BSIEs for these GTO basis sets computed with the PBE functional [24] is given in Figure 5.1. The reference MW precision was set to 1×10^{-8}. The BSIEs systematically increase across the fifth period. UGBS is the best performer, with all errors below 0.1 Hartree. The second best is SARC-ZORA-TZVPP, which exhibits errors of just above 0.1 Hartree for rubidium (Rb) and just below 1 Hartree for xenon (Xe). The other basis sets were developed mainly for correlated wavefunction methods, which likely explains the rather poor convergence observed here for PBE energies.

We have also computed basis set errors for individual orbital energies for all species. Examples for Rb, silver (Ag), and tin (Sn) are given in Figures 5.2 to 5.4, respectively. Both unsigned deviations (UDs) (given in Hartree) and RUDs (given in percent) are shown in the figure. For the three examples given here, the RUDs for UGBS tend to reach

---

[†]Recently ORCA version 5.0.2 was released that fixes a race condition bug relevant for the work presented here. I have redone most elements with the new version, which did not alter the results, but the data shown were computed with version 5.0.1.
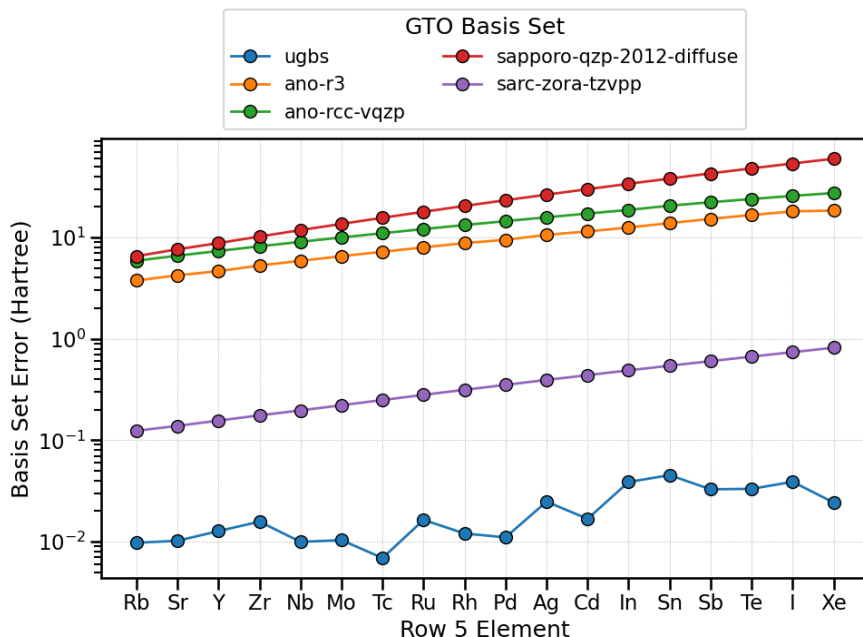
FIGURE 5.1: Basis set incompleteness errors in total energies for row 5 elements for five all-electron GTO basis sets compared to a MW8 reference.

a plateau upon moving from core to valence orbitals. This plateauing leads to an increase in RUDs, due to the smaller orbital energies for the valence region. The same is not observed for the other basis sets, where UDs tend to be largest for core orbitals, and then decrease as one moves toward the valence region. This behavior leads instead to a plateau of the RUDs.

Our preliminary results show that SARC-ZORA-TZVPP and UGBS are not very well converged for total ZORA energies with respect to the CBS limit. Naturally, the errors of relative energies will be more relevant to actual applications than total energies, and we have ongoing work in the group where we plan to extend the analysis to ionization energies

of row 5 elements, and to more chemically relevant transition metal systems. The errors are likely to be larger for molecules, since GTO basis sets are to some extent inherently biased toward atomic orbitals. Nonetheless, our results show that for row 5 elements, in order to obtain relative energies correct to a couple of decimal places, it is necessary for errors of an order of 1×10^{-2}—1×10^{0} in total energies to cancel fortuitously.

FIGURE 5.2: Basis set errors for α and β orbital energies for Rb. Each row corresponds to a different GTO basis set, and each column to orbitals of different spin. The reference data was computed with MWs at a precision of 1×10^{-8}. The red lines show RUDs in percent, while the teal lines show UDs in Hartrees.
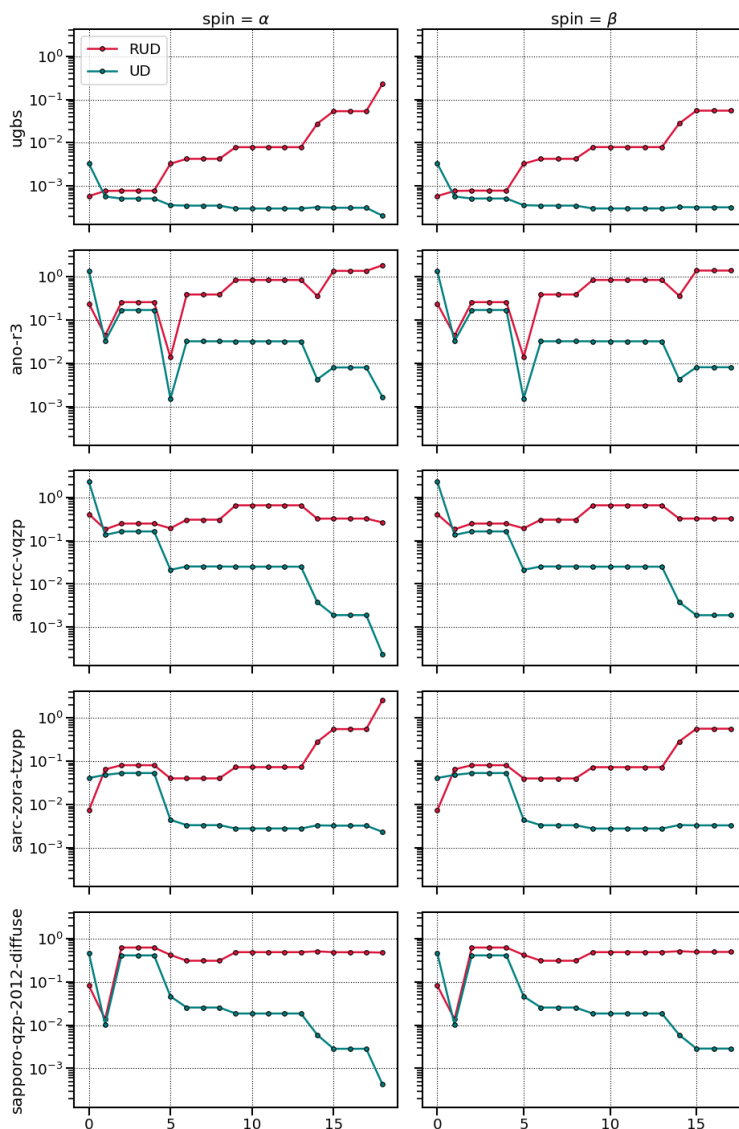
Figure 5.3: Basis set errors for α and β orbital energies for Ags. Each row corresponds to a different GTO basis set, and each column to orbitals of different spin. The reference data was computed with MWs at a precision of 1×10^{-8}. The red lines show RUDs in percent, while the teal lines show UDs in Hartrees.
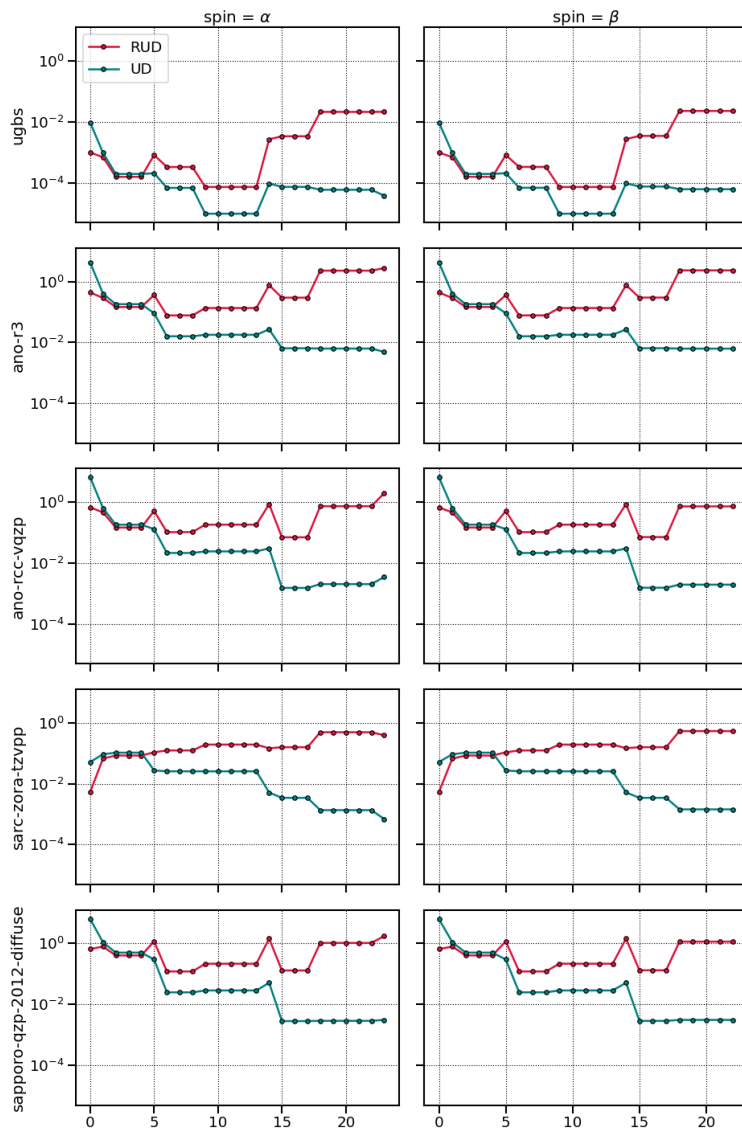
FIGURE 5.4: Basis set errors for α and β orbital energies for Sns. Each row corresponds to a different GTO basis set, and each column to orbitals of different spin. The reference data was computed with MWs at a precision of 1×10^{-8}. The red lines show RUDs in percent, while the teal lines show UDs in Hartrees.
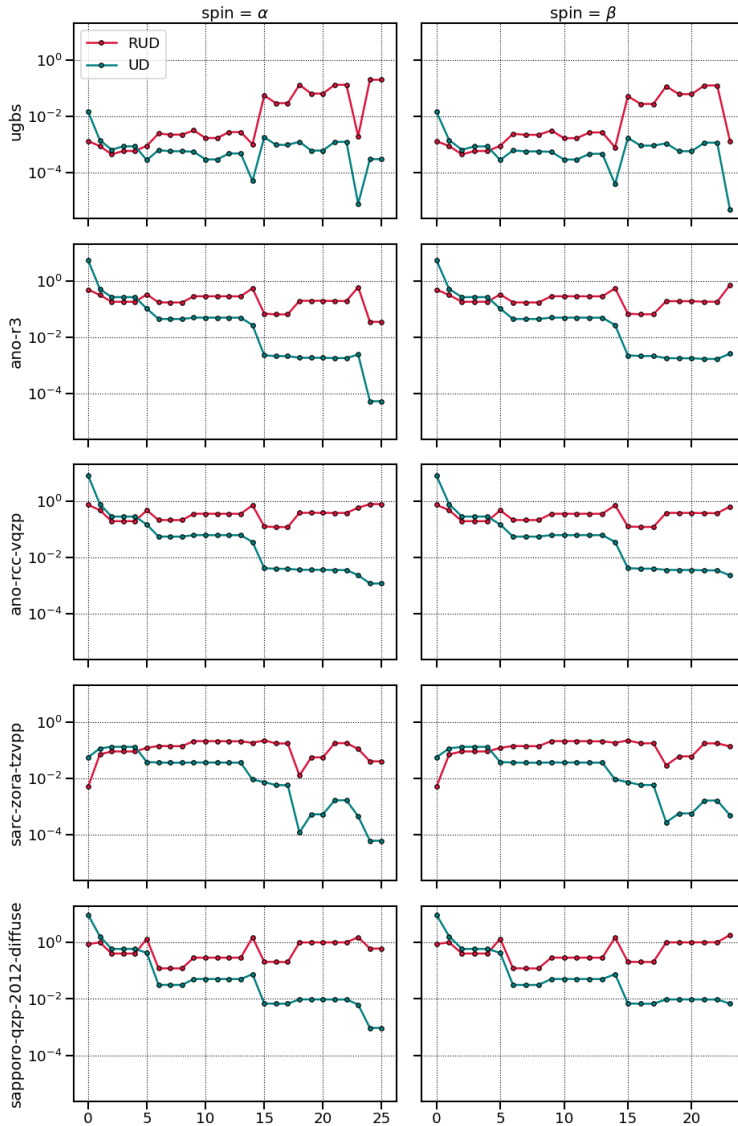
6

CONCLUSIONS AND OUTLOOK

The majority of the work in this thesis has centered around the assessment of basis set incompleteness errors of commonly used GTO basis sets. My work includes the calculation of static polarizabilities and, for the first time, TM-ligand interaction energies with MWs. This has been made possible by the MW implementation available in the MRChem quantum chemistry code, developed in-house at the Hylleraas Centre, due to the robust mathematical foundation in MRA. Using this code, we have been able to quantify basis set errors without ambiguity based on reference data with known errors, something which is difficult to do with conventional GTO basis sets.

In Paper I, we could show that the augmented quintuple zeta basis set aug-pc-4 delivered polarizabilities with basis set errors below 0.5 % for the vast majority of the chemical systems included in our study. The largest basis set errors were observed for open-shell cases, and were approximately 2 %, which should only be significant when very high precision is required. We also demonstrated that MWs can deal with small strengths of the external electric field when computing polarizabilities from FD, since the user can tighten the MW precision to compensate for the weaker responses in the density.

In Paper II, we presented a thorough basis set benchmark of TM-ligand interaction energies for GTO basis sets. We studied 26 association reactions involving ligands commonly used in organometallic chemistry, quantifying BSSEs and BSIEs for these reactions based on objective reference data from MWs. Basis sets from the Jensen, Ahlrichs, Pople, and Dunning families were included, both in augmented and standard forms, ranging from DZ to QZ quality. We showed that the Jensen basis sets overall delivered the smallest errors, with the Ahlrichs closely following. Commonly used variants of the Pople basis sets were shown to deliver larger errors than other comparable basis sets, and we discourage their general use due to the availability of more precise GTO basis sets. Very large basis sets, such as aug-pc-3, were shown to suffer from linear dependencies, which limited the precision we were able to obtain in the interaction energies. This highlights another challenge of basis sets based on non-orthogonal basis functions, which is not present for MWs. We also highlighted an example where a MW protocol for single point corrections is simpler than a corresponding GTO protocol, since MWs by construction are BSSE-free and worrying about whether to perform CP corrections therefore is no longer relevant.

The ZORA implementation (Paper III, in preparation) in MRChem is not complete, and more work needs to be done to sort out the remaining technical challenges. The current implementation only uses the nuclear potential in the ZORA operator κ, and while this is the largest contribution to the scalar relativistic effects we should also include the standard contributions in order to provide functionality similar to other software packages. We have also observed numerical instabilities when our ZORA implementation is used together with the KAIN SCF accelerator, but we are at this time unsure what the cause for this is. ZORA is of course just the beginning of a relativistic theory within the framework of multiwavelets. Work is planned for also implementing infinite order regular approximation (IORA), both in the canonical form and

the so-called "atomic" form. There has also been progress in the group concerning prototyping the implementation of a full four-component implementation for a H atom[†], and there are plans for extending this to the many-electron case and with a full implementation into the MRChem code.

The unique properties of MWs give them tremendous potential as a tool in computational chemistry. The predictable error reduces the need for performing time-consuming mini-benchmarks at the start of new projects, and BSSE-free energies lead to robust results and simpler protocols. MWs are perhaps the largest step toward a black-box situation for basis sets, because they are user-friendly for non-experts. Two major software packages are available today that provide MW functionality within the context of quantum chemistry (MRChem [99, 100] and MADNESS [101]), and the functionality currently available is already sufficient to allow for a diverse set of applications.

Other interesting areas for research is the application of MWs to the development of new GTO basis sets and DFAs, and the generation of good training data for machine learning models. GTO basis sets are today parametrized based on calculations performed with finite basis sets, which introduces an unfortunate bias away from CBS data. One could envision a GTO basis set parametrized completely on CBS reference data obtained from MWs, which perhaps could significantly reduce the average errors produced by such a MW-optimized basis set. The same idea could be applied to the development of new DFAs, since many of these also contain empirically determined parameters. Since the quality of the training data is key to the success of the machine learning models, the use of MWs is a natural choice for generating precise CBS training data. To summarize, MWs have the potential for great impact in the way computational chemistry studies are conducted, and they can be applied to both method development and in computational chemistry

[†]4c hydrogen implementation has been done by Luca Frediani

applications.

However, it takes time to change old habits of computational chemists. Having to download new software (whose methods are founded on mathematical concepts foreign to most chemists) adds an extra barrier-to-entry into the world of MW applications. Future work therefore needs to address the small user-base, for example by showcasing MWs in applications to new areas of chemistry, by relevant benchmarks, by invitations to workshops, and by visibility at conferences and on social media.

Bibliography

[1]   F. Neese, M. Atanasov, G. Bistoni, D. Maganas, and S. Ye. "Chem-
      istry and Quantum Mechanics in 2019: Give Us Insight and
      Numbers". In: *Journal of the American Chemical Society* 141.7 (Jan.
      2019), pp. 2814–2824. ISSN: 1520-5126. DOI: 10.1021/jacs.
      8b13313. URL: http://dx.doi.org/10.1021/jacs.8b13313.

[2]   A. Aspuru-Guzik, R. Lindh, and M. Reiher. "The Matter Simula-
      tion (R)evolution". In: *ACS Central Science* 4.2 (2018), pp. 144–
      152. DOI: 10.1021/acscentsci.7b00550.

[3]   L. Goerigk, A. Hansen, C. A. Bauer, S. Ehrlich, A. Najibi, and
      S. Grimme. "A Look at the Density Functional Theory Zoo with
      the Advanced GMTKN55 Database for General Main Group
      Thermochemistry, Kinetics and Noncovalent Interactions". In:
      Phys. Chem. Chem. Phys. 19.48 (2017), pp. 32184–32215. DOI:
      10.1039/C7CP04913G.

[4]   L. Goerigk and N. Mehta. "A Trip to the Density Functional
      Theory Zoo: Warnings and Recommendations for the User". In:
      Australian Journal of Chemistry 72.8 (2019), p. 563. ISSN: 0004-
      9425. DOI: 10.1071/ch19023. URL: http://dx.doi.org/10.
      1071/CH19023.

[5]   L. Goerigk and M. Casanova-Paéz. "The Trip to the Density
      Functional Theory Zoo Continues: Making a Case for Time-
      Dependent Double Hybrids for Excited-State Problems". In:
      Australian Journal of Chemistry 74 (2021), p. 3. ISSN: 0004-9425.

DOI: 10.1071/ch20093. URL: http://dx.doi.org/10.1071/CH20093.

[6] K. L. Schuchardt, B. T. Didier, T. Elsethagen, L. Sun, V. Guru-moorthi, J. Chase, J. Li, and T. L. Windus. "Basis Set Exchange: A Community Database for Computational Sciences". In: *Journal of Chemical Information and Modeling* 47.3 (2007), pp. 1045–1052. DOI: 10.1021/ci600510j.

[7] B. P. Pritchard, D. Altarawy, B. Didier, T. D. Gibson, and T. L. Windus. "New Basis Set Exchange: An Open, Up-to-Date Resource for the Molecular Sciences Community". In: *Journal of Chemical Information and Modeling* 59.11 (2019), pp. 4814–4820. DOI: 10.1021/acs.jcim.9b00725.

[8] E. R. Davidson and D. Feller. "Basis set selection for molecular calculations". In: *Chemical Reviews* 86.4 (Aug. 1986), pp. 681–696. ISSN: 1520-6890. DOI: 10.1021/cr00074a002. URL: http://dx.doi.org/10.1021/cr00074a002.

[9] D. Feller and D. A. Dixon. "Density Functional Theory and the Basis Set Truncation Problem with Correlation Consistent Basis Sets: Elephant in the Room or Mouse in the Closet?" In: *The Journal of Physical Chemistry A* 122.9 (Feb. 2018). ISSN: 1520-5215. DOI: 10.1021/acs.jpca.8b00392. URL: http://dx.doi.org/10.1021/acs.jpca.8b00392.

[10] B. K. Alpert. "A class of bases in Lˆ2 for the sparse representation of integral operators". In: *SIAM journal on Mathematical Analysis* 24.1 (1993), pp. 246–262.

[11] F. Keinert. "Wavelets and Multiwavelets". In: *Encyclopedia of Complexity and Systems Science*. Ed. by R. A. Meyers. Springer New York, 2009, pp. 5841–5858. ISBN: 978-0-387-30440-3. DOI: 10.1007/978-0-387-30440-3_346.

[12] R. J. Harrison, G. I. Fann, T. Yanai, Z. Gan, and G. Beylkin. "Multiresolution quantum chemistry: Basic theory and initial applications". In: *The Journal of Chemical Physics* 121.23 (Dec. 2004), pp. 11587–11598. ISSN: 1089-7690. DOI: 10.1063/1.1791051. URL: http://dx.doi.org/10.1063/1.1791051.

[13] T. Kato, Y. Yokoi, and H. Sekino. "Basis set limit computation of dynamic polarizability at near-resonance region". In: *International Journal of Quantum Chemistry* 113.3 (May 2012), pp. 286–289. ISSN: 0020-7608. DOI: 10.1002/qua.24148. URL: http://dx.doi.org/10.1002/qua.24148.

[14] S. R. Jensen, S. Saha, J. A. Flores-Livas, W. Huhn, V. Blum, S. Goedecker, and L. Frediani. "The Elephant in the Room of Density Functional Theory Calculations". In: *The Journal of Physical Chemistry Letters* 8.7 (Mar. 2017), pp. 1449–1457. ISSN: 1948-7185. DOI: 10.1021/acs.jpclett.7b00255. URL: http://dx.doi.org/10.1021/acs.jpclett.7b00255.

[15] B. Alpert, G. Beylkin, D. Gines, and L. Vozovoi. "Adaptive Solution of Partial Differential Equations in Multiwavelet Bases". In: *Journal of Computational Physics* 182.1 (2002), pp. 149–190. DOI: https://doi.org/10.1006/jcph.2002.7160.

[16] G. Beylkin, V. Cheruvu, and F. Pérez. "Fast adaptive algorithms in the non-standard form for multidimensional problems". In: *Applied and Computational Harmonic Analysis* 24.3 (May 2008), pp. 354–377. ISSN: 1063-5203. DOI: 10.1016/j.acha.2007.08.001. URL: http://dx.doi.org/10.1016/j.acha.2007.08.001.

[17] L. Frediani, E. Fossgaard, T. Flå, and K. Ruud. "Fully adaptive algorithms for multivariate integral equations using the non-standard form and multiwavelets with applications to the Poisson and bound-state Helmholtz kernels in three dimensions". In: *Molecular Physics* 111.9-11 (July 2013), pp. 1143–1160. ISSN:

1362-3028. DOI: 10.1080/00268976.2013.810793. URL: http://dx.doi.org/10.1080/00268976.2013.810793.

[18] N. Mardirossian and M. Head-Gordon. "Thirty years of density functional theory in computational chemistry: An overview and extensive assessment of 200 density functionals". In: *Molecular Physics* 115.19 (2017), pp. 2315–2372. DOI: 10.1080/00268976.2017.1333644.

[19] M. István. *Simple theorems, proof and derivations in quantum chemistry*. Springer, 2011.

[20] P. Hohenberg and W. Kohn. "Inhomogeneous Electron Gas". In: *Phys. Rev.* 136 (3B Nov. 1964), B864–B871. DOI: 10.1103/PhysRev.136.B864. URL: https://link.aps.org/doi/10.1103/PhysRev.136.B864.

[21] L. H. Thomas. "The calculation of atomic fields". In: *Mathematical Proceedings of the Cambridge Philosophical Society* 23.5 (1927), pp. 542–548. DOI: 10.1017/S0305004100011683.

[22] E. Fermi. "Un Metodo Statistico per la Determinazione di alcune Priopretà dell'Atomo". In: *Rendiconti. Accademia Nazionale dei Lincei* 6 (1927), pp. 602–607.

[23] W. Kohn and L. J. Sham. "Self-Consistent Equations Including Exchange and Correlation Effects". In: *Physical Review* 140 (4A Nov. 1965), A1133–A1138. DOI: 10.1103/PhysRev.140.A1133. URL: https://link.aps.org/doi/10.1103/PhysRev.140.A1133.

[24] J. P. Perdew, K. Burke, and M. Ernzerhof. "Generalized Gradient Approximation Made Simple". In: *Physical Review Letters* 77 (18 1996), pp. 3865–3868. DOI: 10.1103/PhysRevLett.77.3865.

[25] N. Mardirossian and M. Head-Gordon. "How Accurate Are the Minnesota Density Functionals for Noncovalent Interactions, Isomerization Energies, Thermochemistry, and Barrier Heights Involving Molecules Composed of Main-Group Elements?" In: *Journal of Chemical Theory and Computation* 12.9 (Sept. 2016), pp. 4303–4325. ISSN: 1549-9626. DOI: 10.1021/acs.jctc.6b00637. URL: http://dx.doi.org/10.1021/acs.jctc.6b00637.

[26] A. D. Becke. "Density-functional exchange-energy approximation with correct asymptotic behavior". In: *Phys. Rev. A* 38 (6 Sept. 1988), pp. 3098–3100. DOI: 10.1103/PhysRevA.38.3098. URL: https://link.aps.org/doi/10.1103/PhysRevA.38.3098.

[27] C. Lee, W. Yang, and R. G. Parr. "Development of the Colle-Salvetti correlation-energy formula into a functional of the electron density". In: *Phys. Rev. B* 37 (2 Jan. 1988), pp. 785–789. DOI: 10.1103/PhysRevB.37.785. URL: https://link.aps.org/doi/10.1103/PhysRevB.37.785.

[28] A. D. Becke. "Density-functional thermochemistry. III. The role of exact exchange". In: *The Journal of Chemical Physics* 98.7 (1993), pp. 5648–5652. DOI: 10.1063/1.464913.

[29] S. R. Jensen. "Real-space all-electron Density Functional Theory with Multiwavelets". PhD thesis. 2014.

[30] G. te Velde, F. M. Bickelhaupt, E. J. Baerends, C. Fonseca Guerra, S. J. A. van Gisbergen, J. G. Snijders, and T. Ziegler. "Chemistry with ADF". In: *J. Comput. Chem.* 22.9 (2001), pp. 931–967. ISSN: 1096-987X. DOI: 10.1002/jcc.1056. URL: http://dx.doi.org/10.1002/jcc.1056.

[31] F. Jensen. *Introduction to Computational Chemistry*. 2nd ed. John Wiley & Sons, Inc., 2006. ISBN: 0470011874.

[32] S. Boys and F. Bernardi. "The calculation of small molecular interactions by the differences of separate total energies. Some procedures with reduced errors". In: *Molecular Physics* (1970), pp. 553–566. DOI: 10.1080/00268977000101561.

[33] F. B. van Duijneveldt, J. G. C. M. van Duijneveldt-van de Rijdt, and J. H. van Lenthe. "State of the Art in Counterpoise Theory". In: *Chemical Reviews* 94.7 (Nov. 1994), pp. 1873–1885. ISSN: 1520-6890. DOI: 10.1021/cr00031a007. URL: http://dx.doi.org/10.1021/cr00031a007.

[34] J. C. Slater. "Wave Functions in a Periodic Potential". In: *Physical. Reviews* 51 (10 1937), pp. 846–851. DOI: 10.1103/PhysRev.51.846.

[35] J. C. Slater. "Energy Band Calculations by the Augmented Plane Wave Method**The research reported in this paper has been assisted by the National Science Foundation and the Office of Naval Research, as well as by the Army, Navy, and Air Force." In: ed. by P.-O. Löwdin. Vol. 1. Advances in Quantum Chemistry. Academic Press, 1964, pp. 35–58. DOI: 10.1016/S0065-3276(08)60374-3.

[36] P. Blaha, K. Schwarz, F. Tran, R. Laskowski, G. K. H. Madsen, and L. D. Marks. "WIEN2k: An APW+lo program for calculating the properties of solids". In: *The Journal of Chemical Physics* 152.7 (2020), p. 074101. DOI: 10.1063/1.5143061.

[37] O. K. Andersen. "Linear methods in band theory". In: *Phys. Rev. B* 12 (8 Oct. 1975), pp. 3060–3083. DOI: 10.1103/PhysRevB.12.3060. URL: https://link.aps.org/doi/10.1103/PhysRevB.12.3060.

[38] D. D. Koelling and G. O. Arbman. "Use of energy derivative of the radial solution in an augmented plane wave method: application to copper". In: *Journal of Physics F: Metal Physics* 5.11 (Nov.

1975), pp. 2041–2054. ISSN: 0305-4608. DOI: 10.1088/0305-4608/5/11/016. URL: http://dx.doi.org/10.1088/0305-4608/5/11/016.

[39] M. Weinert. "Solution of Poisson's equation: Beyond Ewald-type methods". In: *Journal of Mathematical Physics* 22.11 (Nov. 1981), pp. 2433–2439. ISSN: 1089-7658. DOI: 10.1063/1.524800. URL: http://dx.doi.org/10.1063/1.524800.

[40] E. Wimmer, H. Krakauer, M. Weinert, and A. J. Freeman. "Full-potential self-consistent linearized-augmented-plane-wave method for calculating the electronic structure of molecules and surfaces: O_2 molecule". In: *Phys. Rev. B* 24 (2 July 1981), pp. 864–875. DOI: 10.1103/PhysRevB.24.864. URL: https://link.aps.org/doi/10.1103/PhysRevB.24.864.

[41] D. J. Singh and L. Nordström. *Planewaves, Pseudopotentials and the LAPW Method*. 2nd ed. Springer Science+Business Media, Inc., 2006. ISBN: 978-0-387-29684-5. DOI: 10.1007/978-0-387-29684-5.

[42] L. Lin, J. Lu, and L. Ying. "Numerical methods for Kohn–Sham density functional theory". In: *Acta Numerica* 28 (2019), pp. 405–539. DOI: 10.1017/S0962492919000047.

[43] B. Alpert, G. Beylkin, R. Coifman, and V. Rokhlin. "Wavelet-like bases for the fast solution of second-kind integral equations". In: *SIAM journal on Scientific Computing* 14.1 (1993), pp. 159–184.

[44] R. J. Harrison, G. I. Fann, T. Yanai, and G. Beylkin. "Multiresolution Quantum Chemistry in Multiwavelet Bases". In: *Computational Science — ICCS 2003*. Ed. by P. M. A. Sloot, D. Abramson, A. V. Bogdanov, Y. E. Gorbachev, J. J. Dongarra, and A. Y. Zomaya. Berlin, Heidelberg: Springer Berlin Heidelberg, 2003, pp. 103–110.

[45] T. Yanai, G. I. Fann, Z. Gan, R. J. Harrison, and G. Beylkin. "Multiresolution quantum chemistry in multiwavelet bases: Analytic derivatives for Hartree–Fock and density functional theory". In: *The Journal of Chemical Physics* 121.7 (2004), pp. 2866–2876. DOI: 10.1063/1.1768161.

[46] R. J. Harrison, G. I. Fann, T. Yanai, Z. Gan, and G. Beylkin. "Multiresolution quantum chemistry: Basic theory and initial applications". In: *The Journal of Chemical Physics* 121.23 (2004), pp. 11587–11598. DOI: 10.1063/1.1791051.

[47] T. Yanai, G. I. Fann, Z. Gan, R. J. Harrison, and G. Beylkin. "Multiresolution quantum chemistry in multiwavelet bases: Hartree–Fock exchange". In: *The Journal of Chemical Physics* 121.14 (2004), pp. 6680–6688. DOI: 10.1063/1.1790931.

[48] D. Gines, G. Beylkin, and J. Dunn. "LU Factorization of Nonstandard Forms and Direct Multiresolution Solvers". In: *Applied and Computational Harmonic Analysis* 5.2 (1998), pp. 156–201. DOI: https://doi.org/10.1006/acha.1997.0227.

[49] G. Beylkin, V. Cheruvu, and F. Pérez. "Fast adaptive algorithms in the non-standard form for multidimensional problems". In: *Applied and Computational Harmonic Analysis* 24.3 (2008), pp. 354–377. DOI: https://doi.org/10.1016/j.acha.2007.08.001.

[50] B. Fornberg. "Generation of finite difference formulas on arbitrarily spaced grids". In: *Mathematics of Computation* (1988), pp. 699–706. DOI: 10.1090/S0025-5718-1988-0935077-0.

[51] R. M. Sternheimer. "Electronic Polarizabilities of Ions from the Hartree-Fock Wave Functions". In: *Phys. Rev.* 96 (4 Nov. 1954), pp. 951–968. DOI: 10.1103/PhysRev.96.951. URL: https://link.aps.org/doi/10.1103/PhysRev.96.951.

[52]   G. D. Mahan. "Modified Sternheimer equation for polarizability". In: *Phys. Rev. A* 22 (5 Nov. 1980), pp. 1780–1785. DOI: 10.1103/PhysRevA.22.1780. URL: https://link.aps.org/doi/10.1103/PhysRevA.22.1780.

[53]   S. R. Jensen, T. Flå, D. Jonsson, R. S. Monstad, K. Ruud, and L. Frediani. "Magnetic properties with multiwavelets and DFT: The complete basis set limit achieved". In: *Physical Chemistry Chemical Physics* 18.31 (2016), pp. 21145–21161. DOI: 10.1039/c6cp01294a.

[54]   S. Reine and T. Saue, eds. *European Summerschool in Quantum Chemistry — Book III*. 10th ed. 2017. ISBN: 879-88-908737-8-2.

[55]   M. Repisky, S. Komorovsky, M. Kadek, L. Konecny, U. Ekström, E. Malkin, M. Kaupp, K. Ruud, O. L. Malkina, and V. G. Malkin. "ReSpect: Relativistic spectroscopy DFT program package". In: *The Journal of Chemical Physics* 152.18 (2020), p. 184101. DOI: 10.1063/5.0005094.

[56]   T. Saue, R. Bast, A. S. P. Gomes, H. J. A. Jensen, L. Visscher, I. A. Aucar, R. Di Remigio, K. G. Dyall, E. Eliav, E. Fasshauer, T. Fleig, L. Halbert, E. D. Hedegård, B. Helmich-Paris, M. Iliaš, C. R. Jacob, S. Knecht, J. K. Laerdahl, M. L. Vidal, M. K. Nayak, M. Olejniczak, J. M. H. Olsen, M. Pernpointner, B. Senjean, A. Shee, A. Sunaga, and J. N. P. van Stralen. "The DIRAC code for relativistic molecular calculations". In: *The Journal of Chemical Physics* 152.20 (2020), p. 204104. DOI: 10.1063/5.0004844.

[57]   L. Belpassi, M. De Santis, H. M. Quiney, F. Tarantelli, and L. Storchi. "BERTHA: Implementation of a four-component Dirac–Kohn–Sham relativistic framework". In: *The Journal of Chemical Physics* 152.16 (2020), p. 164118. DOI: 10.1063/5.0002831.

[58] Y. Zhang, B. Suo, Z. Wang, N. Zhang, Z. Li, Y. Lei, W. Zou, J. Gao, D. Peng, Z. Pu, Y. Xiao, Q. Sun, F. Wang, Y. Ma, X. Wang, Y. Guo, and W. Liu. "BDF: A relativistic electronic structure program package". In: *The Journal of Chemical Physics* 152.6 (2020), p. 064113. DOI: 10.1063/1.5143173.

[59] E. v. Lenthe, E. J. Baerends, and J. G. Snijders. "Relativistic regular two-component Hamiltonians". In: *The Journal of Chemical Physics* 99.6 (1993), pp. 4597–4610. DOI: 10.1063/1.466059.

[60] E. van Lenthe, E. J. Baerends, and J. G. Snijders. "Relativistic total energy using regular approximations". In: *The Journal of Chemical Physics* 101.11 (1994), pp. 9783–9792. DOI: 10.1063/1.467943.

[61] E. v. Lenthe. "The ZORA equation". PhD thesis. 1996.

[62] J. Hermann, R. A. DiStasio Jr, and A. Tkatchenko. "First-principles models for van der Waals interactions in molecules and materials: Concepts, theory, and applications". In: *Chemical Reviews* 117.6 (2017), pp. 4714–4758.

[63] Y.-Y. Zhan, Q.-C. Jiang, K. Ishii, T. Koide, O. Kobayashi, T. Kojima, S. Takahashi, M. Tachikawa, S. Uchiyama, and S. Hiraoka. "Polarizability and isotope effects on dispersion interactions in water". In: *Communications Chemistry* 2.1 (2019), pp. 1–8.

[64] D. Hait and M. Head-Gordon. "How accurate are static polarizability predictions from density functional theory? An assessment over 132 species at equilibrium geometry". In: *Physical Chemistry Chemical Physics* 20 (30 2018), pp. 19800–19810. DOI: 10.1039/C8CP03569E.

[65] A. L. Hickey and C. N. Rowley. "Benchmarking Quantum Chemical Methods for the Calculation of Molecular Dipole Moments and Polarizabilities". In: *The Journal of Physical Chemistry A* 118.20 (2014), pp. 3678–3687. DOI: 10.1021/jp502475e.

[66] J. R. Hammond, N. Govind, K. Kowalski, J. Autschbach, and S. S. Xantheas. "Accurate dipole polarizabilities for water clusters n=2–12 at the coupled-cluster level of theory and benchmarking of various density functionals". In: *The Journal of Chemical Physics* 131.21 (2009), p. 214103. DOI: 10.1063/1.3263604.

[67] S. Maekawa and K. Moorthi. "Polarizabilities from Long-Range Corrected DFT Calculations". In: *Journal of Chemical & Engineering Data* 59.10 (2014), pp. 3160–3166. DOI: 10.1021/je500224e.

[68] H.-J. Werner and W. Meyer. "PNO-CI and PNO-CEPA stidies of electron correlation effects V. Static dipole polarizabilities of small molecules". In: *Molecular Physics* 31.3 (1976), pp. 855–872. DOI: 10.1080/00268977600100651.

[69] D. Hait and M. Head-Gordon. "How Accurate Is Density Functional Theory at Predicting Dipole Moments? An Assessment Using a New Database of 200 Benchmark Values". In: *Journal of Chemical Theory and Computation* 14.4 (2018), pp. 1969–1981. DOI: 10.1021/acs.jctc.7b01252.

[70] F. Neese. "Software update: the ORCA program system, version 4.0". In: *Wiley Interdisciplinary Reviews: Computational Molecular Science* 8.1 (2018), e1327. DOI: 10.1002/wcms.1327.

[71] C. Li, W. Huang, C. Zhou, and Y. Chen. "Advances on the transition-metal based catalysts for aquathermolysis upgrading of heavy crude oil". In: *Fuel* 257 (2019), p. 115779. ISSN: 0016-2361. DOI: https://doi.org/10.1016/j.fuel.2019.115779.

[72] J. Medlock and W. Bonrath. "Applications of Transition Metal Catalysis in Drug Discovery and Development. An Industrial Perspective. Edited by Matthew L. Crawley and Barry M. Trost." In: *Angewandte Chemie International Edition* 52.21 (2013), pp. 5435–5435. DOI: https://doi.org/10.1002/anie.201302033.

[73] C. Smith, A. K. Hill, and L. Torrente-Murciano. "Current and future role of Haber–Bosch ammonia in a carbon-free energy landscape". In: *Energy Environ. Sci.* 13 (2 2020), pp. 331–344. DOI: 10.1039/C9EE02873K.

[74] J. Wang, H. Chen, Z. Hu, M. Yao, and Y. Li. "A Review on the Pd-Based Three-Way Catalyst". In: *Catalysis Reviews* 57.1 (Nov. 2014), pp. 79–144. ISSN: 1520-5703. DOI: 10.1080/01614940.2014.977059. URL: http://dx.doi.org/10.1080/01614940.2014.977059.

[75] International Union of Pure ad Applied and Chemistry. *IUPAC Compendium of Chemical Terminology – The Gold Book*. Compiled by A. D. McNaught and A. Wilkinson. Blackwell Scientific Publications, Oxford (1997). Online version (2019-) created by S. J. Chalk. 2009. DOI: 10.1351/goldbook.. URL: https://goldbook.iupac.org/terms/view/T06456.

[76] S. M. Tekarli, M. L. Drummond, T. G. Williams, T. R. Cundari, and A. K. Wilson. "Performance of Density Functional Theory for 3d Transition Metal-Containing Complexes: Utilization of the Correlation Consistent Basis Sets". In: *The Journal of Physical Chemistry A* 113.30 (2009), pp. 8607–8614. DOI: 10.1021/jp811503v.

[77] W. Jiang, M. L. Laury, M. Powell, and A. K. Wilson. "Comparative Study of Single and Double Hybrid Density Functionals for the Prediction of 3d Transition Metal Thermochemistry". In: *Journal of Chemical Theory and Computation* 8.11 (2012), pp. 4102–4111. DOI: 10.1021/ct300455e.

[78] Y. A. Aoto, A. P. de Lima Batista, A. Köhn, and A. G. S. de Oliveira-Filho. "How To Arrive at Accurate Benchmark Values for Transition Metal Compounds: Computation or Experiment?"

In: *Journal of Chemical Theory and Computation* 13.11 (2017), pp. 5291–5316. DOI: 10.1021/acs.jctc.7b00688.

[79] R. S. Grev and H. F. Schaefer. "6-311G is not of valence triple-zeta quality". In: *The Journal of Chemical Physics* 91.11 (1989), pp. 7305–7306. DOI: 10.1063/1.457301.

[80] K. S. Kim, P. Tarakeshwar, and J. Y. Lee. "Molecular Clusters of π-Systems: Theoretical Studies of Structures, Spectra, and Origin of Interaction Energies". In: *Chemical Reviews* 100.11 (2000), pp. 4145–4186. DOI: 10.1021/cr990051i.

[81] A. Brakestad, P. Wind, S. R. Jensen, L. Frediani, and K. H. Hopmann. *Replication Data for: Multiwavelets applied to metal-ligand interactions: Energies free from basis set errors*. Version V1. 2021. DOI: 10.18710/WA5YCF.

[82] P. Pyykkö. "Relativistic Effects in Chemistry: More Common Than You Thought". In: *Annual Review of Physical Chemistry* 63.1 (2012), pp. 45–64. DOI: 10.1146/annurev-physchem-032511-143755.

[83] J. S. Townsend. *Quantum Physics: A Fundamental Approach to Modern Physics*. Sausalito, California: University Science Books, 2010.

[84] P. Tipler and G. Mosca. *Physics for Scientists and Engineers Extended Version*. W. H. Freeman, 2020. ISBN: 9781319321710.

[85] S. Matsika and D. R. Yarkony. "Conical Intersections and the Spin-Orbit Interaction". In: *The Role of Degenerate States in Chemistry*. John Wiley & Sons, Ltd, 2002, pp. 557–581. ISBN: 9780471433460. DOI: https://doi.org/10.1002/0471433462.ch10.

[86] Y. Wang and D. R. Yarkony. "Conical intersection seams in spin–orbit coupled systems with an even number of electrons: A numerical study based on neural network fit surfaces". In:

The Journal of Chemical Physics 155.17 (2021), p. 174115. DOI: 10.1063/5.0067660.

[87] T. B. Demissie, B. D. Garabato, K. Ruud, and P. M. Kozlowski. "Mercury Methylation by Cobalt Corrinoids: Relativistic Effects Dictate the Reaction Mechanism". In: *Angewandte Chemie International Edition* 55.38 (), pp. 11503–11506. DOI: https://doi.org/10.1002/anie.201606001.

[88] N. B. Balabanov and K. A. Peterson. "Systematically convergent basis sets for transition metals. I. All-electron correlation consistent basis sets for the 3d elements Sc–Zn". In: *The Journal of Chemical Physics* 123.6 (2005), p. 064107. DOI: 10.1063/1.1998907.

[89] N. E. Schultz, Y. Zhao, and D. G. Truhlar. "Benchmarking approximate density functional theory for s/d excitation energies in 3d transition metal cations". In: *Journal of Computational Chemistry* 29.2 (2008), pp. 185–189. DOI: https://doi.org/10.1002/jcc.20717.

[90] B. O. Roos, R. Lindh, P.-Å. Malmqvist, V. Veryazov, and P.-O. Widmark. "Main Group Atoms and Dimers Studied with a New Relativistic ANO Basis Set". In: *The Journal of Physical Chemistry A* 108.15 (2004), pp. 2851–2858. DOI: 10.1021/jp031064+.

[91] B. Roos, V. Veryazov, and P.-O. Widmark. "Relativistic atomic natural orbital type basis sets for the alkaline and alkaline-earth atoms applied to the ground-state potentials for the corresponding dimers". In: *Theoretical Chemistry Accounts* 111 (2004), pp. 345–351. DOI: 10.1007/s00214-003-0537-0.

[92] B. O. Roos, R. Lindh, P.-Å. Malmqvist, V. Veryazov, and P.-O. Widmark. "New Relativistic ANO Basis Sets for Transition Metal Atoms". In: *The Journal of Physical Chemistry A* 109.29 (2005), pp. 6575–6579. DOI: 10.1021/jp0581126.

[93]   J. P. Zobel, P.-O. Widmark, and V. Veryazov. "The ANO-R Basis Set". In: *Journal of Chemical Theory and Computation* 16.1 (2020), pp. 278–294. DOI: 10.1021/acs.jctc.9b00873.

[94]   J. P. Zobel, P.-O. Widmark, and V. Veryazov. "Correction to "The ANO-R Basis Set"". In: *Journal of Chemical Theory and Computation* 17.5 (2021), pp. 3233–3234. DOI: 10.1021/acs.jctc.1c00329.

[95]   J. D. Rolfes, F. Neese, and D. A. Pantazis. "All-electron scalar relativistic basis sets for the elements Rb–Xe". In: *Journal of Computational Chemistry* 41.20 (2020), pp. 1842–1849. DOI: 10.1002/jcc.26355.

[96]   E. V. R. de Castro and F. E. Jorge. "Accurate universal Gaussian basis set for all atoms of the Periodic Table". In: *The Journal of Chemical Physics* 108.13 (1998), pp. 5225–5229. DOI: 10.1063/1.475959.

[97]   T. Noro, M. Sekiya, and T. Koga. "Segmented contracted basis sets for atoms H through Xe: Sapporo-(DK)-nZP sets (n = D, T, Q)". In: *Theoretical Chemistry Accounts* 131 (2012). DOI: 10.1007/s00214-012-1124-z.

[98]   D. Feller. "The role of databases in support of computational chemistry calculations". In: *Journal of Computational Chemistry* 17.13 (1996), pp. 1571–1586. DOI: (SICI)1096-987X(199610)17:13<1571::AID-JCC9>3.0.CO;2-P.

[99]   MRCHEM program package **2020**. DOI: 10.5281/zenodo.3786996.

[100] MRCHEM documentation **2020**. https://mrchem.readthedocs.io/en/latest/.

[101] R. J. Harrison, G. Beylkin, F. A. Bischoff, J. A. Calvin, G. I. Fann, J. Fosso-Tande, D. Galindo, J. R. Hammond, R. Hartman-Baker, J. C. Hill, J. Jia, J. S. Kottmann, M.-J. Yvonne Ou, J. Pei, L. E.

Ratcliff, M. G. Reuter, A. C. Richie-Halford, N. A. Romero, H. Sekino, W. A. Shelton, B. E. Sundahl, W. S. Thornton, E. F. Valeev, Á. Vázquez-Mayagoitia, N. Vence, T. Yanai, and Y. Yokoi. "MADNESS: A Multiresolution, Adaptive Numerical Environment for Scientific Simulation". In: *SIAM Journal on Scientific Computing* 38.5 (2016), S123–S142. DOI: 10.1137/15M1026171.

PAPER I

Static Polarizabilities at the Basis Set Limit: A Benchmark of 124 Species

Anders Brakestad, Stig Rune Jensen, Peter Wind, Marco D'Alessandro,
Luigi Genovese, Kathrin H. Hopmann, and Luca Frediani

Supporting Information Available At:
https://pubs.acs.org/doi/10.1021/acs.jctc.0c00128?goto=
supporting-info

Replication Data Available at:
https://doi.org/10.18710/KLQVOK

Article

Static Polarizabilities at the Basis Set Limit: A Benchmark of 124 Species

Anders Brakestad, Stig Rune Jensen, Peter Wind, Marco D'Alessandro, Luigi Genovese, Kathrin Helen Hopmann, and Luca Frediani*

ACCESS | 📊 Metrics & More | 📖 Article Recommendations | 🆂🅸 Supporting Information

ABSTRACT: Benchmarking molecular properties with Gaussian-type orbital (GTO) basis sets can be challenging, because one has to assume that the computed property is at the complete basis set (CBS) limit, without a robust measure of the error. Multiwavelet (MW) bases can be systematically improved with a controllable error, which eliminates the need for such assumptions. In this work, we have used MWs within Kohn–Sham density functional theory to compute static polarizabilities for a set of 92 closed-shell and 32 open-shell species. The results are compared to recent benchmark calculations employing the GTO-type aug-pc4 basis set. We observe discrepancies between GTO and MW results for several species, with open-shell systems showing the largest deviations. Based on linear response calculations, we show that these discrepancies originate from artifacts caused by the field strength and that several polarizabilities from a previous study were contaminated by higher order responses (hyperpolarizabilities). Based on our MW benchmark results, we can affirm that aug-pc4 is able to provide results close to the CBS limit, as long as finite difference effects can be controlled. However, we suggest that a better approach is to use MWs, which are able to yield precise finite difference polarizabilities even with small field strengths.

BSIEs in GTO polarizabilities
MRChem
Powered by MultiWavelets
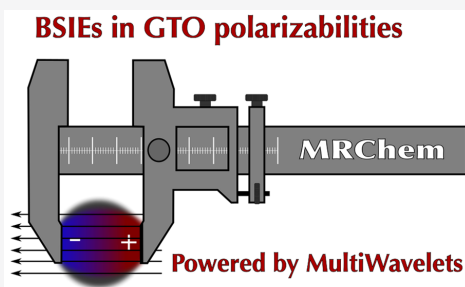
1. INTRODUCTION

Molecular electronic structure calculations are a widespread tool in chemistry, biology, and materials science. Such a diffusion across disciplines has been enabled by Kohn–Sham density functional theory (KS-DFT, hereafter just "DFT")[1] which brought about calculations with accuracy comparable to coupled cluster with singles and doubles (CCSD) at the computational cost of a single-determinant method like Hartree–Fock (HF). A large part of the current development of theoretical methods is concerned with obtaining accurate energies, which are essential to interpret and predict chemical reactivity.

Molecular properties constitute another important area of method development. Electric dipole polarizabilities are related to important processes in chemistry; for example, they hold a key role in our understanding of intra- and intermolecular interactions such as dispersion,[2,3] they are at the foundation of techniques such as Raman spectroscopy and Raman optical activity,[4] and they are employed in the development of accurate force fields for molecular simulations.[5,6] It is therefore highly relevant to assess the accuracy of polarizability predictions within the density functional theory (DFT) framework.

The quality of a given DFT calculation depends on two factors: the density functional approximation (DFA) and the basis set. In order to fairly assess the performance of functionals and basis sets, we must distinguish between these two sources of error. While an ideal (nonexact) functional should be *accurate* and yield a result as close as possible to the corresponding full configuration interaction (FCI) calculation, an ideal basis should be *precise* and minimize the error with respect to the complete basis set (CBS) limit. Most functionals and basis sets are developed so as to provide the best possible energies, which sometimes rely on fortuitous error cancellation. The assessment of accuracy (functional) and precision (basis set) for molecular properties, such as polarizabilites, is therefore challenging.

Hait and Head-Gordon[7] benchmarked the accuracy of electric dipole polarizability predictions for a large number of DFAs against coupled cluster with singles, doubles, and perturbative triples (CCSD(T)) calculations, for a set of 132 species. They employed the aug-pc4 basis set[8−11] for all DFT calculations, assuming that the obtained quantities were close

to the CBS limit, although they noted that this assumption may not hold for certain DFAs. We refer the reader to their excellent paper for details.[7]

Even the largest practical Gaussian-type orbital (GTO) basis sets are far from complete in the mathematical sense. In general, it must be *assumed* that GTO basis sets deliver results close to the CBS limit, even for the large aug-pc4 basis set: one cannot know how close to the limit a given basis set is without a reference value, and simply comparing with a larger GTO basis set does *not* in general guarantee that one converges to the CBS limit. For energies, the variational principle serves as a guide, but quantifying the basis set incompleteness error (BSIE) for other molecular properties is not a trivial task, and two issues lie at the heart of the challenge: (i) atomic orbital (AO) bases are generally developed by minimization of the total energy as the guiding principle and may therefore not be optimal for molecular properties, and (ii) hierarchical constructions of AO bases do not *guarantee* any rate of convergence of the molecular properties. While the Hylleraas–Undheim theorem[12] proves that the polarizability for non-dipolar molecules is a lower bound of the CBS limit, there is no guarantee that a systematic extension of an AO basis will in practice reach the CBS limit, unless the basis can formally be extended to completeness.

Multiwavelets (MWs)[13] have recently emerged as a powerful alternative to the traditional AO bases and are not subject to the same shortcomings as AO bases. MWs are a particular choice of wavelets[14] used to represent functions and operators on a real-space grid. To overcome the hurdles posed by real-space methods, such as large memory footprint and computational cost, MWs exploit adaptive grid refinement[15−17] and Cartesian separated representation of the required operators.[18] Such features are combined with a rigorous formalism with strict error control.[19−21] For molecular energies, it is possible to request a predefined precision with respect to the CBS limit, and for molecular properties such as polarizabilities, a steady progression toward the corresponding limit is observed.[22] MW calculations of polarizabilities performed at high precision can be employed as a true reference because they can be assumed complete to within the given precision. Such capabilities have been recently exploited in our group to perform two extensive benchmark studies on total and atomization energies[20] and on magnetizabilities and NMR shielding constants.[23]

The objective of the present paper has been to use MWs to assess whether aug-pc4 indeed is capable of delivering polarizabilities at the CBS limit, by comparing MW-based polarizabilities to the recent aug-pc4 benchmark.[7] We start by describing the mathematical framework for computing molecular properties with MWs. Next, we report the computational details and present and discuss our results. We also touch upon additional benefits of MWs related to the finite differences (FD) approach, and finish by summarizing our findings.

2. THEORETICAL FRAMEWORK

2.1. Molecular Properties as Energy Derivatives.
Molecular energies are affected by the presence of external fields. In particular, when a static electric field is applied, the total energy of the molecule can be expressed as a Taylor expansion with respect to the external field F[24]

$$E = E_0 + \sum_a \mu_a F_a + \frac{1}{2} \sum_{ab} \alpha_{ab} F_a F_b + \frac{1}{6} \sum_{abc} \beta_{abc} F_a F_b F_c + \frac{1}{24} \sum_{abcd} \gamma_{abcd} F_a F_b F_c F_d + \dots \tag{1}$$

where a, b, c, ... are Cartesian directions. Such an expansion implicitly defines the components of the dipole moment (μ), the polarizability (α), and the hyperpolarizabilities (here limited to the first and second hyperpolarizabilities, β and γ, respectively).

The dipole moment components μ_a can be obtained as a simple expectation value of the corresponding dipole operators $\hat{\mu}_a$. Several approaches can be employed to compute (hyper)polarizabilities. Hait and Head-Gordon[7] have employed a second-order FD expression of the energy. For the diagonal components of the polarizability tensor, the expression reads

$$\alpha_{aa} = -\frac{E(F_a) + E(-F_a) - 2E_0}{F_a^2} + O(F^2) \tag{2}$$

Such an expression is formally equivalent to taking the derivative of eq 1 with respect to the external field and then applying a linear finite difference formula to the dipole moment:

$$\alpha_{ab} = \frac{\mu_a(F_b) - \mu_a(-F_b)}{2F_b} + O(F^2) \tag{3}$$

Both formulas have a leading error term that is quadratic in the applied field and proportional to the second hyperpolarizability. To minimize the error, it is therefore necessary to employ small fields, especially for molecules with large γ.

2.2. Multiwavelets.
Wavelet theory is a relatively new branch of mathematics, dating back to the 1980s.[14,25] It constructs functions with the following properties: they are localized in both real and Fourier space, they achieve completeness as a limit in the L^2 sense, and they provide rigorous error control. *Multi*wavelets are a particular kind of wavelets that include several functions in one interval, as the "multi" prefix suggests. For the construction of MW bases and details about their properties, we refer to the literature on the subject.[13,15]

Finite Field Polarizability with Multiwavelets. In 2004, Harrison and co-workers[19] for the first time used MWs to solve the Kohn−Sham (KS) equations of DFT, demonstrating that arbitrary precision with respect to the CBS limit can be achieved also for general molecular systems;[19,26,27] previously, this was possible only for very small and highly symmetric molecules.[28]

Due to the large number of primitive MW basis functions necessary for the precise represention of the molecular orbitals, it is not practical to solve the KS equations in the traditional way by constructing the primitive Fock matrix and solving the corresponding Roothaan equations. Instead, the equations are rewritten in integral form

$$\varphi_i = -\hat{G}_i \hat{V} \varphi_i \tag{4}$$

using the bound-state Helmholtz integral operator, which is given as the inverse of the kinetic energy operator shifted by the orbital energy $\hat{G}_i = (\hat{T} - \epsilon_i)^{-1}$. There are several benefits with this reformulation: (i) it avoids the explicit construction and diagonalization of the primitive Fock matrix; (ii) it allows

for different and adaptive primitive basis sets for each orbital; (iii) it avoids the application of the kinetic operator as a second derivative, which is not numerically stable in the discontinuous MW basis; and (iv) the implicit construction of a huge virtual orbital space is not necessary, and one solves instead only for the occupied orbitals by iterating eq 4 to self-consistency.

In the presence of a uniform electric field $\vec{F}$, the KS potential operator in eq 4 reads

$$\hat{V} = \hat{V}_{nuc} + \hat{J} + \hat{V}_{xc} - \vec{F} \cdot \hat{\vec{\mu}} \qquad (5)$$

which features the nuclear ($\hat{V}_{nuc}$), Hartree ($\hat{J}$), and exchange-correlation ($\hat{V}_{xc}$) potentials. By solving the corresponding KS equations to obtain the ground state density $\rho = \sum_i |\varphi_i|^2$, we can compute the electric dipole moment as a function of field strength from the expectation value

$$\mu_a(\vec{F}) = \int \hat{\mu}_a \rho(\vec{F})\, dr, \qquad a = x, y, z \qquad (6)$$

This procedure can be used to approximate the electric polarizability through the finite difference formula in eq 3.

Linear Response Polarizability with Multiwavelets. The starting point to obtain linear response properties with multiwavelets is standard perturbation theory. A small perturbation $\hat{h}^{(1)}$ is introduced, and all terms in eq 4 are expanded to first order into a set of Sternheimer equations,[22,29−31] which can be written in integral form

$$\varphi_i^{(1)} = -\hat{G}_i[\hat{V}^{(0)}\varphi_i^{(1)} + (1 - \hat{\rho}^{(0)})(\hat{h}^{(1)} + \hat{V}^{(1)})\varphi_i^{(0)}] \qquad (7)$$

where $\hat{G}_i$ is the same as that for the ground state problem and $\hat{\rho}^{(0)}$ is the ground state density projector, while $\hat{V}^{(0)} = \hat{V}_{nuc}^{(0)} + \hat{J}^{(0)} + \hat{V}_{xc}^{(0)}$ and $\hat{V}^{(1)} = \hat{J}^{(1)} + \hat{V}_{xc}^{(1)}$ are the unperturbed and first-order perturbed potential operators, respectively. At this point, all unperturbed quantities are already known from solving the ground state problem, whereas first-order quantities are obtained by iterating eq 7 to self-consistency. The perturbed orbitals are then used to build the corresponding density perturbation

$$\rho^{(1)} = 2 \sum_i \varphi_i^{(1)} \varphi_i^{(0)} \qquad (8)$$

Here we have assumed real, time-independent perturbations: only one set of real, perturbed orbitals is obtained, which simplify the expression for the perturbed density.

The polarizability tensor is computed as the expectation value of the dipole operator $\hat{\vec{\mu}}$, on a density perturbed by the same operator

$$\alpha_{ab} = \int \hat{\mu}_a \rho_b^{(1)}\, dr, \qquad a, b = x, y, z \qquad (9)$$

For details about the general derivation of time-dependent and imaginary (magnetic) perturbations in a MW framework, we refer the reader to the works by Sekino et al.[22] and Jensen et al.,[23] respectively.

3. COMPUTATIONAL DETAILS

Cartesian coordinates of the species studied here were obtained from Hait and Head-Gordon,[7] and a list of the species and their spin multiplicities is given in Table 1. The set of 124 species includes 92 closed-shell and 32 open-shell systems. The set is slightly smaller than the original one provided in the mentioned benchmark,[7] due to convergence issues encountered for the remaining species (missing species:

Table 1. 124 Species and Their Spin Multiplicities Used in This Study, Sorted Alphabetically[a]

^{1}AlF	^{1}Ar	^{1}Be	^{2}BeH	^{1}BeH$_2$	^{1}BF
^{1}BH$_2$F	^{1}BH$_3$	^{1}BHF$_2$	^{3}BN	^{2}BO	^{2}BS
^{2}C$_2$H$_2$	^{2}C$_2$H$_3$	^{2}C$_2$H$_4$	^{1}CH$_2$BH	^{2}CH$_2$F	^{1}CH$_2$NH
^{1}CH$_3$BH$_2$	^{1}CH$_3$Cl	^{1}CH$_3$F	^{1}CH$_3$NH$_2$	^{1}CH$_3$OH	^{1}CH$_3$SH
^{1}Cl$_2$	^{1}ClCN	^{1}ClF	^{2}CN	^{1}CO	^{1}CO$_2$
^{1}CSO	^{1}F$_2$	^{1}FCN	^{2}FCO	^{2}FH−OH	^{2}H
^{1}H$_2$	^{2}H$_2$CN	^{1}H$_2$O	^{2}H$_2$O−Li	^{1}HBO	^{1}HBS
^{1}HCCF	^{1}HCHO	^{1}HCHS	^{1}HCl	^{1}HCN	^{2}HCO
^{1}HCOOH	^{1}HCP	^{1}He	^{1}HF	^{1}HNC	^{1}HNS
^{2}HO$_2$	^{1}HOCl	^{1}HOF	^{1}HOOH	^{2}Li	^{1}Li$_2$
^{1}LiCl	^{1}LiCN	^{1}LiH	^{1}Mg	^{1}Mg$_2$	^{4}N
^{2}N$_2$H$_2$	^{2}N$_2$H$_4$	^{2}Na	^{1}Na$_2$	^{1}NaCl	^{1}NaCN
^{1}NaLi	^{2}NCO	^{1}Ne	^{3}NH	^{2}NH$_2$	^{1}NH$_2$F
^{1}NH$_2$OH	^{1}NH$_3$	^{1}NH$_3$O	^{1}NOCl	^{1}NP	^{3}O$_2$
^{2}OCl	^{1}OCl$_2$	^{2}OF$_2$	^{4}P		
^{1}P$_2$H$_4$	^{3}PH	^{2}PH$_2$	^{1}PH$_2$OH	^{1}PH$_3$	
^{2}SCl	^{1}SCl$_2$	^{2}SF	^{1}SF$_2$	^{1}SH$_2$	
^{1}SiH$_3$F	^{1}SiH$_4$	^{1}SiO	^{3}SO	^{1}SO$_2$	

^{1}AlF	^{1}Ar	^{1}Be	^{2}BeH	^{1}BeH$_2$	^{1}BF
^{1}BH$_2$F	^{1}BH$_3$	^{1}BHF$_2$	^{3}BN	^{2}BO	^{2}BS
^{2}C$_2$H$_2$	^{2}C$_2$H$_3$	^{2}C$_2$H$_4$	^{1}CH$_2$BH	^{2}CH$_2$F	^{1}CH$_2$PH
^{1}CH$_3$BH$_2$	^{1}CH$_3$Cl	^{1}CH$_3$F	^{1}CH$_3$NH$_2$	^{1}CH$_3$OH	^{1}CH$_3$SH	^{1}CH$_4$
^{1}Cl$_2$	^{1}ClCN	^{1}ClF	^{2}CN	^{1}CO	^{1}CO$_2$	^{1}CS
^{1}CSO	^{1}F$_2$	^{1}FCN	^{2}FCO	^{2}FH−OH	^{1}FNO	^{2}H
^{1}H$_2$	^{2}H$_2$CN	^{1}H$_2$O	^{2}H$_2$O−Li	^{1}HBO	^{1}HBS	^{1}HCCCl
^{1}HCCF	^{1}HCHO	^{1}HCHS	^{1}HCl	^{1}HCN	^{2}HCO	^{1}HCONH$_2$
^{1}HCOOH	^{1}HCP	^{1}He	^{1}HF	^{1}HNC	^{1}HNO	^{1}HNS
^{2}HO$_2$	^{1}HOCl	^{1}HOF	^{1}HOOH	^{2}Li	^{1}Li$_2$	^{1}LiBH$_4$
^{1}LiCl	^{1}LiCN	^{1}LiH	^{1}Mg	^{1}Mg$_2$	^{4}N	^{1}N$_2$
^{1}N$_2$H$_2$	^{1}N$_2$H$_4$	^{2}Na	^{1}Na$_2$	^{1}NaCl	^{1}NaCN	^{1}NaH
^{1}NaLi	^{2}NCO	^{1}Ne	^{3}NH	^{2}NH$_2$	^{1}NH$_2$F
^{1}NH$_2$OH	^{1}NH$_3$	^{1}NH$_3$O	^{1}NOCl	^{1}NP	^{3}O$_2$	^{1}O$_3$
^{2}OCl	^{1}OCl$_2$	^{2}OF$_2$	^{4}P			^{2}P$_2$
^{1}P$_2$H$_4$	^{3}PH	^{2}PH$_2$	^{1}PH$_2$OH	^{1}PH$_3$	^{1}PH$_3$O	^{1}S$_2$H$_2$
^{2}SCl	^{1}SCl$_2$	^{2}SF	^{1}SF$_2$	^{1}SH$_2$	^{2}SiH$_3$	^{1}SiH$_3$Cl
^{1}SiH$_3$F	^{1}SiH$_4$	^{1}SiO	^{3}SO	^{1}SO$_2$		

[a]The numbers of closed-shell and open-shell species are 92 and 32, respectively. Closed-shell species are indicated in blue, while open-shell species are indicated in red.

CH$_3$O, PS, CH$_3$, NO, CH$_2$, BH$_2$, SH, S$_2$). All coordinates and spin multiplicities are available in the form of *XYZ* files in the Supporting Information, together with Python scripts in the form of Jupyter Notebooks for our data analyses and figure generation.

3.1. Multiwavelet Calculations. MW calculations were performed with a prereleased version (1.0.0-alpha) of the MRC$_{hem}$ program package.[32−34] The relative numerical precision was set to $\epsilon_{rel} = 1 \times 10^{-7}$, the MW polynomial order to 11, and the norms of the orbital residuals between consecutive iterations ($\|\phi_i^{n+1} - \phi_i^n\|$) were converged to within $\epsilon_{mo} = 1 \times 10^{-6}$, both for unperturbed and perturbed orbitals.

In general, it is expected that the converged total energy should be correct at least within ϵ_{rel} with respect to the CBS limit (relative precision). The orbital convergence necessary to reach this precision in total energy is roughly $\epsilon_{mo} = \sqrt{\epsilon_{rel}}$ because of quadratic error propagation. However, since we are also interested in properties with linear error propagation (dipole moment and polarizability), we converge the orbitals well beyond this point in order to get the maximum number of digits out of the chosen numerical precision ϵ_{rel},[35] and we then expect around ϵ_{mo} absolute precision in dipole moment and polarizability.

Static polarizabilities were computed with DFT using the LDA[36] and PBE[37] functionals, provided by the XCFun library.[38] Closed-shell species were treated with the spin-restricted formalism, and open-shell species, with the spin-unrestricted formalism. We used the central two-point finite difference formula of eq 3 to compute the diagonal elements α_{aa} of the polarizability tensor. Field strengths of ± 0.001 au were used for all species. Calculations without an applied electric field were first performed to generate initial orbitals for the FD calculations. Initial orbitals for zero-field calculations were generated by the superposition of atomic densities (SAD) method.[39] All MW calculations benefited from the Krylov subspace accelerated inexact Newton (KAIN) convergence accelerator.[40]

To validate our results, we also used MWs to compute static polarizabilities with linear response (LR) for a subset of the species. PBE response calculations were performed for 17 of the 124 species (closed-shell only), while LDA response
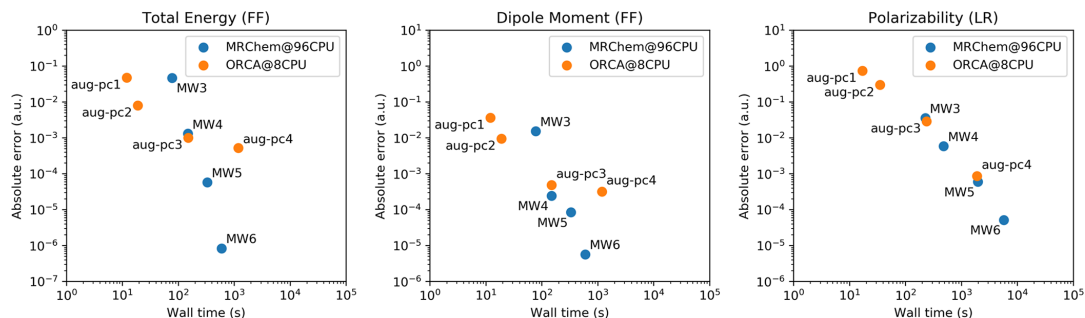
Figure 1. Scaling of computation time with precision for sequences of calculations on SiH_3Cl using MRC_{hem} and ORCA. MWn correspond to $\epsilon_{rel} = 10^{-n}$ and $\epsilon_{mo} = 10\epsilon_{rel}$, and all errors are measured against the corresponding MW7 calculation, which is the parameter chosen for the full benchmark study below. The left and center plots show timings for a *single* finite field (FF) calculation with field strength 0.001 au in the z direction (along the Si−Cl bond) vs errors in total energy and the z component of the dipole moment, respectively. The right-hand plot shows the timings for the full polarizability tensor from linear response (LR) vs the error in its isotropic average. Note: ORCA calculations are on 8 CPU cores, while MRC_{hem} are on 96 cores, so the computational cost is not directly comparable.

calculations were performed for 114 species. Numerical instabilities for GGA functionals at low-density values affected the convergence of the PBE LR calculations, explaining the low success rate. However, the cases that *did* converge are as precise as the corresponding LDA calculations: they converged to within 1×10^{-6}, indicating that they are not affected by these instabilities.

3.2. GTO Calculations. All FD results are taken from the work of Hait and Head-Gordon.[7] They used the energy expression in eq 2 to estimate the polarizability using a field strength of 0.01 au. However, they identified a few cases that were contaminated by hyperpolarizabilities, for which they reduced the field strength to 0.001 au, but this diagnosis was performed only at Hartree−Fock level and simply transferred to the DFT calculations.

In order to assess if further contamination could be present in the DFT results of Hait and Head-Gordon,[7] we performed *analytical* polarizability calculations using the ORCA program package, version 4.1.2,[41] with the PBE functional and the aug-pc4 basis set.[8−11] All species were treated with the spin-unrestricted formalism, and the integrals were computed over an angular Lebedev grid consisting of 770 points and a radial grid consisting of 50, 55, and 60 points for first, second, and third row elements, respectively ("grid7"). Self-consistent field convergence was accelerated by the direct inversion of the iterative subspace (DIIS) method.[42,43] The total energy change was converged to within 1×10^{-9} E_h, and the one-electron energy change to within 1×10^{-6} E_h (as defined by the "VeryTightSCF" ORCA keyword). The (default) resolution of identity (RI) approximation was turned off for all calculations in order to guarantee benchmark quality of the results (some initial test runs indicated a large dependence on the choice of auxiliary basis set).

3.3. Data Analysis. For all error analyses, we used the average polarizability, $\bar{\alpha}$, defined as

$$\bar{\alpha} = \frac{1}{3} \sum_{a=x,y,z} \alpha_{aa} \tag{10}$$

Polarizabilities from different calculations were compared using the relative error (RE) metric, which for species n was given by

$$RE_n = \frac{\bar{\alpha}_n - \bar{\alpha}_n^{REF}}{\bar{\alpha}_n^{REF}} \tag{11}$$

where the reference value may change depending on the comparison. The mean relative error (MRE) over N molecules was defined as

$$MRE = \frac{1}{N} \sum_{n=1}^{N} |RE_n| \tag{12}$$

3.4. Linear and Degenerate Open-Shell Systems. We have given special treatment to seven species in our data analysis (*vide infra*). In order to motivate this decision, it will be useful with a reminder of the electronic structure of linear and open-shell systems with a degenerate ground state. Such systems are particularly challenging to model for mean-field methods such as DFT. Let us consider NO as a prototypical molecule. It has an unpaired electron in a π orbital. Ideally, π_x and π_y are degenerate, but mean-field approaches break the symmetry as soon as one of the two orbitals is populated (the density and hence the KS potential become non-totally symmetric). For such systems, Hait and Head-Gordon[7] reported identical values for α_{xx} and α_{yy}, which is not what we observed: our MW-FD polarizabilities show that one component (the larger one) is virtually identical to the GTO-FD value, whereas the other is slightly smaller. According to Hait and Head-Gordon,[44] the smaller component should in this case be discarded as being unphysical, in connection to the symmetry breaking occurring for mean-field approaches.[45] Since the main objective of the present paper is to quantify the BSIE for the GTO basis set aug-pc4, we decided that the fairest analysis could be made by performing the same procedure as that by Hait and Head-Gordon.[7] We therefore explicitly set $\alpha_{xx} = \alpha_{yy}$ in our MW data set by selecting the component closest to the xx/yy component reported by Hait and Head-Gordon.[7]

The seven species that received the above treatment in our data analysis are SCl, OCl, OH, OF, SF, BN, and NCO. To qualify for the special treatment, they had to fulfill the following three criteria (to within a tolerance of 1×10^{-4}):

1. $\alpha_{xx} = \alpha_{yy}$ in Hait and Head-Gordon's data set
2. $\alpha_{xx} \neq \alpha_{zz}$ in Hait and Head-Gordon's data set
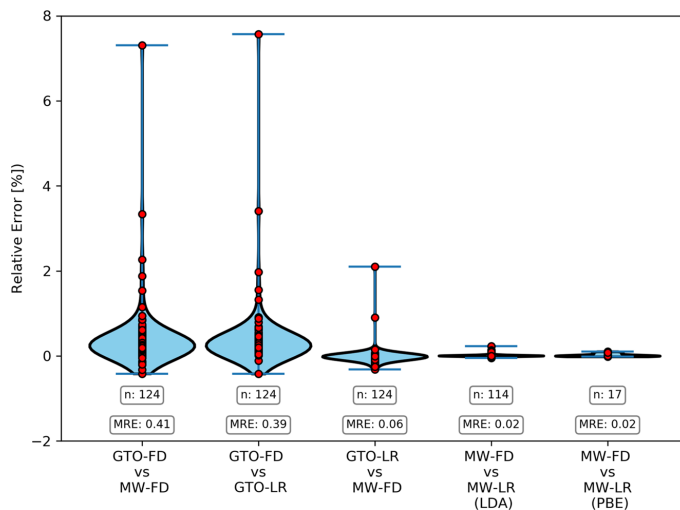3. $\alpha_{xx} \neq \alpha_{yy}$ in our data set

Figure 2. Violin plot summarizing the RE distributions discussed. Red dots indicate data points. The internal validation of our MW results demonstrates that the MW-FD polarizabilities are virtually free from field strength-related effects. GTO-FD polarizabilities display quite large errors, considering the size of the aug-pc4 basis set that was used, while GTO-LR display much smaller errors.

3.5. MW vs GTO: Practical Considerations. *Availability.* MRC$_{hem}$ is one of two programs currently available that offer an all-electron MW basis (the other is MADNESS[46]). Detailed instructions on how to obtain and compile the MRC$_{hem}$ code, as well as a user manual, are available on the documentation web page.[34]

Ease of Use. From a user standpoint, selecting appropriate GTO basis sets for a particular application is not a simple task: The high parametrization of GTO basis sets means the user has to carefully evaluate several factors, for example, which family of GTOs to use (Pople, Jensen, Karlsruhe, Ahlrichs, Dunning, etc.), how many polarization functions to use, how many diffuse functions to use, whether to treat different atoms differently, and so on. Although the result can be converged to *a limit* within the given basis, no knowledge about the *CBS limit* can be inferred from it. Selecting the best basis is not trivial, and suboptimal choices based on "habit" and "popularity" are common (analogous to the "zoo" of DFAs[47]).

For MW calculations, all the user must do is to specify an overall numerical precision, in terms of convergence thresholds for energy and orbitals. This precision parameter is relative to the exact CBS limit, which is a key distinction from GTO. MWs can therefore provide the user with excellent precision and a quantifiable error without expert knowledge about basis sets.

Cost and Performance. At present, a calculation at moderate precision is cheaper to perform with GTOs because of a smaller prefactor. At very high precision, MW calculations become more competitive due to a linear scaling with respect to the precision. The most severe limitation of MWs is the memory requirements, which is rather demanding. For the molecules used in the present work, the total memory needed for the MW-FD calculations was typically between 50 and 150GB (Figure 4 in the Supporting Information), although this is rather efficiently distributed across several compute nodes on a cluster. The number of CPU hours needed for the MW-FD data set is presented in Figure 5 in the Supporting Information.

Figure 1 presents plots of computation time against increasingly larger GTO and MW basis sets for the calculation of total energy, dipole moment, and polarizability for the SiH$_3$Cl molecule: it shows that each additional digit of precision for MWs requires a predictable doubling of CPU time, while moving along the aug-pc$n$ (n = 1, 2, 3, ...) series increases the computational cost by a larger factor, without a guarantee of gaining an additional digit in precision.

4. RESULTS AND DISCUSSION

A challenge in computational benchmark studies is the precision of the basis set: one has to assume that the computed reference property is at the CBS limit. The large GTO basis set aug-pc4[7,48] has been assumed to be close to the CBS limit for electrical properties. Here, we attempt to evaluate if aug-pc4 indeed is at the CBS limit for static polarizability predictions, by quantifying the BSIE associated with this basis set. We do this by comparing our reference MW polarizabilities to a recent aug-pc4 benchmark on DFT static polarizabilities.[7] All data presented herein are available via the Supporting Information accompanying this Article, or as a separate document at the Dataverse open-data repository.[49]

In order to isolate BSIEs, we need a detailed understanding of other potential errors, and in particular the error associated with using a finite field approach. In order to assign errors to the right source, we have considered the following types of calculations: (1) GTO-FD calculations; (2) MW-FD calculations; (3) GTO-LR calculations; (4) MW-LR calculatations.

The comparison of GTO-FD vs MW-FD is the central point of this contribution. The comparison of GTO-FD vs GTO-LR will shed light on potential errors due to finite field effects with GTOs; the comparison of MW-FD vs MW-LR will show how much MW results are affected by the FD approach, and the comparison of MW-FD with GTO-LR will be used to double-check that the discrepancies observed have been attributed correctly. The RE distributions listed here are summarized in Figure 2.
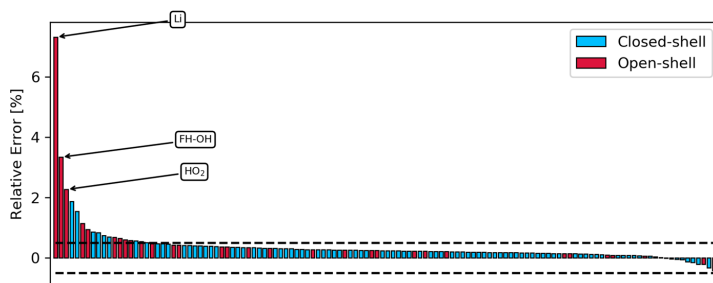
Figure 3. Distribution of REs of PBE polarizabilities for the 124 species, comparing GTO-FD with MW-FD, using the latter as a reference. The dashed lines are located at $\pm 0.5\%$ RE.
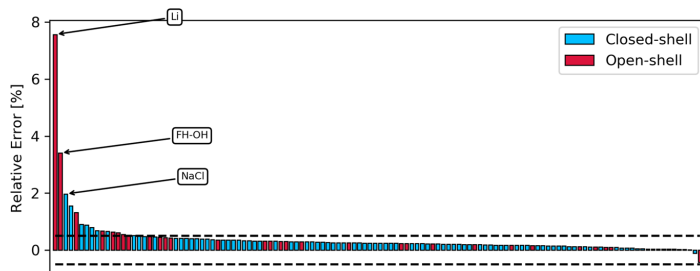

Figure 4. Distribution of REs of PBE polarizabilities for the 124 species, comparing GTO-FD and GTO-LR (both aug-pc-4), using the latter as a reference. The dashed lines are located at $\pm 0.5\%$ RE.
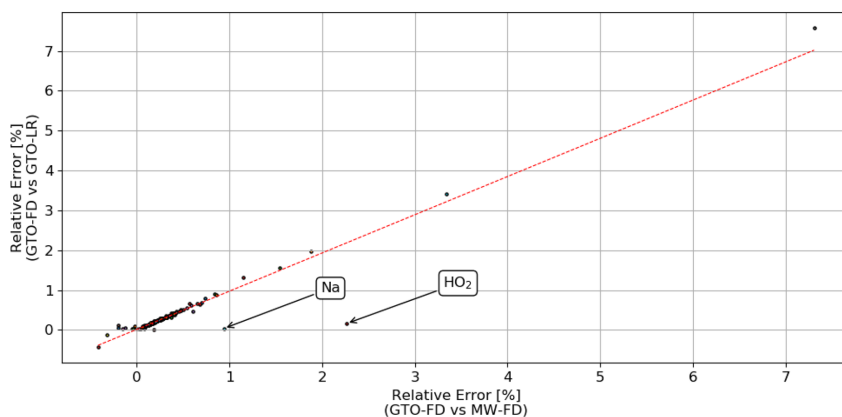

Figure 5. Correlation between the RE distributions presented in Figure 4 (x-axis) and Figure 3 (y-axis). The red dashed line indicates a least-squares linear fit with $r^2 = 0.97$.

4.1. Consistency of the MW Calculations: MW-FD vs MW-LR.

To make sure that our MW-FD polarizabilities were not contaminated by field-related effects, we compared the MW-FD polarizabilities to MW-LR results, using both LDA and PBE, as shown in the right-most plots in Figure 2. The LDA validation included 114 of the 124 species, while the PBE validation included 17 closed-shell species. All results about these validations, including the list of species with converged LR values, are reported in the Supporting Information.

The maximum absolute RE and MRE of the LDA validation were 0.23 and 0.011%, respectively. The PBE validation

yielded similar statistics. The PBE set was limited due to convergence problems. Nevertheless, we see no indication that LDA and PBE behave differently.

Based on the very high numerical precision that has been used throughout, we expect that the remaining discrepancy between MW-FD and MW-LR is due to the field strength of 0.001 au, although this has not been verified numerically. We conclude that our MW-FD polarizabilities have field-related errors *at least* below 1% but usually much lower than this.

4.2. How Good Are FD Results with the aug-pc4 Basis?

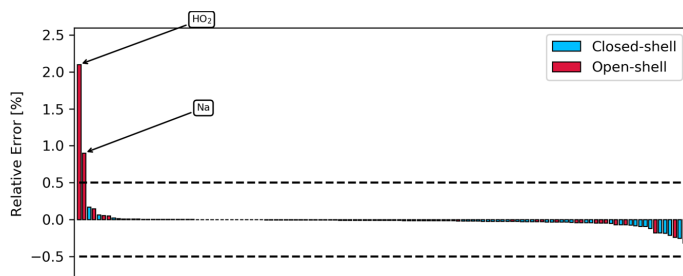To judge the quality of the FD aug-pc4 results, we

Figure 6. Distribution of REs of PBE polarizabilities for the 124 species, comparing GTO-LR with MW-FD, using the latter as a reference. The dashed lines are located at ±0.5% RE.

compared our MW-FD polarizabilities to the published GTO-FD polarizabilities.[7] The distribution of REs for all 124 species, as defined in eq 11 and with MWs as a reference, are presented in the left-most plot in Figure 2 and in more detail in Figure 3. Several features are revealed:

1. The error distribution suggests that FD aug-pc4 on average performs quite well, yielding a RE smaller than ±0.5% for most species.

2. GTOs seem to overestimate static polarizabilities, which may be counterintuitive as *analytical* polarizabilities are variationally approached from below.[12]

3. The most challenging species have open-shell electronic structures.

4. Six species have an RE larger than 1%, which, when considering the size of the basis set employed, should be considered significant errors: Li (7.3%); FH−OH (3.3%); HO_2 (2.3%); NaCl (1.9%); NaCN (1.5%); BeH (1.2%).

4.3. Is It a Basis Set Issue or an FD Issue? In order to evaluate whether the errors in Figure 3 arose from the FD approach, we compared the GTO-FD polarizabilities to computed GTO-LR values. The RE distribution for this comparison, using the analytical polarizabilities as a reference, is presented in the second plot in Figure 2 and in more detail in Figure 4. At first sight, the distribution is very similar to the one presented in Figure 3, indicating that GTO-FD polarizabilities have been contaminated by external field-related effects (the aug-pc4 benchmark study[7] used a field strength of 0.01 au for most species). To rule out the possibility that the two distributions incidentally show similar shapes, we plotted the two distributions against each other, species for species in Figure 5. Linear regression yielded an r^2 value of 0.97. Here it is clear that the error for one species is more or less the same across the two distributions, further indicating that the GTO-FD polarizabilities have been contaminated. Thus, our results show that the observed deviations between MW and GTO (aug-pc4) polarizabilities in Figure 3 are predominantly field-strength-related errors in the GTO-FD values.

4.4. What Is the True BSIE? In order to return to our original objective, the estimation of BSIEs in static polarizability predictions with the aug-pc4 basis set, we ultimately chose to compare GTO-LR and MW-FD values. Based on the above discussion, this comparison should yield the fairest estimation of the BSIE of aug-pc4. The RE distribution is presented in the center plot in Figure 2, and in more detail in Figure 6, and it is clear that the REs have been dramatically reduced for almost all species. Two species stand out with REs

larger than 0.5%: HO_2 (2.1%) and Na (0.9%). While both have open-shell (doublet) electronic structures, it is not clear what the origin of their relatively large REs may be. Despite the two outliers, the comparison in Figure 6 shows that the BSIE for aug-pc4 is very small.

4.5. Multiwavelets Can Handle Smaller Field Strengths than GTOs. Using FD calculations to estimate molecular response properties is a very simple approach, but it requires a careful consideration of the applied field strength. A weak field is required in order to stay within the linear regime, but this at the same time leads to the amplification of numerical errors due to cancellation of significant digits in the nominator of eq 3; a large field reduces numerical noise but simultaneously increases nonlinear effects from higher-order responses, leading to deviations from the correct result. The optimal compromise is therefore the weakest possible field that induces a sufficiently large first-order response in the dipole to obtain a sufficient number of digits in the polarizability. Examples of nonlinear behavior for a few species are presented and briefly discussed in the Supporting Information.

The MW framework guarantees that the computed dipoles are at the CBS limit with a controlled and systematically improvable precision:[50] the number of correct digits in the calculated polarizabilities can be improved systematically by tightening the precision thresholds. Therefore, MWs can make use of very small fields (10^{-3} or less) to eliminate higher-order responses, while still controlling the numerical noise by making use of tighter thresholds. As shown in Figure 1, even aug-pc4 has an error of roughly 10^{-3} in the energy as well as in the dipole moment, whereas the best MW calculation (MW7) yields three additional digits (10^{-6}). Making use of such a small field for GTOs will therefore heavily rely on error cancellation.

5. CONCLUSIONS

We have shown that GTO-FD polarizabilities presented by Hait and Head-Gordon[7] display quite large errors, considering the size of the aug-pc4 basis set used. However, we conclude that these errors mainly originate from field strength-related effects and not from BSIEs. Indeed, GTO-LR polarizabilities computed with aug-pc4 are very close to the CBS limit, which we have confirmed by comparing to very precise MW reference calculations. Specifically, we show that the observed errors exceeding 1% in GTO-FD polarizabilities are attributed to a field strength of 0.01 au, while the MRE of 0.06% in GTO-LR polarizabilities is attributed to the BSIE of aug-pc4.

The internal validation of our MW results demonstrates that MW-FD polarizabilities can be made virtually free from field strength-related effects, because numerical issues arising from using very small fields can be countered by tightening the MW thresholds. Our MW-FD polarizabilities using a field strength of 0.001 au show a MRE of 0.02% relative to a MW-LR reference.

For future benchmarks of any property, we recommend to validate that the reference data indeed is at the CBS limit by comparing to MW results.

■ ASSOCIATED CONTENT

⒮ Supporting Information

The Supporting Information is available free of charge at https://pubs.acs.org/doi/10.1021/acs.jctc.0c00128.

Cartesian coordinates of all species, data sets for all presented results, Python code for all data analyses and figure generation, and a brief discussion of nonlinearity effects and MW-FD validations (ZIP)

■ AUTHOR INFORMATION

Corresponding Author

Luca Frediani − Hylleraas Centre for Quantum Molecular Sciences, Department of Chemistry, UiT, The Arctic University of Norway, 9037 Tromsø, Norway; ⓞ orcid.org/0000-0003-0807-682X; Email: luca.frediani@uit.no

Authors

Anders Brakestad − Hylleraas Centre for Quantum Molecular Sciences, Department of Chemistry, UiT, The Arctic University of Norway, 9037 Tromsø, Norway; ⓞ orcid.org/0000-0001-9361-2759

Stig Rune Jensen − Hylleraas Centre for Quantum Molecular Sciences, Department of Chemistry, UiT, The Arctic University of Norway, 9037 Tromsø, Norway; ⓞ orcid.org/0000-0002-2175-5723

Peter Wind − Hylleraas Centre for Quantum Molecular Sciences, Department of Chemistry, UiT, The Arctic University of Norway, 9037 Tromsø, Norway

Marco D'Alessandro − Istituto di Struttura della Materia, Consiglio Nazionale delle Ricerche, 00133 Roma, Italia

Luigi Genovese − Laboratoire de Simulation Atomistique, Université Grenoble Alpes, CEA, INAC-MEM, 38000 Grenoble, France

Kathrin Helen Hopmann − Hylleraas Centre for Quantum Molecular Sciences, Department of Chemistry, UiT, The Arctic University of Norway, 9037 Tromsø, Norway; ⓞ orcid.org/0000-0003-2798-716X

Complete contact information is available at:
https://pubs.acs.org/10.1021/acs.jctc.0c00128

Notes

The authors declare no competing financial interest.

■ ACKNOWLEDGMENTS

■ REFERENCES

(1) Kohn, W.; Sham, L. J. Self-Consistent Equations Including Exchange and Correlation Effects. *Phys. Rev.* **1965**, *140*, A1133−A1138.

(2) Hermann, J.; DiStasio, R. A.; Tkatchenko, A. First-Principles Models for van der Waals Interactions in Molecules and Materials: Concepts, Theory, and Applications. *Chem. Rev.* **2017**, *117*, 4714−4758.

(3) Zhan, Y.-Y.; Jiang, Q.-C.; Ishii, K.; Koide, T.; Kobayashi, O.; Kojima, T.; Takahashi, S.; Tachikawa, M.; Uchiyama, S.; Hiraoka, S. Polarizability and isotope effects on dispersion interactions in water. *Communications Chemistry* **2019**, *2*, 2399−3669.

(4) Parchaňský, V.; Kapitán, J.; Bouř, P. Inspecting chiral molecules by Raman optical activity spectroscopy. *RSC Adv.* **2014**, *4*, 57125−57136.

(5) Bedrov, D.; Piquemal, J.-P.; Borodin, O.; MacKerell, A. D.; Roux, B.; Schröder, C. Molecular Dynamics Simulations of Ionic Liquids and Electrolytes Using Polarizable Force Fields. *Chem. Rev.* **2019**, *119*, 7940−7995.

(6) Baker, C. M. Polarizable force fields for molecular dynamics simulations of biomolecules. *WIREs Computational Molecular Science* **2015**, *5*, 241−254.

(7) Hait, D.; Head-Gordon, M. How accurate are static polarizability predictions from density functional theory? An assessment over 132 species at equilibrium geometry. *Phys. Chem. Chem. Phys.* **2018**, *20*, 19800−19810.

(8) Jensen, F. Polarization consistent basis sets: Principles. *J. Chem. Phys.* **2001**, *115*, 9113−9125.

(9) Jensen, F. Polarization consistent basis sets: II. Estimating the Kohn-Sham basis set limit. *J. Chem. Phys.* **2002**, *116*, 7372−7379.

(10) Jensen, F. Polarization consistent basis sets. III. The importance of diffuse functions. *J. Chem. Phys.* **2002**, *117*, 9234−9240.

(11) Jensen, F.; Helgaker, T. Polarization consistent basis sets. V. The elements Si-Cl. *J. Chem. Phys.* **2004**, *121*, 3463−3470.

(12) Hylleraas, E. A.; Undheim, B. Numerische Berechnung der 2 S-Terme von Ortho- und Par-Helium. *Eur. Phys. J. A* **1930**, *65*, 759−772.

(13) Alpert, B. K. A Class of Bases in L^2 for the Sparse Representation of Integral Operators. *SIAM Journal on Mathematical Analysis* **1993**, *24*, 246−262.

(14) Keinert, F. *Wavelets and Multiwavelets*, 1st ed.; Chapman and Hall: 2003.

(15) Alpert, B.; Beylkin, G.; Gines, D.; Vozovoi, L. Adaptive solution of partial differential equations in multiwavelet bases. *J. Comput. Phys.* **2002**, *182*, 149−190.

(16) Beylkin, G.; Cheruvu, V.; Perez, F. Fast adaptive algorithms in the non-standard form for multidimensional problems. *Applied and Computational Harmonic Analysis* **2008**, *24*, 354−377.

(17) Frediani, L.; Fossgaard, E.; Flå, T.; Ruud, K. Fully adaptive algorithms for multivariate integral equations using the non-standard form and multiwavelets with applications to the Poisson and bound-state Helmholtz kernels in three dimensions. *Mol. Phys.* **2013**, *111*, 1143−1160.

(18) Beylkin, G.; Cramer, R.; Fann, G.; Harrison, R. J. Multi-resolution separated representations of singular and weakly singular operators. *Applied and Computational Harmonic Analysis* **2007**, *23*, 235−253.

(19) Harrison, R. J.; Fann, G. I.; Yanai, T.; Gan, Z.; Beylkin, G. Multiresolution quantum chemistry: Basic theory and initial applications. *J. Chem. Phys.* **2004**, *121*, 11587.

(20) Jensen, S. R.; Saha, S.; Flores-Livas, J. A.; Huhn, W.; Blum, V.; Goedecker, S.; Frediani, L. The Elephant in the Room of Density Functional Theory Calculations. *J. Phys. Chem. Lett.* **2017**, *8*, 1449−1457.

(21) Kato, T.; Yokoi, Y.; Sekino, H. Basis set limit computation of dynamic polarizability at near-resonance region. *Int. J. Quantum Chem.* **2013**, *113*, 286−289.

(22) Sekino, H.; Maeda, Y.; Yanai, T.; Harrison, R. J. Basis set limit Hartree−Fock and density functional theory response property

evaluation by multiresolution multiwavelet basis. *J. Chem. Phys.* **2008**, *129*, 034111.

(23) Jensen, S. R.; Flå, T.; Jonsson, D.; Monstad, R. S.; Ruud, K.; Frediani, L. Magnetic properties with multiwavelets and DFT: the complete basis set limit achieved. *Phys. Chem. Chem. Phys.* **2016**, *18*, 21145−21161.

(24) Jensen, F. *Introduction to Computational Chemistry*, 2nd ed.; Wiley: 2007.

(25) Daubechies, I.; Grossmann, A.; Meyer, Y. Painless non-orthogonal expansions. *J. Math. Phys.* **1986**, *27*, 1271−1283.

(26) Yanai, T.; Fann, G. I.; Gan, Z.; Harrison, R. J.; Beylkin, G. Multiresolution quantum chemistry in multiwavelet bases: Hartree−Fock exchange. *J. Chem. Phys.* **2004**, *121*, 6680.

(27) Yanai, T.; Fann, G. I.; Gan, Z.; Harrison, R. J.; Beylkin, G. Multiresolution quantum chemistry in multiwavelet bases: Analytic derivatives for Hartree−Fock and density functional theory. *J. Chem. Phys.* **2004**, *121*, 2866.

(28) Kobus, J.; Laaksonen, L.; Sundholm, D. A numerical Hartree-Fock program for diatomic molecules. *Comput. Phys. Commun.* **1996**, *98*, 346−358.

(29) Mahan, G. Modified Sternheimer equation for polarizability. *Phys. Rev. A: At., Mol., Opt. Phys.* **1980**, *22*, 1780−1785.

(30) Andrade, X.; Botti, S.; Marques, M. A. L.; Rubio, A. Time-dependent density functional theory scheme for efficient calculations of dynamic (hyper)polarizabilities. *J. Chem. Phys.* **2007**, *126*, 184106.

(31) D'Alessandro, M.; Genovese, L. Locality and computational reliability of linear response calculations for molecular systems. *Physical Review Materials* **2019**, *3*, 023805.

(32) MRCPP library 2020. DOI: 10.5281/zenodo.3749748.

(33) MRC$_{hem}$ program package 2020. DOI: 10.5281/zenodo.3786996.

(34) MRC$_{hem}$ documentation 2020. https://mrchem.readthedocs.io/en/latest/.

(35) It is not feasible to converge beyond ϵ_{rel} due to numerical noise, so we leave a factor of 10 between ϵ_{mo} and ϵ_{rel} to be on the safe side.

(36) Vosko, S. H.; Wilk, L.; Nusair, M. Accurate spin-dependent electron liquid correlation energies for local spin density calculations: a critical analysis. *Can. J. Phys.* **1980**, *58*, 1200−1211.

(37) Perdew, J. P.; Burke, K.; Ernzerhof, M. Generalized Gradient Approximation Made Simple. *Phys. Rev. Lett.* **1996**, *77*, 3865−3868.

(38) Ekström, U.; Visscher, L.; Bast, R.; Thorvaldsen, A. J.; Ruud, K. Arbitrary-Order Density Functional Response Theory from Automatic Differentiation. *J. Chem. Theory Comput.* **2010**, *6*, 1971−1980.

(39) Van Lenthe, J. H.; Zwaans, R.; Van Dam, H. J. J.; Guest, M. F. Starting SCF calculations by superposition of atomic densities. *J. Comput. Chem.* **2006**, *27*, 926−932.

(40) Harrison, R. J. Krylov subspace accelerated inexact Newton method for linear and nonlinear equations. *J. Comput. Chem.* **2004**, *25*, 328−334.

(41) Neese, F. Software update: the ORCA program system, version 4.0. *Wiley Interdiscip. Rev.: Comput. Mol. Sci.* **2018**, *8*, e1327.

(42) Pulay, P. Convergence acceleration of iterative sequences. the case of scf iteration. *Chem. Phys. Lett.* **1980**, *73*, 393−398.

(43) Pulay, P. Improved SCF convergence acceleration. *J. Comput. Chem.* **1982**, *3*, 556−560.

(44) Hait, D.; Head-Gordon, M. Private communication, 2019.

(45) However, we believe that the reason for the two different components is not a consequence of the mean-field treatment but that it naturally derives from elementary considerations of degenerate perturbation theory. We are currently investigating this issue and will report on it elsewhere.

(46) Harrison, R. J.; Beylkin, G.; Bischoff, F. A.; Calvin, J. A.; Fann, G. I.; Fosso-Tande, J.; Galindo, D.; Hammond, J. R.; Hartman-Baker, R.; Hill, J. C.; Jia, J.; Kottmann, J. S.; Yvonne Ou, M.-J.; Pei, J.; Ratcliff, L. E.; Reuter, M. G.; Richie-Halford, A. C.; Romero, N. A.; Sekino, H.; Shelton, W. A.; Sundahl, B. E.; Thornton, W. S.; Valeev, E. F.; Vázquez-Mayagoitia, A.; Vence, N.; Yanai, T.; Yokoi, Y. MADNESS: A Multiresolution, Adaptive Numerical Environment for Scientific Simulation. *SIAM Journal on Scientific Computing* **2016**, *38*, S123−S142.

(47) Goerigk, L.; Mehta, N. A Trip to the Density Functional Theory Zoo: Warnings and Recommendations for the User. *Aust. J. Chem.* **2019**, *72*, 563−573.

(48) Hait, D.; Head-Gordon, M. How Accurate Is Density Functional Theory at Predicting Dipole Moments? An Assessment Using a New Database of 200 Benchmark Values. *J. Chem. Theory Comput.* **2018**, *14*, 1969−1981.

(49) Brakestad, A.; Jensen, S. R.; Wind, P.; D'Alessandro, M.; Genovese, L.; Hopmann, K. H.; Frediani, L. Replication Data for: Static polarizabilities at the basis set limit: A benchmark of 124 species. 2020. DOI: 10.18710/KLQVOK.

(50) The inherent limits are dictated by the double precision in the numerical representation.

Paper II

Multiwavelets applied to metal–ligand interactions: Energies free from basis set errors

Anders Brakestad, Peter Wind, Stig Rune Jensen,
Luca Frediani, and Kathrin H. Hopmann

J. Chem. Phys. **154** (2021), 214302,
DOI: 10.1063/5.0046023

Supporting Information Available At:
https://aip.scitation.org/doi/suppl/10.1063/5.0046023

Replication Data Available at:
https://doi.org/10.18710/WA5YCF

PAPER III

Scalar relativistic effects with Multiwavelets: Implementation and benchmark

Anders Brakestad, Stig Rune Jensen, Kathrin Helen Hopmann, and Luca Frediani

Manuscript in preparation

Scalar relativistic effects with Multiwavelets: Implementation and benchmark

Anders Brakestad,[†,‡,¶] Stig Rune Jensen,[†,‡,¶] Kathrin Helen Hopmann,[‡] and Luca Frediani[*,†,‡]

†*Hylleraas Centre for Quantum Molecular Sciences, UiT The Arctic University of Norway, 9037 Tromsø, Norway*

‡*Department of Chemistry, UiT The Arctic University of Norway, 9037 Tromsø, Norway*

¶*First authorship is shared between AB and SRJ*

E-mail: luca.frediani@uit.no

Abstract

Relativistic methods are steadily gaining momentum in the quantum chemistry community, because their importance for accurate modeling of heavier elements (5th row and below) is nowadays widely recognized. However, relativistic calculations also pose a challenge to traditional basis sets. The core region, where relativistic effects manifest, are difficult to model due to the nuclear cusp Multiwavelets overcome this challenge, due to a foundation in multiresolution analysis that leads to robust error control and adaptive algorithms that automatically refine the basis set description until the desired precision is reached. In this work we present a ZORA implementation in the MW code MRChem, and we provide a small benchmark of total energies for the 5th row elements.

1 Introduction

Quantum chemical modeling of the heavier elements of the periodic table (5th-7th row) is important, because such elements are employed in a large number of technological applications. It is also challenging, because their correct modeling requires relativistic effects be taken into account. Relativity can play a role in a variety of properties, from the color of elements, to their physical properties and to their catalytic behaviour[1–4]. While relativistic effects may be more pronounced from the 5th row of the periodic table, it should be acknowledged that the properties of lighter elements also can be influenced by relativity[5].

Several strategies exist today for including relativistic effects in quantum chemistry calculations. The simplest and most widely employed is the use of effective core potentials (ECPs), also known as pseudopotentials in the physics community. Most chemical transformations involve the outer shell electrons, and the core electrons are largely unaffected. As such it is convenient to consider a core composed not only by the bare nucleus, but also by one or more shells of core electrons. The approach has two important advantages: i) the calculation becomes faster, and ii) relativistic effects, which are predominant for core electrons, can be implicitly accounted for by parametrizing the core potentials to relativistic calculations. The main drawbacks of such an approach are the need to parametrize and choose an ECP, leading to practical issues similar to those arising when basis sets are considered, and the lack of explicit description of core electrons which prevents using such an approach for core related properties such as X-Ray spectroscopy[6] or NMR shielding constants[3].

The alternative to ECPs is the explicit inclusion of all core electrons in the calculation. The Dirac equation for the electron, and the resulting four-component wave function, constitutes the starting point for such a treatment. Its extension to the molecular framework leads to the usual electronic structure methods, albeit using four-component spinors instead of the non-relativistic orbitals. Although this is the most accurate description available, it is also the most computationally expensive: spinors are 4-component complex functions. Additionally, spin is not a good quantum number in a relativistic framework and the simplified

picture of two electrons with opposite spin sharing the same orbital is no longer valid. Most operators couple the different components of a spinor, thus leading roughly to a factor 100 in computational cost, because coupling four complex functions requires 8×8 matrices instead of a real scalar.

Although progress has been made to make 4-component calculations faster and easily available[7–10], it is still convenient to attempt approximations that promise great reduction in the computational cost at the price of reduced accuracy. The first step in such a hierarchy of approximations is the elimination of the small components through a Foldy–Wouthuysen (FW) transformation. The choice of transformation leads to different kinds of methods, such as the Pauli Hamiltonian, the Regular Approximation (RA), the Douglas-Kroll-Hess Hamiltonian, or the exact two-component (X2C) method. Further reduction to a scalar method is also possible for the Pauli Hamiltonian and the RA.

In particular, the RA has two interesting features: (1) the part of the FW transformation can be expanded in a convergent series to recover the exact elimination and (2) the renormalization part can be exactly incorporated in the wave function. The zero-order regular approximation (ZORA) is the simplest form of Hamiltonian keeping only the zeroth order in both parts. The reduction to a scalar method is then carried out by applying the Dirac identity and discarding the spin-polarization term. In practical terms, the advantage of ZORA is that the standard algorithms of quantum chemistry can be mostly kept in their original form, just including the contribution from the modified ZORA kinetic energy. As shown below, this simply amounts to including an additional function κ where necessary in the equations. This can at the same time be a challenge as κ is mostly unity (no effect) besides a tiny region around each nucleus, where standard approaches generally struggle to get an accurate description. The problem is further aggravated for heavier nuclei, where such a correction is important, and at the same time the number of basis sets available is more limited and less is known about their true precision. Some efforts to assess the precision of Gaussian type orbitals (GTOs) for heavier elements have been undertaken, but it is

anyway challenging to assess the precision without an external reference. One such option for helium-like ions (He, Ne^{8+}, Ar^{16+}, etc) is constituted by the rescaling properties of the ZORA Hamiltonian in a two-component framework, which should then yield the (rescaled) exact Dirac energies for such a system. However, for many-electron systems, and/or for a scalar relativistic approach, assessing the true precision of a GTO basis is challenging.

Examples of all-electron relativistic basis sets include the universal Gaussian basis set UGBS[11], the atomic natural orbitals basis sets[12–16], the X2C basis sets[17], and the segmented all-electron relativistically contracted basis sets in the SARC series[18–22]. Importantly, such basis sets have to be fitted to the chosen Hamiltonian (ZORA, DKH2, etc). This comes on top of the required fitting of the basis set to a given electronic structure method, and if relevant, to a particular property[22]. Thus, although some of the known all-electron relativistic basis sets may provide good results for a particular method and property, their transferability is limited.

In recent years, Multiwavelets have emerged as a powerful alternative to traditional GTOs[23]. Their foundation in the robust mathematics of multiresolution analysis[24] leads to a basis set that is not empirically parametrized. Robust error control[25–27] means the user can set a finite but arbitrary target precision, and adaptive algorithms[28–30] ensure that the representations of molecular orbitals are automatically refined until the required precision is reached. The large number of available GTO basis sets reflect an underlying challenge in that no single basis set is good enough to describe all properties of interest to sufficient precision. Multiwavelets are in this sense a great step towards a black-box situation for basis sets, where just simple numerical considerations are required from the user, which makes them easy to use to non-experts. One can think of the MW basis set as being constructed to the necessary precision on-the-fly, and it should in principle be applicable for the computation of any property.

In this work we present a MW implementation of the ZORA method into the MRChem code. We use this to give a benchmark of total energies for all 5th row elements, and compare

to various all-electron GTO basis sets. In the next section we derive the ZORA equations, and give some details on the MW implementation. Then we mention the computational details, show some preliminary results, and end with some concluding remarks.

2 Theory and implementation

2.1 From the Dirac equation to the scalar ZORA Hamiltonian

We will briefly expose how the scalar ZORA method is derived, starting from the 4-component Dirac equation of an electron:

$$\left(\beta c^2 + V + c\boldsymbol{\alpha} \cdot \boldsymbol{p}\right)\Psi = E\Psi \tag{1}$$

where we assume atomic units ($m_e = 1$, $\hbar = 1$, $e = -1$), $\boldsymbol{p} = (-i\partial/\partial x, -i\partial/\partial y, -i\partial/\partial z)$ is the momentum operator, c is the speed of light, V is the external potential, Ψ is a 4-component wave function, and $\boldsymbol{\alpha}$ and β are defined as follows:

$$\beta = \begin{pmatrix} I_2 & 0 \\ 0 & -I_2 \end{pmatrix} \quad \boldsymbol{\alpha} = \begin{pmatrix} 0 & \boldsymbol{\sigma} \\ \boldsymbol{\sigma} & 0 \end{pmatrix}$$

$$\sigma_x = \begin{pmatrix} 0 & 1 \\ 1 & 0 \end{pmatrix} \quad \sigma_y = \begin{pmatrix} 0 & -i \\ i & 0 \end{pmatrix} \quad \sigma_z = \begin{pmatrix} 1 & 0 \\ 0 & -1 \end{pmatrix} \tag{2}$$

The first step towards the scalar ZORA consists in applying the Foldy–Wouthuysen transformation to the four-component Dirac Hamiltonian:

$$H^{FW} = U^{\dagger} H^D U \tag{3}$$

where the transformation matrix $U = W_1 W_2$ is a product of a decoupling matrix W_1 and a renormalization matrix W_2:

$$W_1 = \begin{pmatrix} 1 & -R^\dagger \\ R & 1 \end{pmatrix} \qquad W_2 = \begin{pmatrix} 1/\sqrt{1 + R^\dagger R} & 0 \\ 0 & 1/\sqrt{1 + RR^\dagger} \end{pmatrix} \qquad (4)$$

and R is the exact coupling between the large and the small components of a 4-spinor:

$$R = \frac{1}{2c^2 - V + E} c\boldsymbol{\sigma} \cdot \boldsymbol{p}$$

The inverse potential term depends on the eigenvalue E. Such a dependence can be expanded in a Taylor series as follows:

$$R = \frac{1}{2c^2 - V} \left(1 + \frac{E}{2c^2 - V} \right) \boldsymbol{\sigma} \cdot \boldsymbol{p} = \frac{1}{2c^2 - V} \sum_{k=0}^{\infty} \frac{(-E)^k}{(2c^2 - V)^k} \boldsymbol{\sigma} \cdot \boldsymbol{p}$$

Restricting the expansion to the zero-th order, leads to the so-called Regular Approximation. Once the renormalization W_2 is also considered, the following two-component Hamiltonian is obtained:

$$H^{RA} = \frac{1}{\sqrt{1 + R^\dagger R}} \left[V + \boldsymbol{\sigma} \cdot \boldsymbol{p} \frac{c^2}{2c^2 - V} \boldsymbol{\sigma} \cdot \boldsymbol{p} \right] \frac{1}{\sqrt{1 + R^\dagger R}}$$

The ZORA Hamiltonian is then obtained by Taylor-expanding the renormalization operator and retaining only the zero-order term:

$$H^{ZORA} = V + \boldsymbol{\sigma} \cdot \boldsymbol{p} \frac{c^2}{2c^2 - V} \boldsymbol{\sigma} \cdot \boldsymbol{p}$$

The following step consists in isolating and neglecting the spin polarization part from the kinetic energy by virtue of the Dirac identity $(\boldsymbol{\sigma} \cdot \boldsymbol{A})(\boldsymbol{\sigma} \cdot \boldsymbol{B}) = \boldsymbol{A} \cdot \boldsymbol{B} + i\boldsymbol{\sigma} \cdot (\boldsymbol{A} \times \boldsymbol{B})$:

$$H^{ZORA} = V + \boldsymbol{p} \frac{c^2}{2c^2 - V} \cdot \boldsymbol{p} = V + \frac{1}{2} \boldsymbol{p} \kappa \cdot \boldsymbol{p}$$

where in the last expression we have implicitly defined $\kappa = (1 - \frac{V}{2c^2})^{-1}$.

Given the scalar ZORA Hamiltonian, a Kohn-Sham density functional theory (DFT)

implementation is then obtained by replacing the kinetic energy operator with the ZORA counterpart:

$$\left(\frac{1}{2} \boldsymbol{p} \cdot \kappa \boldsymbol{p} + V \right) \varphi_i = \epsilon_i \varphi_i$$

It should be noted that in practical implementations the potential defining κ is usually *not* the full Kohn-Sham (KS) potential. Given the form of κ, the most important contribution is the nuclear attraction. Introducing Coulomb ($\hat{J}$) and exchange and correlation ($\hat{V}_{xc}$) is possible, but the corresponding operator would have to be recomputed numerically at each iteration, which is computationally demanding. Additionally, operations such as function multiplications are difficult to perform in traditional LCAO basis representations. In practice, a fixed pre-computed atomic potential is most often used, which is called the atomic-ZORA approximation.

2.2   ZORA equations in a Multiwavelet framework

To obtain a Multiwavelet implementation of the ZORA eigenvalue problem, it is necessary to transform the differential equation into an integral equation, in analogy with the non-relativistic case[25,27]. The standard KS equations can be concisely written as follows:

$$\hat{F}\varphi_i = \sum_j F_{ij}\varphi_j, \tag{5}$$

where $\hat{F}$ is the Fock operator, φ_i refer to an occupied molecular orbital, and F_{ij} are the matrix elements of the Fock operator between two occupied orbitals, assuming a general non-canonical (non-diagonal) form.

Within the framework of KS-DFT the Fock operator consists of the kinetic energy $\hat{T}$, the nuclear attraction $\hat{V}_{nuc}$, the Coulomb repulsion $\hat{J}$, the Hartree-Fock exchange $\hat{K}$ and the exchange and correlation potential $\hat{V}_{xc}$:

$$\hat{F} = \hat{T} + \hat{V}_{nuc} + \hat{J} - \hat{K} + \hat{V}_{xc}. \tag{6}$$

In the non-relativistic domain, the coupled KS differential equations (5) can be rewritten in integral form, by making use of the bound-state Helmholtz kernel. For the derivation we refer to the literature[31,32]. We report here the final expression:

$$\varphi_i = -2\hat{G}_{\mu_i} \left(\hat{V} \varphi_i - \sum_{j \neq i} F_{ij} \varphi_j \right), \tag{7}$$

where $\hat{G}_{\mu_i}$ is the integral convolution operator associated with the bound-state Helmholtz kernel $G(r) = e^{-\mu_i r}/r$, using $\mu_i = \sqrt{-2F_{ii}}$. In the ZORA Hamiltonian, the kinetic energy operator becomes:

$$\hat{T} = \boldsymbol{p} \cdot \frac{c^2}{2c^2 - V_Z} \boldsymbol{p} = -\frac{c^2}{2c^2 - V_Z} \nabla^2 - \nabla \frac{c^2}{2c^2 - V_Z} \cdot \nabla = -\frac{1}{2} \kappa \nabla^2 - \frac{1}{2} \nabla \kappa \cdot \nabla. \tag{8}$$

Here we denote the ZORA potential V_Z, which can be chosen to be the nuclear potential only (nZORA), a superposition of pre-computed atomic potentials (aZORA) or the full self-consistent KS potential (ZORA). Using the full (semi-local) KS potential does not pose any issue in the Multiwavelet framework, other than the computational overhead of having to update the potential at every iteration, since all the potentials are anyway treated on an equal footing using a numerical grid. The Hartree-Fock exchange, however, remains a challenge, because it cannot be written in a closed form and as such is not amenable to the approach presented here.

Inserting the ZORA kinetic operator into Eq. (5) we obtain:

$$\left(-\frac{1}{2} \kappa \nabla^2 - \frac{1}{2} \nabla \kappa \cdot \nabla + V \right) \varphi_i = \sum_j F_{ij} \varphi_j. \tag{9}$$

In order to make use of the same framework as the non-relativistic implementation of Eq. (7), it is necessary to isolate the Laplacian and the diagonal element of the sum on the right-hand side, which together make up the bound-state Helmholtz operator $\hat{G} = (\nabla^2 + 2F_{ii})^{-1}$. As can be seen from Eq. (9), this cannot be achieved directly since there is a factor κ separating

the two. We can however get it to the desired form by subtracting a "kappa-energy" term $(\kappa F_{ii} \varphi_i)$ on both sides of the equation

$$\left(-\frac{1}{2}\kappa\nabla^2 - \frac{1}{2}\nabla\kappa\cdot\nabla + V + \kappa F_{ii}\right)\varphi_i = \kappa F_{ii}\varphi_i + \sum_j F_{ij}\varphi_j, \tag{10}$$

and then divide through by κ. With standard algebraic manipulations we obtain:

$$-\frac{1}{2}\left(\nabla^2 + 2F_{ii}\right)\varphi_i = \frac{1}{2}\frac{\nabla\kappa}{\kappa}\cdot\nabla\varphi_i - \left(\frac{V}{\kappa} + \frac{V_Z}{2c^2}F_{ii}\right)\varphi_i + \frac{1}{\kappa}\sum_{j\neq i}F_{ij}\varphi_j, \tag{11}$$

which can be converted to an integral equation, reusing the non-relativistic bound-state Helmholtz operator $\hat{G}_{\mu_i}$:

$$\varphi_i = -2\hat{G}_{\mu_i}\left[-\frac{1}{2}\frac{\nabla\kappa}{\kappa}\cdot\nabla\varphi_i + \left(\frac{V}{\kappa} + \frac{V_Z}{2c^2}F_{ii}\right)\varphi_i - \frac{1}{\kappa}\sum_{j\neq i}F_{ij}\varphi_j\right]. \tag{12}$$

In general, it cannot be expected that the iterative solution of Eq. (12) will work for arbitrary "shifts" in the equation as has been performed in the derivation above. In the current setting it is justified by recalling that $\kappa \simeq 1$ almost everywhere, except close to the nuclei. However, our tests indicate that the convergence is starting to break down when the ZORA contribution is getting more significant, either "physically" by going down the periodic table, or "artificially" by letting $c \to 0$. One has to keep in mind, though, that this is a regime where the ZORA method itself becomes questionable and should be used with care. In the non-relativistic limit ($c \to \infty$ and $\kappa \to 1$) the first term on the right-hand side of Eq. (12) vanishes and the second and third fall back to their non relativistic counterparts, thus recovering the non-relativistic form as in Eq. (7).

An alternative approach to obtain the desired $(\nabla^2 + 2F_{ii})$ term from Eq. (9) is to add a Laplacian term $(\frac{1}{2}\nabla^2)$ directly, thus avoiding division by κ. Our tests indicate that the strategy presented above works better, despite the additional singularity introduced. The main reason seems to be that the former strategy removes the Laplacian altogether, which

is ill-conditioned in the discontinuous Multiwavelet basis, whereas the latter keeps part of it on the right-hand side.

2.3 Implementation

A prototype implementation of the ZORA method as outlined above has been made in a development version of the MRChem package,[33] and is expected to appear in the next official release v1.1. MRChem is a numerical quantum chemistry code based on a multiwavelet framework, in which all functions and operators are represented on their own fully adaptive multi-resolution numerical real-space grid. This allows for efficient all-electron treatment of medium to large molecules (hundreds of atoms) at Hartree-Fock/KS-DFT level of theory.

The κ function is computed as a point-wise map of the chosen ZORA potential V_Z through

$$\kappa(r) = \frac{1}{1 - V_Z(r)/2c^2},$$ (13)

and similarly for its inverse

$$\kappa^{-1}(r) = 1 - V_Z(r)/2c^2.$$ (14)

Both of these functions are represented on their own adaptive numerical grid, and subsequently treated as standard multiplicative potential operators in the SCF procedure of solving Eq. (12).

The nuclear potential $\hat{V}_{nuc}$ is by far the most important contribution to the ZORA potential, and it needs to be treated with special care. In a non-relativistic setting, the nuclear singularity is removed by replacing the analytic $1/r$ potential with a smoothed approximation of the form[25]

$$u(r) = \frac{\text{erf}(r)}{r} + \frac{1}{3\sqrt{\pi}} \left(e^{-r^2} + 16e^{-4r^2} \right),$$ (15)

and then parametrized as $u(r/s)/s$, where s is a scalar smoothing parameter (when $s \to 0$, then $u(r/s)/s \to 1/r$). The smoothing parameter is usually chosen from the nuclear charge

Z and the desired precision ϵ as[25]

$$s = \left(\frac{0.00435\epsilon}{Z^5} \right)^{1/3}.$$ (16)

We have for now kept this form of the nuclear potential also in the ZORA setting, but its effect on the energy through the ZORA potential V_Z needs to be further investigated.

3 Computational details

MW calculations were performed with a development version of MRChem. A MW precision of 1×10^{-6} was used for validation tests of small atoms and molecules, while a precision of 1×10^{-8} was used in a small benchmark of the 5th row elements. GTO calculations were performed with the ORCA[34] version 5.0.1.[a] The resolution of the identity approximation was turned off (`!nori`), extra tight SCF convergence was requested (`!verytightscf`), and the largest available integration grid was requested (`!defgrid3`), to try and isolate any effects originating from the basis sets. All calculations were performed with the PBE functional[35]. The GTO basis sets studied are given in Table 1.

Table 1: GTO basis sets included in the 5th row benchmark of total energies.

Basis set	Relativistically contracted	Ref
UGBS	yes	[11]
ANO-R3	yes	[12,13]
ANO-RCC-VQZP	yes	[14–16]
Sapporo-QZP-2012-Diffuse	no	[36]
Sarc-ZORA-TZVPP	yes	[22]

---

[a]A race condition bug was recently reported in version 5.0.1. We have recomputed most elements with version 5.0.2 which addresses the bug, but no major differences were observed in our data. The data presented were obtained from version 5.0.1.

4   Results and discussion

Basis set errors in total energies, by comparison to multiwavelet reference data at a precision of 1×10^{-8}, for five different GTO basis sets are given in Figure 1. The errors systematically increase with the nuclear charge for all basis sets, but UGBS behaves a bit more erratically. UGBS delivers errors smaller than 0.1 Hartree, while the SARC basis set shows errors between 0.1 Hartree to 1.0 Hartree. The ANO and Sapporo basis sets have not been developed for use in DFT calculations, and so their poorer convergence displayed should perhaps be expected.
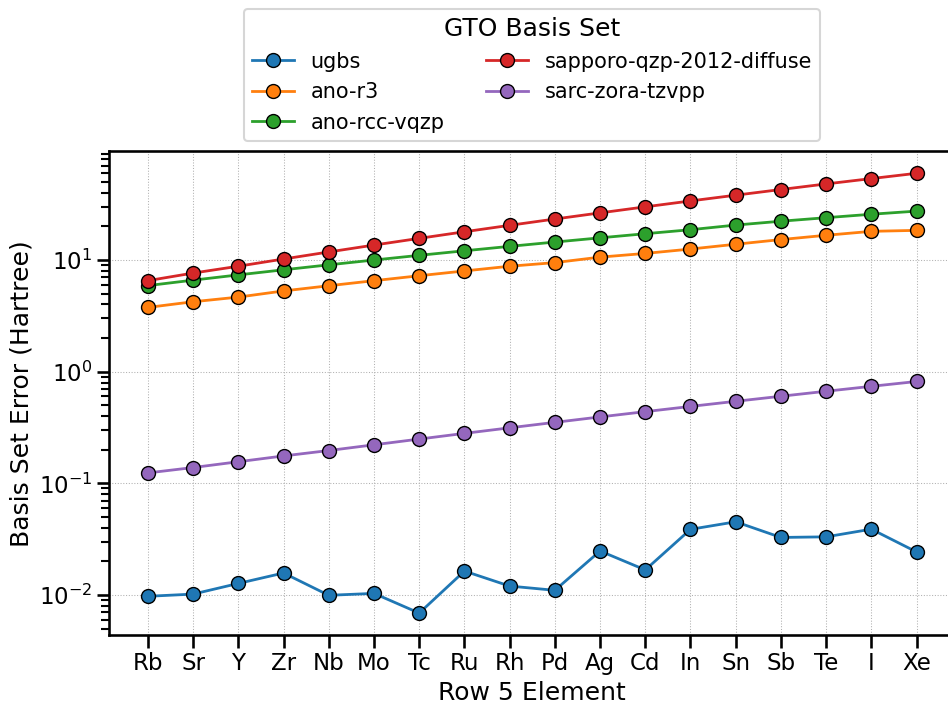

Figure 1: Basis set incompleteness errors in total energies for row 5 elements for five all-electron GTO basis sets compared to a MW8 reference.

We have also computed basis set errors for individual orbital energies for all species. Examples for Rb, Ag, and Sn are given in Figures 2 to 4, respectively. Both unsigned

deviations (UDs, given in Hartree) and relative unsigned deviations (RUDs, given in percent) are shown in the figure. For the three examples given here, the RUDs for UGBS tend to reach a plateau upon moving from core to valence orbitals. This plateauing leads to an increase in RUDs, due to the smaller orbital energies for the valence region. The same is not observed for the other basis sets, where UDs tend to be largest for core orbitals, and then decrease as one moves toward the valence region. This behavior leads instead to a plateau of the RUDs.
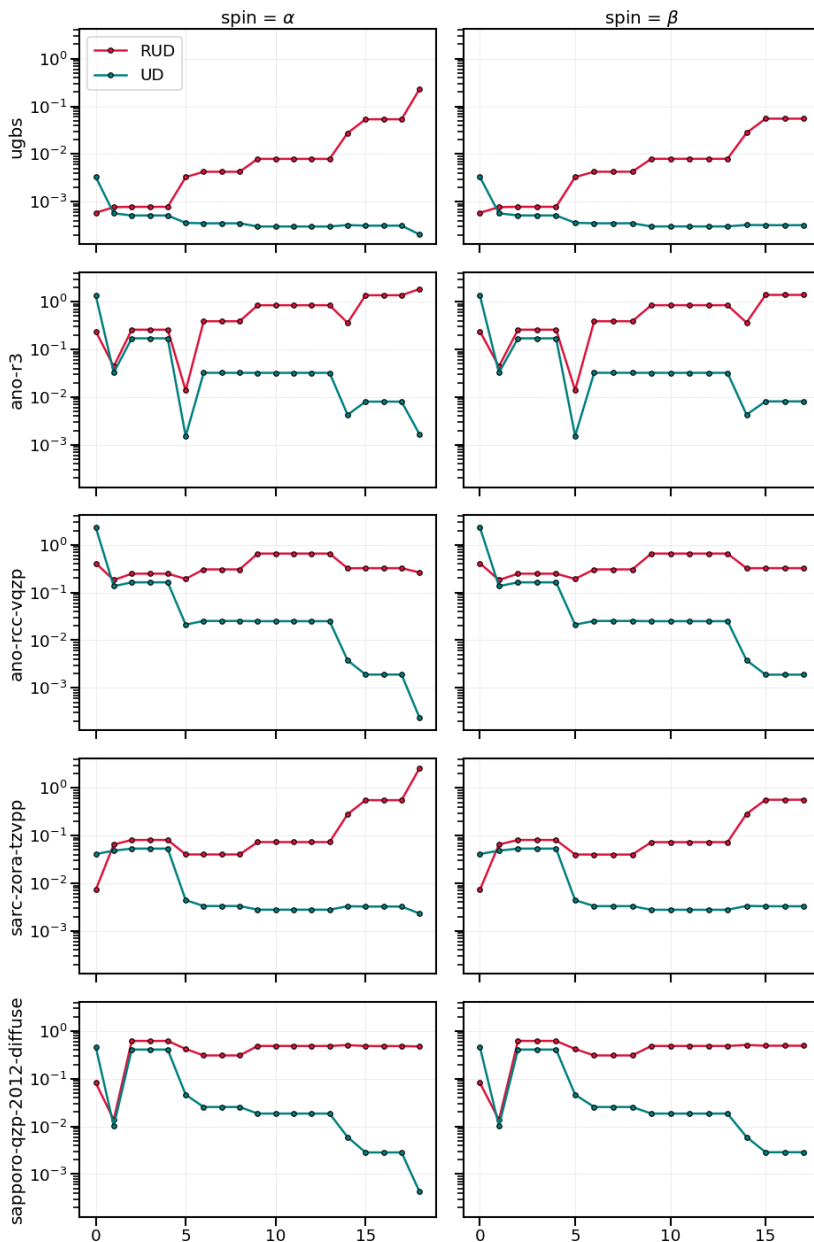
Figure 2: Basis set errors for α and β orbital energies for Rb. Each row corresponds to different GTO basis sets, and each column to orbitals of different spins. The reference data was computed with multiwavelets at a precision of 1×10^{-8}. The red lines show relative unsigned deviations in percent, while the teal lines show unsigned deviations in Hartrees.
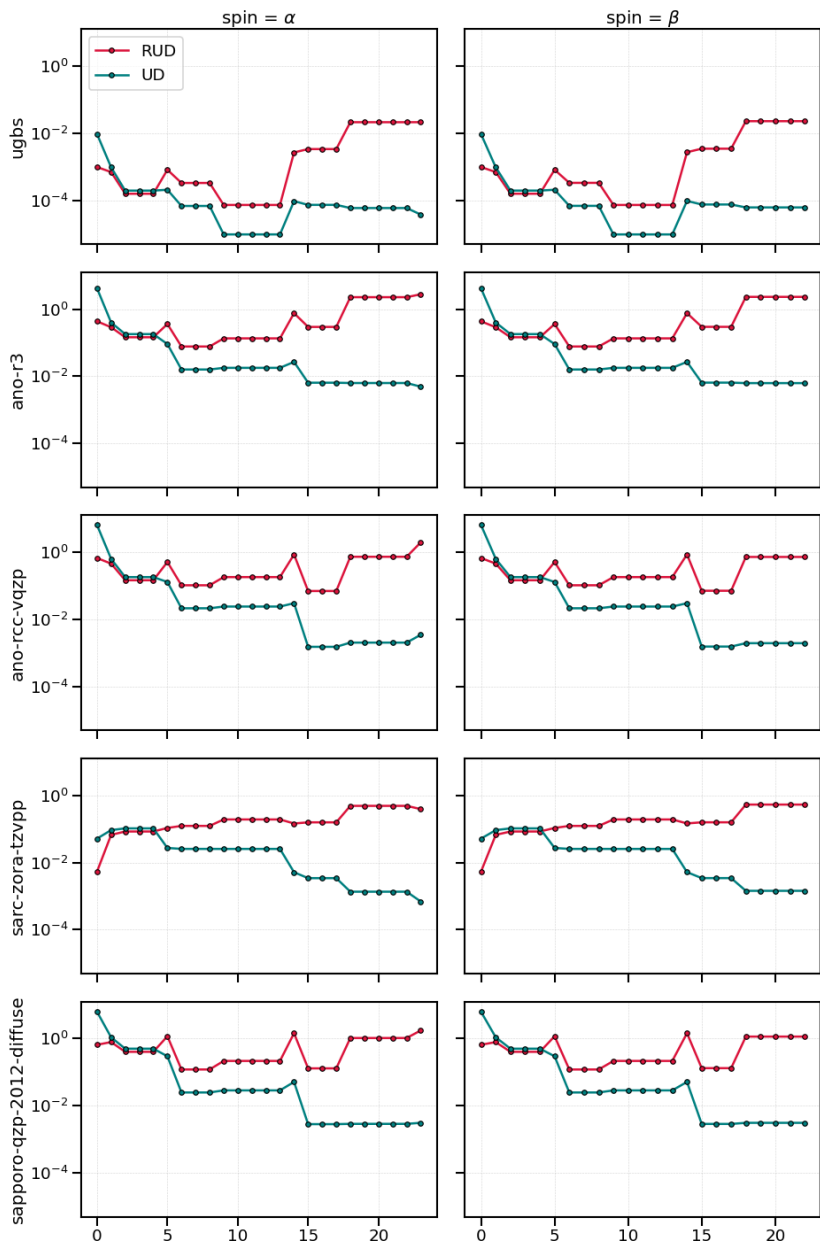
Figure 3: Basis set errors for α and β orbital energies for Ag. Each row corresponds to different GTO basis sets, and each column to orbitals of different spins. The reference data was computed with multiwavelets at a precision of 1×10^{-8}. The red lines show relative unsigned deviations in percent, while the teal lines show unsigned deviations in Hartrees.
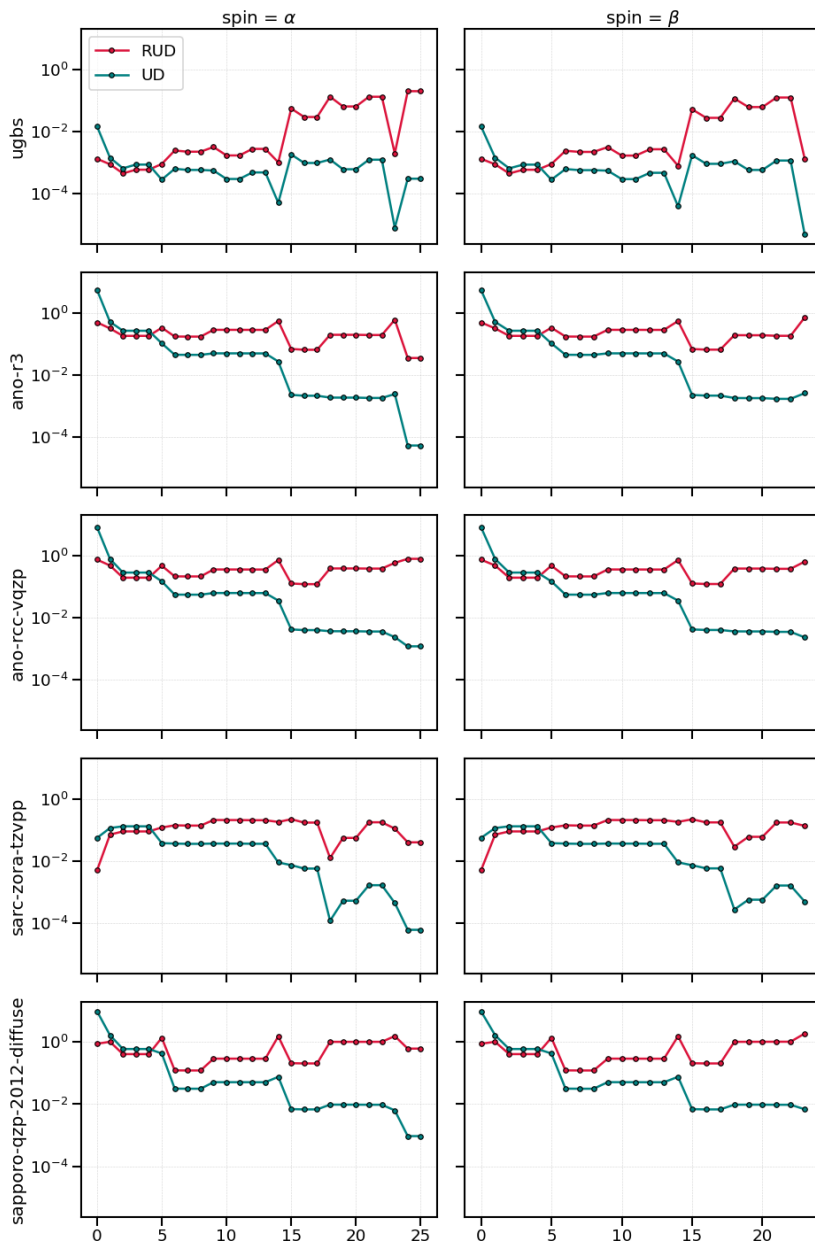
Figure 4: Basis set errors for α and β orbital energies for Sn. Each row corresponds to different GTO basis sets, and each column to orbitals of different spins. The reference data was computed with multiwavelets at a precision of 1×10^{-8}. The red lines show relative unsigned deviations in percent, while the teal lines show unsigned deviations in Hartrees.

16

5 Conclusions

We have combined Multiwavelets with the nuclear ZORA method, and implemented this into the MRChem program. This implementation has been used to compute total energies for the 5th row elements at the CBS limit, which have been compared to results from various GTO basis sets. We found that the UGBS basis set overall gave the smallest errors of approximately 0.01 Hartree. Short term we plan to extend the ZORA potential to include Coulomb contributions as well, and long term we will work towards a full four-component Hamiltonian within a MW framework.

Acknowledgement

References

(1) Pyykkö, P. Relativistic Effects in Chemistry: More Common Than You Thought. *Annual Review of Physical Chemistry* **2012**, *63*, 45–64.

(2) Demissie, T. B.; Garabato, B. D.; Ruud, K.; Kozlowski, P. M. Mercury Methylation by Cobalt Corrinoids: Relativistic Effects Dictate the Reaction Mechanism. *Angewandte Chemie International Edition 55*, 11503–11506.

(3) Vícha, J.; Marek, R.; Straka, M. High-Frequency 13C and 29Si NMR Chemical Shifts in Diamagnetic Low-Valence Compounds of TlI and PbII: Decisive Role of Relativistic Effects. *Inorganic Chemistry* **2016**, *55*, 1770–1781.

(4) Lein, M.; Rudolph, M.; Hashmi, S. K.; Schwerdtfeger, P. Homogeneous Gold Catal-

ysis: Mechanism and Relativistic Effects of the Addition of Water to Propyne. *Organometallics* **2010**, *29*, 2206–2210.

(5) Jorge, F. E.; Ferreira, I. B.; Soprani, D. D.; Gomes, T. Estimating the Impact of an All-Electron Basis Set and Scalar Relativistic Effects on the Structure, Stability, and Reactivity of Small Copper Clusters. *Journal of the Brazilian Chemical Society* **2015**,

(6) Rudek, B.; Toyota, K.; Foucar, L.; Erk, B.; Boll, R.; Bomme, C.; Correa, J.; Carron, S.; Boutet, S.; Williams, G. J.; Ferguson, K. R.; Alonso-Mori, R.; Koglin, J. E.; Gorkhover, T.; Bucher, M.; Lehmann, C. S.; Krässig, B.; Southworth, S. H.; Young, L.; Bostedt, C.; Ueda, K.; Marchenko, T.; Simon, M.; Jurek, Z.; Santra, R.; Rudenko, A.; Son, S.-K.; Rolles, D. Relativistic and resonant effects in the ionization of heavy atoms by ultra-intense hard X-rays. *Nature Communications* **2018**, *9*.

(7) Repisky, M.; Komorovsky, S.; Kadek, M.; Konecny, L.; Ekström, U.; Malkin, E.; Kaupp, M.; Ruud, K.; Malkina, O. L.; Malkin, V. G. ReSpect: Relativistic spectroscopy DFT program package. *The Journal of Chemical Physics* **2020**, *152*, 184101.

(8) Saue, T.; Bast, R.; Gomes, A. S. P.; Jensen, H. J. A.; Visscher, L.; Aucar, I. A.; Di Remigio, R.; Dyall, K. G.; Eliav, E.; Fasshauer, E.; Fleig, T.; Halbert, L.; Hedegård, E. D.; Helmich-Paris, B.; Iliaš, M.; Jacob, C. R.; Knecht, S.; Laerdahl, J. K.; Vidal, M. L.; Nayak, M. K.; Olejniczak, M.; Olsen, J. M. H.; Pernpointner, M.; Senjean, B.; Shee, A.; Sunaga, A.; van Stralen, J. N. P. The DIRAC code for relativistic molecular calculations. *The Journal of Chemical Physics* **2020**, *152*, 204104.

(9) Zhang, Y.; Suo, B.; Wang, Z.; Zhang, N.; Li, Z.; Lei, Y.; Zou, W.; Gao, J.; Peng, D.; Pu, Z.; Xiao, Y.; Sun, Q.; Wang, F.; Ma, Y.; Wang, X.; Guo, Y.; Liu, W. BDF: A relativistic electronic structure program package. *The Journal of Chemical Physics* **2020**, *152*, 064113.

(10) Belpassi, L.; De Santis, M.; Quiney, H. M.; Tarantelli, F.; Storchi, L. BERTHA: Imple-

mentation of a four-component Dirac–Kohn–Sham relativistic framework. *The Journal of Chemical Physics* **2020**, *152*, 164118.

(11) de Castro, E. V. R.; Jorge, F. E. Accurate universal Gaussian basis set for all atoms of the Periodic Table. *The Journal of Chemical Physics* **1998**, *108*, 5225–5229.

(12) Zobel, J. P.; Widmark, P.-O.; Veryazov, V. The ANO-R Basis Set. *Journal of Chemical Theory and Computation* **2020**, *16*, 278–294.

(13) Zobel, J. P.; Widmark, P.-O.; Veryazov, V. Correction to "The ANO-R Basis Set". *Journal of Chemical Theory and Computation* **2021**, *17*, 3233–3234.

(14) Roos, B. O.; Lindh, R.; Malmqvist, P.-Å.; Veryazov, V.; Widmark, P.-O. Main Group Atoms and Dimers Studied with a New Relativistic ANO Basis Set. *The Journal of Physical Chemistry A* **2004**, *108*, 2851–2858.

(15) Roos, B.; Veryazov, V.; Widmark, P.-O. Relativistic atomic natural orbital type basis sets for the alkaline and alkaline-earth atoms applied to the ground-state potentials for the corresponding dimers. *Theoretical Chemistry Accounts* **2004**, *111*, 345–351.

(16) Roos, B. O.; Lindh, R.; Malmqvist, P.-Å.; Veryazov, V.; Widmark, P.-O. New Relativistic ANO Basis Sets for Transition Metal Atoms. *The Journal of Physical Chemistry A* **2005**, *109*, 6575–6579.

(17) Pollak, P.; Weigend, F. Segmented Contracted Error-Consistent Basis Sets of Double- and Triple-ζ Valence Quality for One- and Two-Component Relativistic All-Electron Calculations. *Journal of Chemical Theory and Computation* **2017**, *13*, 3696–3705.

(18) Pantazis, D. A.; Neese, F. All-electron scalar relativistic basis sets for the lanthanides. *Journal of chemical theory and computation* **2009**, *5*, 2229–2238.

(19) Pantazis, D. A.; Neese, F. All-electron scalar relativistic basis sets for the actinides. *Journal of chemical theory and computation* **2011**, *7*, 677–684.

(20) Pantazis, D. A.; Neese, F. All-electron scalar relativistic basis sets for the 6 p elements. *Theoretical Chemistry Accounts* **2012**, *131*, 1–7.

(21) Aravena, D.; Neese, F.; Pantazis, D. A. Improved segmented all-electron relativistically contracted basis sets for the lanthanides. *Journal of chemical theory and computation* **2016**, *12*, 1148–1156.

(22) Rolfes, J. D.; Neese, F.; Pantazis, D. A. All-electron scalar relativistic basis sets for the elements Rb–Xe. *Journal of Computational Chemistry* **2020**, *41*, 1842–1849.

(23) Alpert, B. K. A Class of Bases in L^2 for the Sparse Representation of Integral Operators. *SIAM Journal on Mathematical Analysis* **1993**, *24*, 246–262.

(24) Keinert, F. In *Encyclopedia of Complexity and Systems Science*; Meyers, R. A., Ed.; Springer New York, 2009; pp 5841–5858.

(25) Harrison, R. J.; Fann, G. I.; Yanai, T.; Gan, Z.; Beylkin, G. Multiresolution quantum chemistry: Basic theory and initial applications. *The Journal of Chemical Physics* **2004**, *121*, 11587–11598.

(26) Kato, T.; Yokoi, Y.; Sekino, H. Basis set limit computation of dynamic polarizability at near-resonance region. *International Journal of Quantum Chemistry* **2012**, *113*, 286–289.

(27) Jensen, S. R.; Saha, S.; Flores-Livas, J. A.; Huhn, W.; Blum, V.; Goedecker, S.; Frediani, L. The Elephant in the Room of Density Functional Theory Calculations. *The Journal of Physical Chemistry Letters* **2017**, *8*, 1449–1457.

(28) Alpert, B.; Beylkin, G.; Gines, D.; Vozovoi, L. Adaptive Solution of Partial Differential Equations in Multiwavelet Bases. *Journal of Computational Physics* **2002**, *182*, 149–190.

(29) Beylkin, G.; Cheruvu, V.; Pérez, F. Fast adaptive algorithms in the non-standard form for multidimensional problems. *Applied and Computational Harmonic Analysis* **2008**, *24*, 354–377.

(30) Frediani, L.; Fossgaard, E.; Flå, T.; Ruud, K. Fully adaptive algorithms for multivariate integral equations using the non-standard form and multiwavelets with applications to the Poisson and bound-state Helmholtz kernels in three dimensions. *Molecular Physics* **2013**, *111*, 1143–1160.

(31) Kalos, M. H. Monte Carlo Calculations of the Ground State of Three- and Four-Body Nuclei. *Phys. Rev.* **1962**, *128*, 1791–1795.

(32) Beylkin, G.; Mohlenkamp, M. J. Numerical operator calculus in higher dimensions. *Proceedings of the National Academy of Sciences* **2002**, *99*, 10246–10251.

(33) MRCHEM program package **2020**. DOI: 10.5281/zenodo.3786996.

(34) Neese, F. Software update: the ORCA program system, version 4.0. *Wiley Interdisciplinary Reviews: Computational Molecular Science* **2018**, *8*, e1327.

(35) Perdew, J. P.; Burke, K.; Ernzerhof, M. Generalized Gradient Approximation Made Simple. *Physical Review Letters* **1996**, *77*, 3865–3868.

(36) Noro, T.; Sekiya, M.; Koga, T. Segmented contracted basis sets for atoms H through Xe: Sapporo-(DK)-nZP sets (n = D, T, Q). *Theoretical Chemistry Accounts* **2012**, *131*.